DESIGN, SIMULATION, CONSTRUCTION AND PERFORMANCE EVALUATION OF A THERMOSYPHON SOLAR WATER HEATER

BY

SELFA JOHNSON ZWALNAN B.Eng. (A.T.B.U) 2002

MSc/ENG/03852/10-11

A THESIS SUBMITTED TO THE SCHOOL OF POSTGRADUATE STUDIES
AHMADU BELLO UNIVERSITY, ZARIA

IN PARTIAL FULFILLMENT OF THE REQUIREMENTS FOR THE AWARD OF
MASTERS DEGREE IN MECHANICAL ENGINEERING

DEPARTMENT OF MECHANICAL ENGINEERING
FACULTY OF ENGINEERING
AHMADU BELLO UNIVERSITY, ZARIA
NIGERIA

JULY, 2015

DECLARATION

I declare that the work in the thesis entitled 'Design, Simulation, Construction and Performance Evaluation of A Thermosyphon Solar Water Heater' has been performed by me in the Department of Mechanical Engineering under the supervision of Dr G.Y Pam, and Prof. E.J Bala. The information derived from the literature has been duly acknowledged in the text and a list of references provided. No part of this thesis was previously presented for another degree or diploma at this or any other Institution.

SELFA JOHNSON ZWALNAN _____ _____

(Signature) (Date)

CERTIFICATION

This thesis titled 'DESIGN, SIMULATION, CONSTRUCTION AND PERFORMANCE EVALUATION OF A THERMOSYPHON SOLAR WATER HEATER' by SELFA JOHNSON ZWALNAN meets the regulations governing the award of the degree of Master of Science in the Department of Mechanical Engineering of the Ahmadu Bello University, Zaria, and is approved for its contribution to knowledge and literary presentation.

Dr. G.Y Pam	_____	_____
(Chairman, Supervisory Committee)	(Signature)	(Date)
Prof. E.J Bala	_____	_____
(Member, Supervisory Committee)	(Signature)	(Date)
Dr. M.Dauda	_____	_____
(Head of Department)	(Signature)	(Date)
Prof. A.Z. Hassan	_____	_____
(Dean, School of Postgraduate Studies)	(Signature)	(Date)

DEDICATION

This thesis is dedicated to God and the memory of my wonderful Dad, Johnson Buture Zwalnan.

ACKNOWLEDGEMENTS

This thesis would not have been possible without the guidance, encouragement and support of several individuals who, in one way or another contributed and extended their valuable assistance in the preparation and completion of this study. First and foremost, I offer my sincere gratitude to my supervisors Dr. G.Y. Pam and Prof. E.J. Bala for their quality supervision, advice, and guidance right from the very beginning of this research as well as giving me extraordinary experience throughout this work. I am in deed much indebted to you for using your precious time to read through the thesis and provide your critical comments. My special thanks go to the Head of Department Mechanical Engineering and all the staff of the department. I would like to acknowledge my wife and my children for their endless love, continuous support and encouragement while I have been away for the study. I would like to acknowledge my parents for their prayers for me to finish this work. I would not forget the encouragement and support I got from my class mates and very special friends like Christopher Nyachaka and Muhammed Baba. You guys are wonderful. My gratitude would not be complete without the mention of Peter Piro for his quality assistance and all staff of mechanical engineering workshop for their valuable help during the construction process. You really are special people.

ABSTRACT

A thermosyphon solar water heating system which captures and utilises the abundant solar energy to provide domestic hot water was designed, simulated, constructed and tested. The system was designed to supply a daily hot water capacity of $0.1m^3$ at a minimum temperature of 70^oC for domestic use. The design approach was in three parts; firstly, since solar radiation and weather data which are driving function for solar systems design vary randomly with time, the monthly average daily solar radiation and weather data obtained from the typical meteorological year (TMY) solar data of Zaria were used to determine the design month as the month (August) with the least monthly average daily solar energy ratio. Solar radiation and weather data of the design month were used to design the system. Secondly, the design month solar radiations and weather data were used as input into the design equations coded using MATLAB programming language to determine the system characteristic and components sizes. A parametric study was also carried out to study the effects and sensitivity of varying some design parameters such as number of glass covers N_g, collector tube centre to centre distance W, absorber plate thickness δ, collector tube internal diameter d_i and collector tilt angle β on the design objective function (the heat removal factor F_R). Thirdly, based on the values of the system characteristics and components sizes obtained from the design calculations and the parametric study, a model for the performance simulation of the system was formulated using the Transient System Simulation (TRNSYS) software. This model was used to predict the annual hourly performance of the system for recommended average day of the months using the TMY solar radiation and weather data of Zaria as input function. The system was then constructed based on the component sizes adopted for the simulation owing to the satisfactory performance of the system as revealed from the simulated results. To validate the simulated system performance, system performance tests

were conducted for 3 days and the results were compared with the simulated results. The root mean square error (RMSE) and the Nash-Sutcliffe Coefficient of Efficiency (NSE) statistical tools were used to analyse the experimental and simulated results in order to validate the predictive power of the software. The results of this research led to the conclusion that a thermosyphon solar system with collector area of 2.24 m^2 operated under the weather condition of Zaria, would be capable of supplying a daily domestic water of $0.1m^3$ at temperature ranging from 59^oC for the worst month (August) to 81^oC for the best month (April).The computed Nash-Sutcliffe Coefficient of Efficiency (NSE) values of 0.663, 0.956 and 0.885 and the low RMSE values of 8.09^oC, 3.65^oC and 5.31^oC between the modeled tank inlet temperature and the observed tank inlet temperature for the three days tests conducted indicated that the model formulated using TRNSYS software was valid and closely agreed, capable of predicting the performance of the system with a 66.3 %, 95.6% and 88.5 % degree of accuracy for the 3 days that the experiments were conducted respectively.

TABLE OF CONTENTS

LIST OF FIGURES

LIST OF TABLES

LIST OF APPENDICES

NOMENCLATURE

Ac	Collector area (m^2)
A_i	Anisotropic index
A_e	Edge insulation area (m^2)
A_{st}	Tank surface area (m^2)
b_o	Incidence angle modifier constant
C_b	Contact resistance *(*kJ/hr.m.K).
C_p	Fluid specific heat (kJ/kgK)
d_o	Outer diameter of collector outlet pipe (m)
d_R	Riser diameter (m)
d_i	Diameter of collector inlet pipe (m)
d_o	Diameter of collector outlet piping (m)
Di	Inner tube diameter (m)
D	Outer tube diameter (m)
E_R	Energy ratio
f	Square root of ratio of beam to total radiation
F_R	Heat removal factor
F'	Collector efficiency factor
F	Standard fin efficiency for straight fins with rectangular profile
F''	Collector flow factor
F	Solar fraction over a specified time horizon
H_d	Header diameter (m)
H_L	Header length (m)

h_c Horizontal distance between collector outlet and inlet (m)

h_o Horizontal distance between outlet of tank and inlet of collector (m)

H_t Tank height (if vertical) or diameter (if horizontal) (m)

H_R Height of collector return to tank above bottom of tank (m)

$\overline{H}$ Monthly average daily radiation on a horizontal surface (MJ/m^2 day)

$\overline{H}_0$ Monthly average extraterrestrial daily radiation on a horizontal surface

$\overline{H}_T$ Monthly average total radiation on tilted surface (MJ/m^2day)

H_b Total beam radiation on horizontal surface (MJ/m^2day)

H_d Total diffuse radiation on horizontal surface (MJ/m^2day)

h_{fi} Internal fluid heat transfer coefficient (kJ/hr.m^2.K).

h_w Wind heat transfer coefficient (kJ/hr.m^2.K).

KL Product of extinction coefficient and the thickness of each cover plate

k_f Thermal conductivity of fluid in the tank (kJ/h m ^oC)

k_{ins} Thermal conductivity of insulation material (kJ/hr m ^oK)

$\overline{K}_T$ Monthly average clearness index,

k Plate conductivity (kJ/hr m ^oK)

K_{ei} Thermal conductivity of edge insulation materials (kJ/hr m ^oK)

L Length of each pipe (m)

L_i Length of collector inlet pipe form the storage tank (m)

L_o Length of collector outlet pipe to the tank inlet (m

NB_1 Number of right angle bends (or equivalent) in inlet pipe 2

NB_2 Number of right angle bends (or equivalent) in collector outlet piping

N_g Number of glass covers

N_R Number of parallel collector risers

N_x Number of collector nodes for thermal head calculations

$\dot{m}$ Collector fluid mass flow rate (kg/hr.m^2)

$\dot{m}_L$ Desired load mass flow rate, (kg/s)

$\dot{m}$ Mass flow rate of fluid in the collector (kg/s)

N Number of turns

N_g Number of glass covers

Q_u Useful energy gain per unit time (MJ/m^{2}day)

Q_L Quantity of heat required to meet load (MJ/day)

Q_{aux} Auxiliary energy requirement to meet the desired load (MJ/day)

Q_{Ls} Load met by solar energy (MJ/m^{2}day)

R_b Monthly average ratio of beam radiation on a tilted surface to beam radiation on a horizontal surface.

R Index of refraction of cover material

Re Reynolds number

T_{pm} Mean plate temperature (K)

T_{ci} Collector fluid inlet temperature (K)

Ta Ambient temperature (K)

T_{co} Collector fluid outlet temperature (K)

T_L Desired load (hot water) temperature, (^{o}C)

t_{ins} Thickness of insulation material (m)

T_{ci} Fluid inlet temperature (^{o}C)

T_{st} Storage temperature (^{o}C)

T_{fm} Collector means fluid temperature (K)

T_{ci} Collector inlet fluid temperature (^{o}C)

T_{sti} Storage tank inlet temperature (^{o}C)

t_p Plate thickness (m)

U_e Edge loss coefficient of collector per unit aperture area (kJ/hr-m^2-K)

U_o Loss coefficient of collector outlet and inlet pipe plus insulation (kJ/hr m$^{2\,o}$K)

V_t Tank volume (m^3)

U_L Overall collector loss coefficient (kJ/ m^{2}hr.K)

U_t Collector top loss coefficient (kJ/hr.m^2.K).

U_b Back loss coefficient (kJ/hr.m^2.K).

U_{st} Tank loss coefficient (kJ/hr.m^2.K).

W Tube spacing (m)

x_{ei} Insulation thickness at the edge (m)

Greek symbols

ε_p Absorber plate emittance

α_p Absorptance of absorber plate

β Collector slope (degrees)

ρ_{fs} Fluid density at standard conditions (kg/m^3)

θ_T Incident angle of beam radiation on tilted surface (degrees)

θ_z Zennit angle (degrees)

δ Declination (Degrees)

σ Boltzmann constant

$\emptyset$ Latitude of the location (Degrees)

ω Solar hour angle (Degrees).

$\bar{\theta}_b$ Monthly average (equivalent) beam incident angle (degrees)

ω_s Sunset hour angle (Degrees).

$\overline{\tau\alpha}$ Monthly average daily transmittance-absorptance product

ρ_d Reflectance of the cover system for diffuse radiation

$(\tau\alpha)_b$ Transmittance-absorptance product of beam radiation

$(\tau\alpha)_d$ Transmittance-absorptance product of diffuse radiation

$(\tau\alpha)_g$ Transmittance-absorptance product of ground reflected radiation

ρ_g Diffuse reflectance of the ground

δ_t Absorber plate thickness (m)

ε_g Emittance of glass (0.88)

ε_P Emittance of plate

μ Dynamic viscosity, (kg/m s)

ρ Density of water (kg/m^3)

υ Kinematic viscosity (m^2/s)

β' Thermal cubic expansion coefficient

η_C Collector efficiency over a specified time horizon

ABBREVIATIONS

T_2	Temperature of the upper glazing
T_1	Temperature of the lower glazing
TK_{expt}	Hourly experimental tank inlet temperature
TK_{sim}	Hourly simulated tank inlet temperature
$\overline{TK}_{expt}$	Daily average experimental tank inlet temperature
RMSE	Root Mean Square Error
NSE	Nash-Sutcliffe Coefficient of Efficiency
TMY	Typical meteorological year
R_s	Hourly simulated solar radiation on the collector surface
R_{exp}	Hourly experimental solar radiation on the collector surface
$\overline{R}_{exp}$	Daily average experimental solar radiation on the collector surface
$T1_{top}$	Top surface temperature of the first glazing from the top
$T2_{top}$	Top surface temperature of the second glazing from the top

CHAPTER ONE

INTRODUCTION

1.1 Background of the Study

Energy is considered a prime agent in the generation of wealth and a significant factor in economic development. The importance of energy in economic development is recognized universally, and historical data verified that there is a strong relationship between the availability of energy and economic activity (Soteris, 2004). Although in the early seventies, after the oil crises, the concern was on the cost of energy, however during the past two decades, the risk and reality of environmental degradation have become more apparent. The growing evidence of environmental problems is due to a combination of several factors, since the environmental impact of human activities has grown dramatically (Soteris, 2004). This is due to the increase of the world population, energy consumption and industrial activities. Achieving solutions to the environmental problems that humanity faces today requires long term potential actions for sustainable development. Renewable energy resources appear to be one of the most efficient and effective solutions.

Of all the renewable sources of energy available, solar thermal energy is the most abundant one and is available in both direct as well as indirect forms. The Sun emits energy at a rate of 3.8×10^{23} kW, of which, approximately 1.8×10^{14} kW is intercepted by the earth, which is located about 150 million km from the sun. About 60% of, this amount reaches the surface of the earth. The rest is reflected back into space and absorbed by the atmosphere. About 0.1% of this energy, when converted at an efficiency of 10% would generate four times the world's total generating capacity of about 3000 GW(Mirunalini, *et al.*,2010). It is also worth noting that the total annual solar radiation falling on the earth ismore than 7500 times the world's total annual primary energy consumption of 450 EJ (Mirunalini, *et al.*, 2010). The annual solar radiation reaching the earth's surface, approximately 3,400,000 EJ,

is an order of magnitude greater than all the estimated (discovered and undiscovered) non-renewable energy resources, including fossil fuels and nuclear energy (Mirunalini *et al.* , 2010). However, 80% of the present worldwide energy utilisation is based on fossil fuels.

World demand for fossil fuels (starting with oil) is expected to exceed annual production, probably within the next two decades (Mirunalini *et al.*, 2010). International economic and political crisis and conflicts can also be initiated by shortages of oil or gas. Moreover, burning fossil fuel releases harmful emissions such as carbon dioxide, nitrogen oxides, aerosols, etc. which affect the local, regional and global environment. By means of different mechanisms, solar radiation may be converted into other forms of energy, such as photovoltaic conversion into electrical energy, photochemical conversion into chemically bound energy, and photo thermal conversion into heat. The heat converted from solar radiation, is well suited to provide domestic hot water and space heating. In most parts of the world, the yearly solar radiation received by a single family house is several times greater than the energy needed for domestic hot water and space heating(Mirunalini *et al.*, 2010).

For many years, solar domestic hot water (DHW) systems have gained great attention due to their considerable energy conservation, environmental protection and relatively good economy. The purpose of using a solar DHW system is to convert the solar radiation into thermal energy, and then to use it for domestic hot water heating, thus reducing the over dependence on and consumption of conventional energy. Recently, environmental issues have led to an even greater interest in solar DHW systems. There are several fundamental conditions that make solar DHW systems very different from conventional fossil-fuel systems. Firstly, the power density of solar radiation is relatively low and the collector has to cover a large area. Thus, the solar DHW systems cannot be as compact as conventional units. Secondly, the solar radiation varies considerably during the day, in the course of a

year and between different locations. Therefore, the solar energy received by a collector is an irregular function of time and location, and the power output of the collector cannot be controlled in the same way as conventional heating systems. Consequently, heat storage and auxiliary energy are required to match the supply to the load.

1.2 Statement of the Problem.

There is a strong consensus among climate scientists that the environmental problems now observed is caused by human activities targeted to meeting our energy demand, especially the combustion of fossil fuels. When oil, gas, or coal are burned to generate electricity or provide heat, the products of the combustion which include carbon dioxide and nitrous oxide, lead to global warming and acid rain deposition, respectively . The expected impacts of global warming include sea-level rise flooding of coastal areas increased frequency and severity of floods, draughts, storms, and heat waves, reduced agricultural production, massive species extinction, and the spread of vector-borne diseases such as malaria and dengue fever (Christopher and Homola, 2006). Thus, the manners in which we produce and consume energy (conventional way) are to a large extent responsible for this impending environmental problem (Intergovernmental Panel on Climate Change (IPCC), 2001).

According to Christopher and Homola (2006), rising economic losses due to weather-related disasters are part of a trend being linked to climate change. The World Health Organization estimates that climate change is already responsible for 150,000 deaths annually (Christopher and Homola, 2006).

Domestic hot water use again represents a large proportion of domestic energy need. This energy need accounts for approximately one third of the total annual energy consumption for domestic purposes and therefore a greater portion of the family income is spent on domestic hot water (Retscreen International, 2004).

1.3 The Present Research

This research involves the design, simulation, construction and performance tests of a solar domestic hot water heating thermosyphon system for Zaria, Nigeria, located on latitude 11.2^{o} N and longitude 7.8^{o}N. The design method employed is the simulation based method, where mathematical models for the determination of the system design parameters and characteristics were coded into a computer programme using the Matrix Laboratory (MATLAB) software in a manner that represents the conceptual design of the system.

The effects and sensitivity of the system design parameters on the collector heat removal factor were studied through programmes codes written in MATLAB in order to determine the size of the various components of the collector that will give better performance.

The system performance was simulated using the Transient Systems Simulation (TRNSYS) software for recommended average days of the months. The system was then constructed based on the adopted system configuration and components' sizes obtained from the studies. The performance of the system was then experimentally determined and the results obtained from the test were compared with the simulated results in order to validate the formulated model used for the performance simulation.

1.4 Aim and Objectives

The aim of this research is to design, simulate, construct and test the performance of a solar domestic hot water thermosyphon system for the city of Zaria, Nigeria.

The specific objectives are:

i. To carry out a parametric study on the effect and sensitivity of the tilt angle, β, number of glasing , N, absorber plate thickness, δ, collector tube diameter, d_i and collector tube centre to centre distance, W, on the objective function which is the

percentage expression of the heat removal factor, F_R, using Matrix Laboratory (MATLAB) programming language.

ii. To predict through simulation using TRNSYS, the annual performance of the system.

iii. To validate the predicted system performance through experiments.

iv. To estimate the cost of the system.

1.5 Significance of the Research.

Environmental concerns about global warming, local pollution and reduction of over dependence on conventional energy source for domestic hot water need in Zaria, is the primary impetus for this research. This research would provide alternative way to providing hot water for domestic use in various homes. It also has the potential of reducing family utility bills and thereby improving family savings.

CHAPTER TWO

LITERATURES REVIEW

2.1 Solar Potential and Resources of a Location

Every location on earth receives sunlight at least part of the year. The amount of solar radiation that reaches any one "spot" on the earth's surface varies according to geographic location, time of the day, season, local landscape and local weather. The shape of the earth makes the sun to strike its surface at different angles ranging from 0º (just above the horizon) to 90º (directly overhead). When the sun's rays are vertical, the earth's surface gets all the energy possible. The more slanted the sun's rays are, the longer they travel through the atmosphere, becoming more scattered and diffuse (www.eere.energy.gov , 2012**).**

The earth revolves around the sun in an elliptical orbit and is closer to the sun during part of the year. When the sun is nearer the earth, the earth's surface receives a little more solar energy. The earth is nearer the sun when it is summer in the southern hemisphere and winter in the northern hemisphere. However, the presence of vast oceans moderate the hotter summers and colder winters one would expect to see in the southern hemisphere as a result of this difference.

The 23.5º tilt in the earth's axis of rotation is a more significant factor in determining the amount of sunlight striking the earth at a particular location. Tilting results in longer days in the northern hemisphere from the spring (vernal) and longer days in the southern hemisphere during the other six months. Days and nights are both exactly 12 hours long on the equinoxes, which occur each year on or around March 23 and September 22. Countries like the United States, which lie in the middle latitudes, receive more solar energy in the summer not only because days are longer, but also because the sun is nearly overhead. The sun's rays are far more slanted during the shorter days of the winter months (www.eere.energy.gov, 2012**).**

The rotation of the earth is responsible for hourly variations in sunlight. In the early morning and late afternoon, the sun is low in the sky. Its rays travel further through the atmosphere than at noon when the sun is at its highest point. On a clear day, the greatest amount of solar energy reaching a solar collector is around solar noon (Qin, 1998).

2.2 Solar Water Heating Systems

Solar water heating systems use solar energy to heat water. Depending on the type of solar collector used, the weather conditions, and the hot water demand, the temperature of the water heated can vary from tepid to nearly boiling. Most solar systems are meant to furnish 20 to 85% of the annual demand for hot water, the remainder being met by conventional heating sources, which either raise the temperature of the water further or provide hot water when the solar water heating system cannot meet demand (e.g. at night) (Alternative energy tutorials, 2012). Solar hot water systems can be used wherever moderately hot water is required. Solar water heating technology has been embraced by a number of developing countries with both strong solar resources and costly or unreliable conventional energy supplies (Alternative energy tutorials, 2012).

2.2.1 Direct open-loop hot water system

An active open-loop direct solar water heating system uses a pump to circulate the water around the system. The cooler water is pumped directly from the home to a central water storage or immersion tank and passes through the solar collector for heating. The hot water leaves the flat plate collector and returns to the tank flowing in a continuous loop. From the tank, the water is pumped back into the house as hot usable water using a low voltages (12 volt) pump, which can be powered by a small photovoltaic cell making the system greener. A direct system is usually used in warmer climates with few cold days (Alternative energy tutorials, 2012).

However, a passive direct hot water system does not use pumps or control mechanisms to transfer the heat generated to the storage tank. Instead, passive systems are open-loop systems which use the natural force of gravity to help circulate the water. This type of system uses a solar flat plate collector combined with a horizontally mounted storage tank of some kind, located immediately above the collector. The water heated by the sun rises naturally due convection current through the solar collector pipes and enters the storage tank situated above the collector. As the heated water enters the storage tank above, the cooler water is forced out and flows down to the bottom of the collector aided, by gravity as cold water is denser than hot water. This cycle of hot water rising and cooler water falling is known as a "thermosyphon flow" and continuously repeats itself unaided while the sun is shining.

For the thermosyphoning process to work correctly, the base of the water storage tank must be situated at least 1 to 2 feet (300 to 500mm) above the top of the flat plate collector(see figure 2.1). This distance is also known as the system's "head height" (Alternative energy tutorials, 2012).

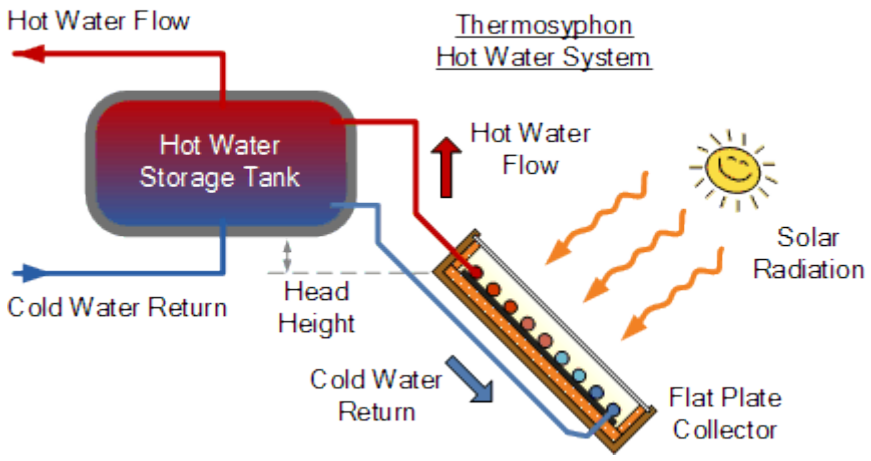

Figure 2.1: A typical thermosyphon hot water system (Alternative energy tutorials, 2012).

2.2.2 Indirect hot water system

An indirect hot water system, also known as a closed-loop system, differs from the previous system (figure 2.1) in that it uses a heat exchanger that is separate from the solar flat plate collector to heat the water in the storage tank. Indirect hot water systems are active systems and require pumps to circulate the heat transfer liquid around the closed-loop system from the collector to the heat exchanger in the tank. The system contains an antifreeze solution, typically a 50% Glycol/water mixture, in the primary closed-loop instead of just water, which is heated and is kept separate from the main domestic hot water supply. A simple schematic diagram of an indirect solar hot water system is shown in figure 2.2

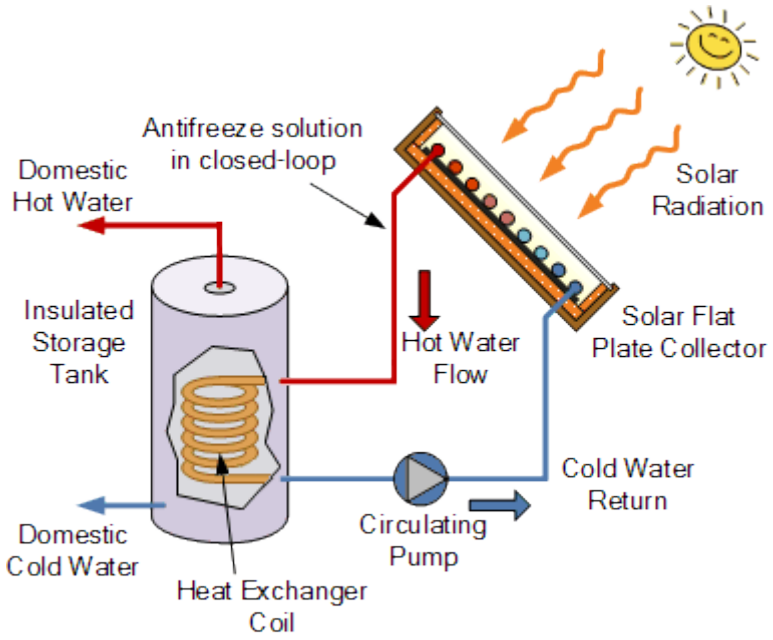

Figure 2.2: Typical indirect hot water system (Alternative Energy Tutorials, 2012).

The heat exchanger transfers the heat from the collector's antifreeze solution to the water contained in the water storage tank. The heat exchanger is a copper coil inside the lower

part of the storage tank. One main advantage to this indirect system is that the antifreeze solution gives all year round operation in areas where the temperature falls below the freezing point as well as protecting the system from corrosion of the collectors by untreated tap water containing gases and various dissolved salts.

2.3 Solar Collector

A **flat plate solar collector** is a heat exchanger that converts the radiant solar energy from the sun into heat using the well-known greenhouse effect. It collects, or captures solar energy and uses that energy to heat water in the home and it can even be used to heat outdoor swimming pools and hot tubs. For most residential and small commercial hot water applications, the *solar flat plate collector* tends to be more cost effective due to their simple design, low cost, and relatively easier installation compared to other forms of hot water heating systems. Also, solar flat plate collectors are more than capable of delivering the necessary quantity of hot water at the required temperature (Alternative Energy Tutorials, 2012).

A solar flat plate collector typically consists of a large heat absorbing plate, usually a large sheet of copper or aluminum as they are both good conductors of heat, which is painted and chemically etched black to absorb as much solar radiation as possible for maximum efficiency. This blackened heat absorbing surface has several parallel copper tubes called risers, which contain the heat transfer fluid, typically water, running length ways across the plate. These copper pipes are bonded, soldered or brazed directly to the absorber plate to ensure maximum surface contact and heat transfer as sunlight heats the absorbing surface. As the plate gets hotter this heat is conducted through the risers and absorbed by the fluid flowing inside the copper pipes which is then used by the house hold. The pipes and absorber plate are enclosed in an insulated metal or wooden box with a sheet of glazing material, either glass or plastic on the front to protect the enclosed absorber plate and

create an insulating air space. This glazing material does not absorb the sun's thermal energy to any significant extent and therefore most of the incoming radiation is received by the blackened absorber. The air gap between the plate and glazing material traps this heat preventing it from escaping back into the atmosphere. As the absorber plate warms up, it transfers heat to the fluid within the collector but it also loses heat to its surroundings. To minimise this loss of heat, the bottom and sides of a flat plate collector are insulated with material such as, high temperature rigid foam or aluminum foil insulation. Figure 2.3 depicts a typical flat plate collector.

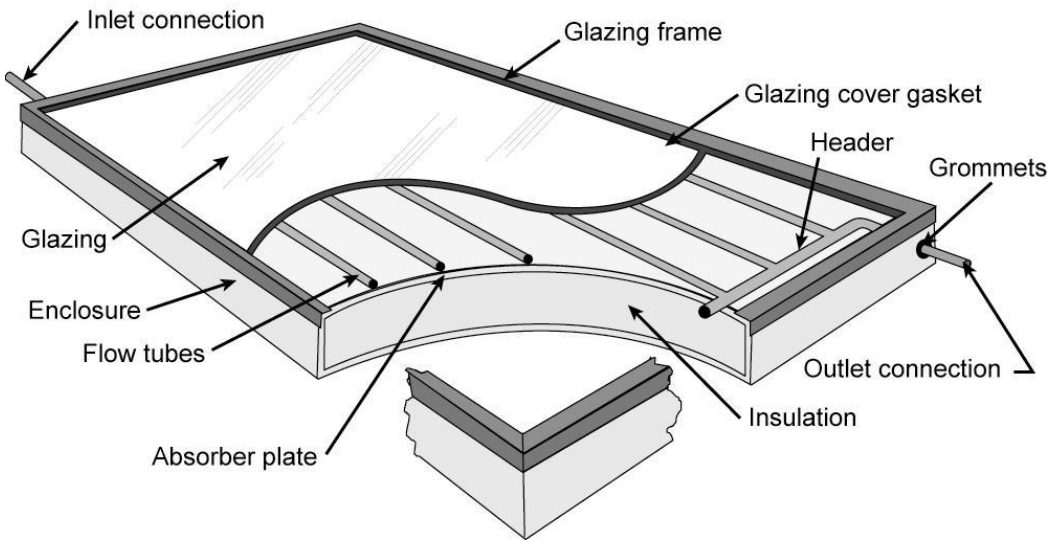

Figure 2.3: Typical cross sections of a flat plate solar collector (Alternative Energy Tutorials, 2012)

Flat-plate collectors are most suitable for low temperature applications such as domestic hot water and space heating. They collect both direct and diffuse radiation. It is not required that they track the sun, thus initial cost and maintenance are minimised. A properly designed flat-plate collector has a life expectancy of 10 to 25 years, or sometimes longer (Qin, 1998). All copper and glass systems currently exhibit the longest lives. Using softened water will help. Tubes should be 1/2 inch (0.012700m) in diameter or greater for

low pressure drop and longer life. The better the attachment of tube to-plate (such as by soldering), the better the heat transfer, but the greater the manufacturing cost (Qin, 1998).

2.3.1 Selective surfaces.

A collector manufactured with a black coating absorber plate absorbs the high frequency incoming solar radiation very well and emits low frequency infrared radiation poorly. This is a highly desirable combination of properties for a collector. The absorptance should be 0.9 or higher and emittance may be 0.1 or lower. Such coatings are approximately equal in effect to one cover glass. Thus, a selective coating plus one cover glass may be expected to be about equal in efficiency to a collector with two cover glasses and a flat black painted surface.

Electroplated black nickel, black chrome, copper oxide and anodized aluminum are common types of selective coatings (Rhushi *et al.,* 2011). A summary of the thermal properties of some selected thermal absorbers is presented in table 2.1

Table 2.1: Summary of absorber coatings optical properties both selective and nonselective.

	Absorptanceα	**Emittanceε**
Black Chrome	0.87-0.93	0.10
Alkyd Enamel	0.90	0.90
Black Acrylic Paint	0.92-0.96	0.86-0.93
Black Inorganic Paint	0.89-0.97	0.84-0.90
Black Silicone	0.86-0.94	0.83-0.89
Matt Black	0.95-0.98	0.89-0.97
Black Zinc	0.90	0.10

Source: Duffie and Beckman (1991)

2.3.2 Collector covers.

The transparent covers serve to admit solar radiation to the absorber while reducing convection and radiation heat losses from the collector. The covers also protect the absorber from dirt, rain, and other environmental contaminants. The material used for covers include glass and/or plastic sheets. Glass has been the principal material used to glaze solar collectors because it has the highly desirable property of transmitting as much as 90% of the incoming short-wave solar radiation, while virtually none of the long wave radiation emitted by the flat plate can escape outward by transmission. Glass of low iron content has a relatively high transmittance (0.85 - 0.90 at normal incidence) for the solar spectrum from 0.30μm to 3.0μm, (Rhushi *et al.,* 2010**)**. Absorptance of solar radiation by the collector can be increased with the use of thinner tempered glass and by using glass that has low iron content. Although glass is subject to impact damage and is more expensive than plastic, it does not degrade in sunlight or at high collector temperatures, and is generally considered to be more durable than plastic. Each additional cover, whether it is glass or plastic, reduces convection heat losses, but results in added expense and less solar radiation transmitted to the absorber. Most commercially available collectors come with one or two glazing. The decision to use one or two covers depends on the type of absorber coating, the required collection temperatures, average ambient air temperature, the local wind conditions, and of course, the cost of the covers. The use of a selective surface is about equal to using one additional cover. Thus, for most cases, only one glass cover is needed if the absorber has a selective coating (Unified Facilities Criteria, 2004).

Two covers are generally recommended for use in Northern climates where winter ambient air temperatures are low. For flat-plate collectors used mostly for winter heating, one rule of thumb is to use one glass cover where average winter air is greater than 25^{o}C and two glasses covers in colder climates (Unified Facilities Criteria, 2004).

2.4 Thermosyphon System.

Unlike other types of solar DHW systems, the operation of a thermosyphon system depends on a large number of design and weather parameters. The flow in the collector loop is essentially controlled and adjusted by temperature distribution (Qin, 1998).

The basic working principle of this kind of system is that when solar radiation is absorbed in the collector, the collector heats up the water present in the collector tubes, the water becomes less dense than the cold water in the tank and thus, rises to the highest point in the assembly, the top of the storage tank. At the same time the cold water from the bottom of the tank flows into the collector and is in turn being heated. This process is repeated continuously, forming what is termed a thermosyphon water circulation pattern (Qin, 1998).

Since the flow is controlled by the density difference, the reverse may also happen during the night when the temperature of the collector and riser are lower than the temperature of the tank water. To avoid heat loss from the storage tank a check valve is used in the system to prevent reverse flow (Qin, 1998).

2.5 Sizing a Solar Hot Water System

Sizing a **solar flat plate collector** for use in a solar hot water or heating system depends upon the hot water demand. If the home's hot water consumption or maximum water temperature is reduced, hot water demand may be met with a smaller solar array that is easy to install. Also, smaller systems are cheaper to install and will pay for themselves sooner through energy savings. System sizing of course depends on hot water temperature and consumption but general rules of thumb can be used to help give an idea of a system's size.

For locations with minimum monthly average daily global solar radiation on horizontal surface of 3.0 kWh/m^2, 0.1 m^2collector surface area may heat about 0.01m^3 (10 litres)of water per day to well over 70^{o}C. Therefore a single collector of 1.86m^2 to 2.79m^2 will heat about 0.3m^3 (300 litres) of water, which is about the size of a standard hot water storage tank to 70^{o}C (Alternative Energy Tutorials, 2012). In general, about 0.01m^3 (2 gallons) of water storage requires 0.0929$m^2$of collector area to heat it to a temperature of 70^{o}C. So, for a family of four persons this translates into 3.72m^2 to 5.57m^2 of collector area for hot water of 0.23m^3 (230 litres) to 0.45m^3 (454 litres) at 70^{o}C (Alternative Energy Tutorials, 2012). Then, a solar hot water heating system for a family of four, each would need at least two standard solar flat plate collectors of about 2.95m^2 (1.22m x 2.44m) (Alternative Energy Tutorials, 2012).

2.6 Collector Orientation

Solar hot water collectors should be oriented geographically to maximise the amount of daily and seasonal solar energy that they received. Geographic orientation and collector tilt can affect the amount of solar radiation a system receives. Both the orientation and tilt of the collector will affect a solar water heating system's performance. In general, the optimum orientation for a solar collector in the northern hemisphere is due south. Even though solar collectors can collect heat from the diffuse component of solar radiation, solar systems are designed to use the direct component. Direct radiation is in the form of parallel rays coming straight from the sun. To best capture this energy, the solar collector should be tilted so that it is more nearly perpendicular to the solar rays. The "optimum" tilt angle varies even as the sun changes its position throughout the day and year. However, since the solar system cannot be continuously moved, the following general rules can be stated **(**Unified Facilities Criteria, 2004):

i. For all year domestic hot water (DHW) heating, tilt angle should be equal to the latitude.

ii For all year DHW heating and winter space heating, use a tilt angle equal to the latitude plus 10 to 15 degrees.

iii For all year DHW heating, winter space heating and summer cooling, use same as (i).

In addition to choosing the best collector tilt angle, consideration must be given to the orientation of a collector (i.e., the direction the collector faces). Normally true south is the best and most frequent choice. However, slightly west of south (10 degrees) may be preferable in some locations if an early morning haze or fog is a regular occurrence. Some deviations from these tilt and orientation angles are allowable without significantly affecting the performance of the solar collector. The tilt angle may vary plus or minus 10 degrees and the orientation angle up to 20 degrees either side of true south (Unified Facilities Criteria, 2004). For these deviations, the solar collectors would still collect 95% - 100% of their rated capacity in most locations. Additional deviations would require more collector area to capture the same amount of energy.

In collector orientation, keeping the collectors out of the shade, especially between 9 a.m. and 3 p.m, when most of the useful energy collection occurs is also very important. In designing, effort should be made to anticipate any future structures or vegetation (trees) that could block future solar access (Christopher and Homola, 2006).

2.7 Solar Water Heating System Applications.

Solar water heating applications can be classified based upon the end-use application of the technology. The most common solar water heating applications are service hot water and swimming pools.

2.6.1 Service hot water

There are a number of service hot water applications. The most common application is the use of domestic hot water systems (DHWS), generally sold as “off-the-shelf” or standard kits as depicted in figure 2.4.

Figure 2.4 “off-the-shelf” or standard kits Solar Domestic Hot Water (Thermosiphon) System .
Photo Credit: (Retscreen International, 2004).

Other common uses include providing process hot water for commercial and institutional applications, including multi-unit houses and apartment buildings, housing developments, in school health centre, hospitals, office buildings, restaurants and hotels. Small commercial and industrial applications such as car washes, laundries and fish farms are other typical examples of service hot water. Solar water heating systems can also be used for large industrial loads and for providing energy to district heating networks.

2.7.2 Swimming pools

The water temperature in swimming pools can also be regulated using solar water heating systems, extending the swimming pool season and saving on the conventional energy

costs. The basic principle of these systems is the same as with solar service hot water systems, with the difference that the pool itself acts as the thermal storage.

2.8 Solar Water Heating System Load

In solar heating system design, it is necessary to estimate the long-term (annual and/or monthly) average heating loads. The water heating load or the amount of energy required to warm water from the inlet cold water to a desired temperature is dependent on several factors such as hot water consumption rate, cold water inlet and desired hot water set temperatures, location and orientation of the building, and system characteristic. This load also includes any heat loss from the storage tank, piping system, the amount of energy that is required to reheat the water that was already heated but not used (Alireza and Kamran, 2009).

2.8.1 Average daily hot water consumption

The average domestic hot-water loads for a family or apartment building is normally found from experimental measurements. A number of results from different regions have been reported. From these reports, it was found that the average daily hot-water consumption differs considerably for different areas. This may be due to many effects such as climate differences and life style. Otto and Nielesn carried out measurement for family houses in Denmark and found that the average daily hot-water at 50^{o}C load is about 32 litres per person, which is lower than the commonly accepted design value of 40 litres/person (Qin, 1998).

2.8.2 Hot water load profile

The hourly distribution of hot water consumption can vary from day to day, from season to season and from family to family. A hot water consumption of 140 l/day distributed during

a day according to Domestic hot water consumption pattern as per ISO 9459-3 (1997) is shown in figure 2.5.

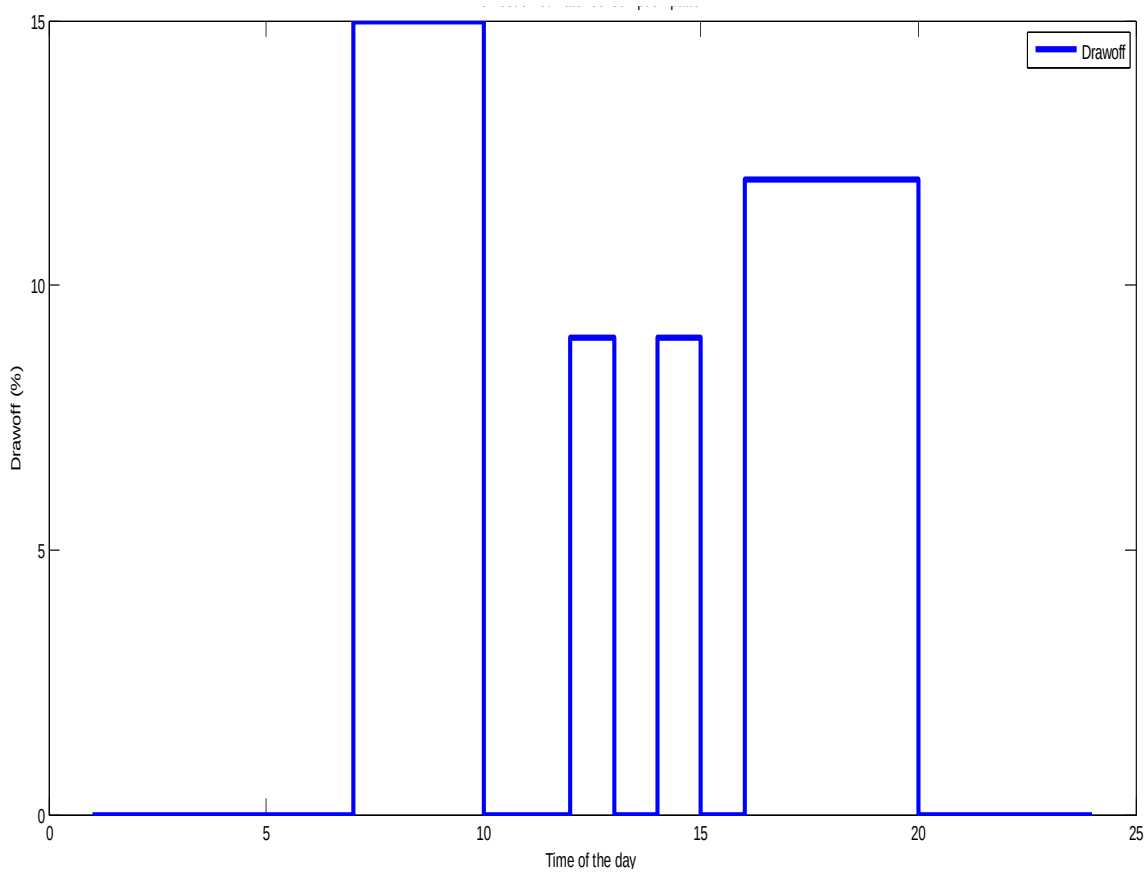

Figure 2.5.Domestic hot water consumption pattern as per ISO 9459-3 (ISO, 1997).

2.9 Review of Related Work.

Jae-Mo (1999) carried out a very detailed thermal analysis of a flat-plate solar collector to predict the thermal performance. This analysis was based on the established theory about flat-plate solar collector: the radiation absorption, heat loss from the collector, and temperature distribution on the plate. The calculation of useful energy and top heat loss from the collector is based on the aperture area to make a more accurate prediction of collector performance. The correlation for natural convection heat transfer between the covers and between the plate and cover was selected with the consideration of the low conductivity of plastics. The semi-gray radiation model was adopted to determine the optical properties of the collector cover and absorber plate. Comparison of the results

between calculated with experimental showed good agreement. The collector tests were performed by Florida Solar Energy Centre. The calculations based on the information from test reports yielded an accurate prediction of the thermal performance of flat-plate solar collectors. Based on the analysis, a flat-plate solar collector design programme (CoDePro) has been developed.

Morrison and Braun (1985) have conducted a study on a system modeling and operation characteristics of a thermosyphon solar water heater with vertical or horizontal storage tank. They found that the system performance is maximised when the daily collector volume flow rate is approximately equal to the daily load flow rate, and that the system with a horizontal tank did not perform as well as the one with a vertical tank.

Shariah and Shialabi (1997) have studied optimisation of design parameters for a thermosyphon solar water heater for two regions in Jordan represented by two cities, namely Amman and Aqaba through the use of TRNSYS simulation programme. Their results indicated that the solar fraction of the system can be improved by 10±25% when each studied parameter is chosen properly.

Mryna (1997) developed a low-flow solar domestic hot water system and founded that low-flow systems are capable of reducing equipment and installation costs, which together account for approximately two-thirds of the total SDHW system cost. Low-flow systems allow equipment to be considerably sized down; piping and pumps are smaller. Cost advantages are in terms of decreased material costs, less parasitic pumping power required from the utility and reduced costs with installing lightweight systems. The thermodynamic advantage of low-flow systems is increased tank stratification, which leads to improved system performance.

Govind *et al.* (2006) proposed a methodology to determine the design space for synthesis, analysis, and optimisation of solar water heating systems. The proposed methodology incorporates different design constraints to identify all possible designs or a design space on a collector area versus storage volume diagram. The design space was determined by tracing constant solar fraction lines on a collector area versus storage volume diagram. It was observed that there exists a minimum as well as a maximum storage volume for a given solar fraction and collector area. Similarly, existence of a minimum and a maximum collector area was also observed for a fixed solar fraction and storage volume.

Belessiotis and Mathioulakis (2002) developed an efficient and simple simulation approach for thermosyphon solar water heaters and used the proposed methodology for energy optimization of the system in the design phase and for evaluation of test results of an existing system in order to improve it further.

Delfín *et al.* (2000) carried out a simulation study of a solar domestic water heating system, with different collector efficiencies and different volume storage tanks using a programme based on Matrix Laboratory (MATLAB). The results of simulations performed on an annual basis for a solar system which consists of a solar flat collector, a water storage tank, a source of auxiliary energy, and a device for blending water. , operated in Santander (Spain), which provides hot water for a family (four persons) shows that systems with greater volume yield higher solar fraction values. However, when a larger storage tank was used, the solar fraction was less sensitive to a variation of these operation parameters.

Chaurasia and Twidel (2007) suggested that transparent insulation material may be successfully introduced in integrated collector-storage (ICS) solar water heaters to increase

the efficiency and to provide hot water at higher temperature as compared to conventional ICS solar water heater with glass glazing.

Fanney and Klein (1985) experimentally found that for low flow rates (less than 0.0025 kg/s.m^2 compared to the manufacturer's recommended flow rate of 0.020 kg/s.m^2) there was an

imbalance in the flow through a collector array. The flow was not divided equally between three

individual collectors. The imbalanced flow condition was detected by monitoring thermocouples attached to the absorber plates (Duffie and Beckman, 1991).

Rhushi *et al.* (2011) studied and simulated with a computer programme in C-language the performance of a solar water heater using a flat plate collector. The Program calculates instantaneous beam and diffuse radiations for the given location of the collector, number of days for the given date, angle of incidence of beam radiation on the collector, total solar flux incident on the collector, transmissivity – absorbtivity product for beam and diffuse radiations, incident flux absorbed by the absorber plate, collector heat removal factor, overall loss coefficient, water outlet temperature and the instantaneous efficiency. The developed simulation program not only predicts performance of a given solar collector system, but also could be used to size the solar hot water systems for different applications. Comparison between simulated results and the collector test results, showed that generalised program predicts the values very near to the experimental values and hence the approach of design analysis based upon mathematical modeling is cheap and efficient compared to the analysis of physical models, which in some cases may become very tedious.

Suleiman (2011) carried out a study of adsorption bed of a solar powered adsorption refrigeration system to determine the effects of generation, evaporation and condensation temperatures on the performance of the cooling system of three different collectors. A transient simulation of the cooling system with an evaporator temperature of 0^{o}C and condenser temperature of 25 ^{o}C was subsequently carried out with the TRNSYS software over a period of a typical year. The result of the simulation showed that the flat plate collector system gave average values of refrigeration effect of 4814.83 kJ, solar coefficient of performance (COPs) of 0.024, a cooling coefficient of performance (COP) of 0.608 and a heating efficiency of 0.46. The Evacuated tube collector powered system achieved average values of refrigeration effect of 5528.05 kJ, COPs of 0.025, a COP of 0.612 and a heating efficiency of 0.61. The Parabolic trough collector powered system however gave average values of refrigeration effect of 5654.73 kJ, COPs of 0.025, a COP of 0.613 and a heating efficiency of 0.76.

This research developed Matrix Laboratory (MATLAB) codes for the conceptual design and parametric study of a thermosyphon water heating system based on typical solar and weather data of Zaria, Nigeria.

2.10 Theoretical Background

2.10.1 Angle of incidence of beam radiation

This is defined as the angle between the beam radiation to a surface and the normal to that surface. The angle of incidence, θ_T, of beam radiation for fixed flat plate collector surfaces in the northern hemisphere sloped to the north or south relating to other angles which describe the direction of beam radiation is given by the equation (Duffie and Beckman, 1991).

$$\theta_T = Cos^{-1}[cos(\emptyset - \beta)\cos\delta Cos\omega + \sin(\emptyset - \beta)\sin\delta] \quad (2.1)$$

For horizontal surfaces the angle of incidence of beam radiation is the zenith angle of the sun, θ_z, which must be between 0^o and 90^o when the sun is above the horizon. In this situation tilt angle is zero and therefore θ_z is expressed as (Duffie and Beckman, 1991)

$$\theta_Z = Cos^{-1}[cos(\emptyset)\cos\delta Cos\omega + \sin(\emptyset)\sin\delta]$$

(2.2)

where:

$\theta_T$is the incident angle of beam radiation on tilted surface (degrees)

β is the angle of tilt of the collector,

δ is the declination (degrees)

∅is the latitude of the location (degrees)

$\omega$is the solar angle hour (degrees).

Equations (2.1) through (2.2) describe the hourly incident direction of beam radiation. However for the monthly average beam radiation, Duffie and Beckman (1991) worked out the monthly average (equivalent) beam incident angle $\bar{\theta}_b$, as a function of collector slope, month, latitude, and azimuth angle as shown in figure 2.6.

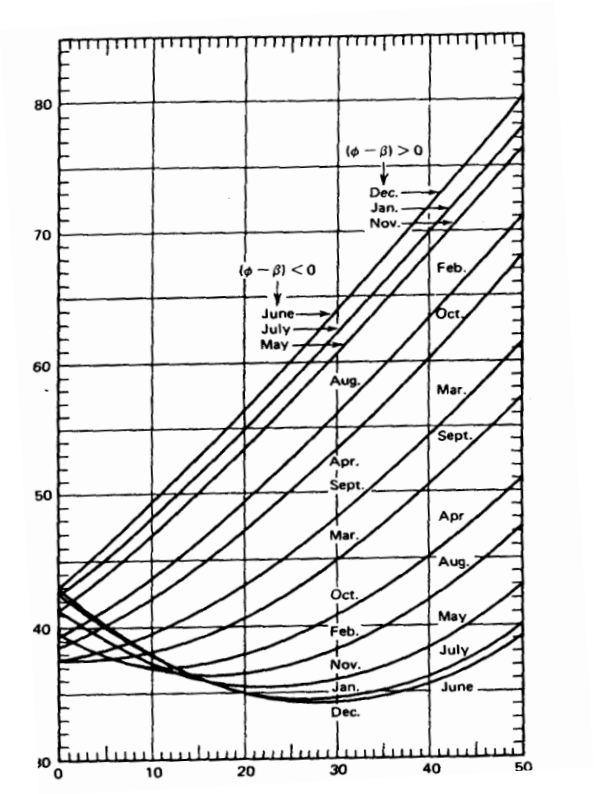

Figure2.6: Monthly mean incident angle for beam radiation for surfaces facing the equator in the
northern hemisphere.(Duffie and Beckman , 1991).

2.10.2 Declination

The declination is the angular position of the sun's ray north or south of the equator. It is the angle between a line extending from the sun to the centre of the earth and the projection of the line upon the earth's equatorial plane. Its value in degrees is given by Cooper's equation as (Duffie and Beckman, 1991):

$$\delta = \left(23.45 sin\left(2\pi \frac{n+284}{365}\right)\right) \qquad (2.3)$$

Where *n* is the day of year (i.e. *n*=1 for January 1, *n*=32 for 1st February, etc.). Declination varies between -23.45° on December 21 and +23.45° on June 21. Table 2.2 shows the recommended average days for the month and values of n by month.

Table 2.2: Recommended average days for each month of the year and values of *n* by month.

Average day of the month			
Month	Date	n, Day of the Year	Declination.
January	17	17	-20.9
February	16	47	-13
March	16	75	-2.4
April	15	105	9.4
May	15	135	18.8
June	11	162	23.1
July	17	198	21.2
August	16	228	13.5
September	15	258	2.2
October	15	288	-9.6
November	14	318	-18.9
December	10	344	-23

Source: Duffie and Beckman (1991).

2.10.3 Solar hour angle

The solar hour angle is the angular displacement of the sun east or west of the local meridian; morning negative and afternoon positive. The solar hour angle is equal to zero at solar noon and varies by 15 degrees per hour from solar noon. For example at 7 a.m. (solar time) the solar hour angle is equal to –75° (7 a.m. is five hours from noon; five times 15 is equal to 75, with a negative sign because it is morning).The solar hour angle ω is expressed as:

$$\omega = 15(S_T - 12) \text{ in degrees.} \qquad (2.4)$$

where S_T = solar time in hours. i. e 1.30 is equivalent to 13.5Hrs

2.10.4 The sunset hour angle

The sun set hour angle on an inclined surface is the solar hour angle corresponding to the time when the sun sets. It is an indication of how long the sun is up during the day. It is given by the following equation (Duffie and Beckman, 1991):

$$\omega_s = cos^{-1}(-tan\emptyset tan\delta) \quad (2.5)$$

where:

ω_s is the sunset angle in degrees

$\emptyset$ is the latitude of the location in degrees

2.10.5 Extraterrestrial radiation and clearness index

Solar radiation outside the earth's atmosphere is called extraterrestrial radiation. Daily extraterrestrial radiation on a horizontal surface, H_0, for latitude in the range of -60 to +60 degrees can also be deduced from (Anna, 2006) as:

$$H_0 = \frac{86400G_{sc}}{\pi}\left(1 + 0.033cos\left(360\frac{n}{365}\right)\right)(cos\emptyset \cos\delta sin\omega_s + \frac{\pi}{180}\omega_s \sin\emptyset \sin\delta) \quad (2.6)$$

where:

$G_{sc}$is the solar constant equal to 1,367 W/m^2

Before reaching the surface of the earth, radiation from the sun is attenuated by the atmosphere and the clouds. The effect expressed in a dimensionless index called the clearness index. If expressed on daily basis it is defined as the daily clearness index. Thus, the monthly average clearness index, $\overline{K_T}$, is defined as the ratio of the monthly average daily radiation on a horizontal surface to the monthly average daily extraterrestrial radiation, written as:

$$\overline{K_T} = \frac{\overline{H}}{\overline{H}_0} \quad (2.7)$$

where:

$\overline{H}$ is the monthly average daily solar radiation on a horizontal surface and

$\overline{H}_0$ is the monthly average extraterrestrial daily solar radiation on a horizontal surface.

2.10.6 Tilted beam and diffused components of radiation

For the purposes of solar process design and performance calculations, it is necessary to know the radiation on the plane of the collector from measurements or estimates of radiation on horizontal surfaces. However, the most commonly available data is that of total hourly or daily radiation on horizontal surfaces, whereas the need is for beam and diffuse radiation on horizontal and tilted surfaces. It is well known that while the isotropic diffuse model is easy to use, it tends to underestimate the monthly average daily or hourly global irradiation on a tilted surface. Models developed by Reindl *et al*. (1990); and Young *et al.*, (2012), modified the Hay and Davies (1980) model and of Klucher (1979) to take into account the circumsolar diffuse and horizontal brightening components on a tilted surface, giving a model referred to as the Hay–Davies–Klucher–Reindl (HDKR) diffuse model. The (HDKR) model estimates total radiation on tilted surface as (Young *et al,* 2012):

$$H_T = (H_b + H_d A_i) R_b + H_d (1 - A_i) \left(\frac{1+Cos\beta}{2}\right) \left[1 + f \sin^3 \frac{\beta}{2}\right] + H \left(\frac{1-Cos\beta}{2}\right)$$

(2.8)

where:

H_b is the total beam radiation on horizontal surface

H_d is the total diffuse radiation on horizontal surface

A_i is an anisotropic index which is a function of the transmittance of the atmosphere for beam radiation expressed as:

$$A_i = \frac{H_b}{H_o}$$

(2.9)

f is the square root of ratio of beam to total radiation expressed as:

$$f = \left(\frac{H_b}{H}\right)^{1/2}$$

(2.10)

The geometric factor $\bar{R}_b$ which is the ratio of the average daily beam radiation on tilted surface to that on horizontal surface is a function of transmittance of the atmosphere, but Duffie and Beckman (1991), suggested that it can be estimated by assuming that it has value which would be obtained if there were no atmosphere. For surfaces that are sloped toward the equator in the northern hemisphere, i.e. surfaces with surface azimuth angle = 0^o, the geometric factor is expressed as (Duffie and Beckman, 2006).

$$\bar{R}_b = \frac{\cos(\emptyset+\beta)\cos\delta\sin{\omega_s}^1+(\frac{\pi}{180}){\omega_s}^1\sin(\emptyset+\beta)\sin\delta}{\cos\emptyset\cos\delta\sin\omega_s+\frac{\pi}{180}\omega_s\sin\emptyset\sin\delta}$$

(2.11)

where: $${\omega_s}^1 = min\begin{pmatrix}\cos^{-1}(-\tan\emptyset\tan\delta)\\ \cos^{-1}(-\tan(\emptyset+\beta)\tan\delta)\end{pmatrix}$$

(2.12)

and "min" means the smaller of the two values in the bracket.

The total radiations, H, are obtained from radiation data, but the distribution of this total radiation term into the diffuse and beam components must be estimated based on the sun angle and the clearness of the sky. Studies of available monthly mean radiation have shown that the average fraction of solar radiation which is diffuse, $\frac{\bar{H}_d}{\bar{H}}$ is a function of clearness index K_T.and sunset angle, ω_s. The Colleares-Pereira and Rabl correlation of the ratio of radiation which is diffuse is expressed as (Duffie and Beckman, 1991):

$$\frac{\bar{H}_d}{\bar{H}} = 0.775 + 0.00606(\omega_s - 90) - [0.505 + 0.0045(\omega_s - 90)]\cos(115K_T - 103)$$

(2.13)

Where the beam component can be calculated as:

$$\overline{H}_b = \overline{H} - \overline{H}_d$$

(2.14)

2.11 Transmittance-Absorptance Product

For solar collector analysis, it is necessary to evaluate the effective transmittance-absorptance product, $(\tau\alpha)$ of the radiation passing through the cover system and striking the absorber plate. For any solar radiation incident on a solar collector, some of the radiation passing through the cover system and striking the absorber plate is reflected back to the cover system, while the remainder is absorbed by the plate. In turn, the reflected radiation from the plate will be partially reflected at the cover surface and back to the plate. The monthly average daily transmittance-absorptance products are determined by finding independently the angular dependence of the transmittance τ and absorptance α and the transmittance-absorptance product obtained as (Rai, 2008):

$$(\overline{\tau\alpha})_{eff} = \frac{\overline{\tau\alpha}}{1-(1-\alpha)\rho_d} \qquad (2.15)$$

The quantity$\rho_d$refers to the reflectance of the cover system for diffuse radiation incident from the bottom side. For cover system which consists of two similar materials, the value of ρ_d is taken as 0.22 (Rai, 2008).

2.12 Monthly Average Absorbed Radiation.

The prediction of solar performance requires information on the solar energy absorbed by the collector absorber plate. The method for the evaluation of long term solar system performance requires that the average radiation absorbed by a collector be evaluated for monthly periods. The solar energy incident on a tilted collector consists of three different components: beam radiation, diffuse radiation, and ground-reflected radiation. The details of the calculation depend on which diffuse-sky model is used. The calculation of the specific hourly, daily or monthly (depending on the time horizon) absorbed radiation for

the south facing surfaces determined according to the (HDKR) model is expressed as (Duffie and Beckman, 1991) :

$$S = (H_b + H_d A_i)(\tau\alpha)_b R_b + H_d R_D + H\rho_g(\tau\alpha)_g \left(\frac{1-cos\beta}{2}\right)$$

(2.16)

where: R_D is given by

$$R_D = (1 - A_i)(\tau\alpha)_d \left(\frac{1+cos\beta}{2}\right)\left[1 + f\, sin^3\left(\frac{\beta}{2}\right)\right]$$

(2.17)

$\overline{H}$ is the monthly average daily radiation on a horizontal surface in MJ/m^2

H_b is the monthly average daily beam radiation on a horizontal surface in MJ/m^2

H_d is the monthly average daily diffused radiation on a horizontal surface in MJ/m^2

R_b is the monthly average ratio of beam radiation on a tilted to horizontal surface

$(\tau\alpha)_b$ is the monthly average transmittance-absorptance product of beam radiation

$(\tau\alpha)_d$ is the monthly average transmittance-absorptance product of diffuse radiation

$(\tau\alpha)_g$ is the monthly average transmittance-absorptance product of ground reflected radiation

β = is the collector slope in degrees

ρ_g = is the diffuse reflectance of ground (0.2) (Duffie and Beckman, 1991).

CHAPTER THREE

MATERIALS AND METHODS

3.1 System Description (Thermosyphon)

The system consists of a flat plate solar collector, tilted from the horizontal, a thermally insulated horizontal storage tank and interconnecting pipes connecting the solar collector and the storage tank. The flat plate collector casing was made of dry wood to minimise heat loss. The flat plate collector has 12 evenly spaced copper pipes called risers embossed by semi-circular grooves formed in the flat plate absorber. The casing was covered at the top with a 4mm thick glass sealed with a rubber gasket. The absorber plate was painted with black fine matte paint to achieve high absorption coefficient. The underside of the absorber insulated with dry wood to reduce conduction losses. The hot water storage tank which was moulded from a mixture of fibre glass and chemical binders is properly lagged with saw dust to minimise heat loss to the surroundings. The hot water storage tank was linked to a source of water from the mains water supply through the cold water inlet as seen in figure 3.1. Control valves to control the inflow of water into the storage tank from the main supply were incorporated along the length of the pipe linking the mains water supply to the storage tank. To prevent draining back of water into the collector when the temperature in the collector is lower than that in the tank, especially in the night when there is no solar radiation, another control valve was installed between the pipe connecting the collector hot water outlet and storage tank hot water inlet. The hot water to meet the domestic load is collected through the hot water outlet.

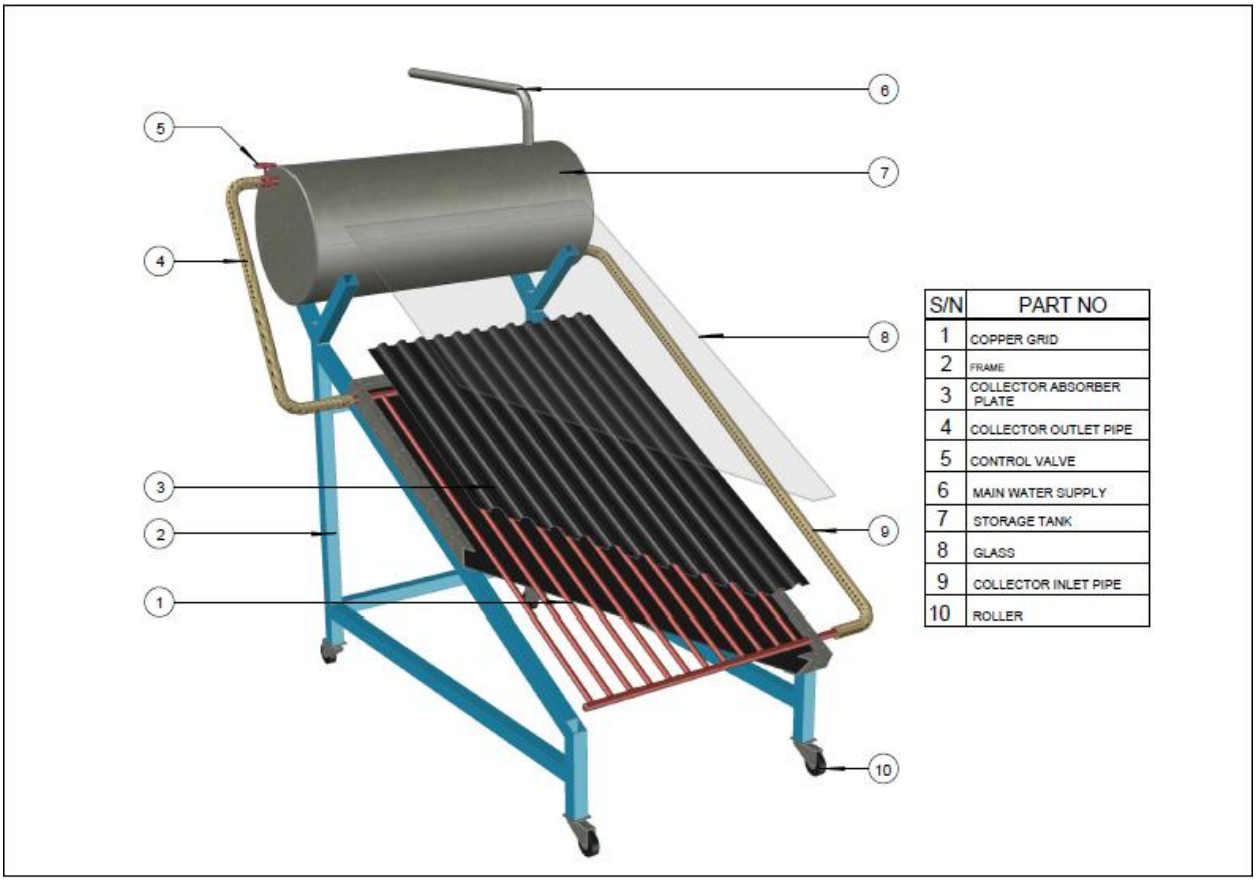

S/N	PART NO
1	COPPER GRID
2	FRAME
3	COLLECTOR ABSORBER PLATE
4	COLLECTOR OUTLET PIPE
5	CONTROL VALVE
6	MAIN WATER SUPPLY
7	STORAGE TANK
8	GLASS
9	COLLECTOR INLET PIPE
10	ROLLER

Figure 3.1: Exploded view of the thermosyphon water heating system.

3.2 Working Principle.

Solar radiation from the atmosphere falling on the collector heats the absorber surface within the solar collector or the actual storage tank. A heat-transfer fluid (water) flowing through the tubes attached to the absorber plate picks up the heat from it and moves to the top of the storage tank, and a denser water flows by gravity from the bottom of the storage tank to the collector to again pick the heat falling on the collector from the sun. As hot water leaves the top of the collector and enters the storage tank from a certain point at the top, it mixes with water at this level if the temperature difference is within 0.5^{o}C. If its temperature is lower than that at the top by more than 0.5^{o}C it flows down and mixes with the water of a segment where the temperature difference is within 0.5^{o}C. In the case when the temperature of water entering the storage tank is higher than that at the top of the

storage tank by more than 0.5^{o}C, a new segment is created at the top, increasing the number of segments by one. When hot water is drawn to the load, the same case applies for cold water from the mains entering the tank from the bottom, this water mixes with that at the bottom if the temperatures are within 0.5^{o}C of each other, otherwise a new segment is created (Soteris and Christos, 2000).The process is self-controlled because it continues until there is no radiation from the sun. The heated water is reheated by other forms of conventional heaters when the solar system fails to meet up the water temperature requirement.

3.3 Materials Selection

3.3.1 Flat plate collector

The flat plate solar collector is selected because it is relatively simple. Its characteristics are known. It is the easiest and least expensive to fabricate, install, and maintain. Moreover, it is capable of using both the diffuse and the direct or beam solar radiation. For residential and commercial use, flat plate collectors can produce heat at sufficiently high temperatures to heat domestic hot water, in buildings; they also can operate a cooling unit, particularly if the incident sunlight is increased by the use of a reflector. Flat plate collectors easily attain temperatures of 40 to 80ºC (Rhushi *et al*., 2011).

3.3.1.1Glazing material

Glass is selected as material for glazing. This is because glass is capable of transmitting solar energy. From the standpoint of the utilisation of solar energy, the important desirable characteristics of a glazing material are low reflectance, *(ρ*), low absorptance, *(α*), and high transmittance, *(τ).* For a glass, reflectance and absorptance is very low and the transmissivityis high. The choice of glass for the glazing is to admit as much solar radiation as possible and to reduce the upward loss of heat to the lowest attainable value. Glass has been the principal material used to glaze solar collectors because it has the

highly desirable property of transmitting as much as 90% of the incoming short-wave radiation (solar), while virtually none of the long wave radiation emitted by the flat plate can escape outward by transmission (Rhushi *et al*., 2010).

The effect of dirt and dust on collector glazing is surprisingly small, and the cleansing effect of occasional rain seems to be adequate to maintain the transmittance within 2 - 4% of its maximum value (Rhushi *et al*., 2011).

3.3.1.2 Absorber plates and tubes.

The primary function of the absorber plate and tubes in the collector is to absorb as much as possible the radiation reaching their surfaces through the glazing, to lose as little heat as possible upward to the atmosphere and downward through the back of the container, and to transfer the retained heat to the circulating fluid. Aluminum sheet was selected as the absorber plate for this design because it has the properties mentioned above. Its durability, ease of handling, its availability and relatively low cost are other major factors considered in its selection. Copper tube was selected and preferred over any other metal for water passages because of its high conductivity and compatibility with water. Absorber plates are usually given a surface coating (black is commonly paint was used) that increases the fraction of available solar radiation absorbed by the plate (absorptance α). The matte black paints, for which α = 0.92 to 0.98was selected (Duffie and Beckman, 1991).

3.3.1.3 Thermal insulators

Fiber glass-wool and hard foam material were selected for the thermal insulation of the flat plate, storage tank and connecting pipes. These insulation materials are known to be dimensionally and chemically stable at high temperatures, and resistant to weathering and dampness from condensation (Rhushi *et al*., 2011).

3.3.1.4 Collector casing

Dry wood was selected for the construction of the hot water collector casing, this is because dry wood is a very poor conductor of heat. Its relatively low cost and availability are other major factors in its selection.

3.3.2 Storage tank.

Fibre glass and resin chemical binder were selected for the moulding of the hot water storage tank. This is because of its low conductivity, corrosion resistance and compatibility with water.

3.4 System Design Assumptions

In the design analysis of the system, the following assumptions were made:

i. The collector operates in steady state.
ii. Temperature gradient through the cover thickness is negligible.
iii. There is one-dimensional heat flow through the back and side insulation and through the
cover system.
iv. The temperature gradient around and through the tubes is negligible.
v. The temperature gradient through the absorber plate is negligible.
vi. The radiation model employed to calculate heat transfer in the system assumes that the radiation remains constant through the hours and days.
vii. Fluid flow distribution is one dimensional.
viii Temperature distributions in the collector tubes and the storage tank are linear.
ix Flow inside the tubes is laminar and uniformly distributed.

3.5 Design Considerations

A solar domestic hot water system would be designed based on the following considerations:

i. A design month which would be determined from the mean daily heat load (W) and the mean daily solar irradiance (W/m^2) from the months of the year;

ii. The amount of water ($0.1\ m^3$) required, to determine the system load;

iii. The range of operating temperatures between 0^oC and 100^oC for the selection of material; and

iv. The cost of materials.

3.6 Design Theories

3.6.1 Solar resources and weather data.

Solar radiation and meteorological data which are very important driving functions for all solar system design often seem to be highly random and irregular. However, long-term statistical analysis indicates that these variables are predictable to some degree of accuracy. Therefore, the dynamic nature of solar data can be smoothed out by formulating a representative data which can characterise the mean-value behavior of any location over a long period (Qin, 1998). Based on this method, Typical Meteorological Year (TMY) weather data for the location (Zaria) latitude 11.2^o N and longitude 7.8^oE obtained from www.weatheranalytic.comwas used as input functions to design and simulate the annual performance of the thermosyphon solar water heater system. Typical Meteorological Year (TMY) weather data is defined as a year which sums up all the climatic information characterising a period as long as the mean life of the system.

3.6.2 Flat-Plate Collector

The header-riser flat-plate collector consists of two horizontal headers and a series of parallel, vertical risers as shown in Figure 3.2

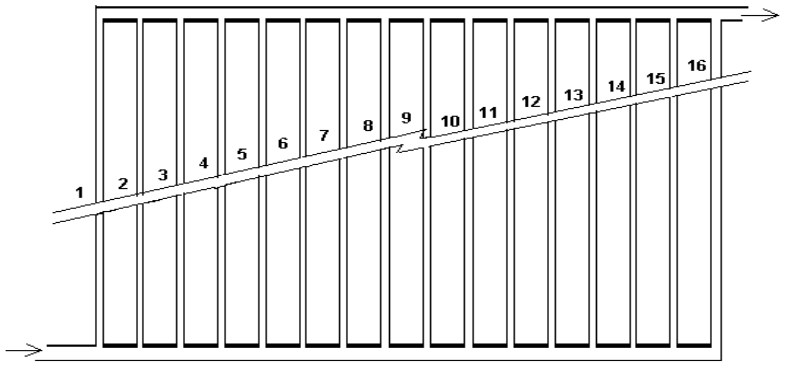

Figure 3.2: Conventional header/riser flat-plate collectors (Fallziah and Balbir, 2003).

In a steady state, the performance and characterization of a flat-plate solar collector can be described by the system mathematical models and energy balance equations as follows:

3.6.2.1 Collector heat removal factor

The collector heat removal factor, F_R, is the ratio of actual useful energy gain of a collector to the useful gain if the whole collector surface were at the fluid inlet temperature.$F_R$is analogous to the heat exchanger effectiveness.For a header-riser flat-plate collector, the collector heat removal factor can be expressed as (Duffie and Beckman, 1991):

$$F_R = \frac{\dot{m}C_p}{A_c U_L}\left[1 - exp\left(-\frac{A_c U_L F'}{\dot{m}C_p}\right)\right]$$

(3.1)

where:

F_R is the heat removal factor

$\dot{m}$ is the collector fluid mass flow rate (kg/hr.m^2)

C_p is the fluid specific heat (kJ/kg K)

$A_c$is the collector area *(m^2)*

$U_L$is the overall collector loss coefficient (kJ/ m^{2}hr.K)

where *F'* is the collector efficiency factor expressed as (Duffie and Beckman, 1991)..

$$F' = \frac{1/U_L}{W\left[\frac{1}{U_L[D_i+(W-D_i)F]}+\frac{1}{C_b}+\frac{1}{\pi D_i h_{fi}}\right]}$$

(3.2)

where

W represents tube spacing, (m)

Cb is the contact resistance, (W/m. K) and $\frac{1}{C_b} = 0$

C_p Specificheat of the material,(kJ/kg K)

h_{fi} is the internal fluid heat transfer coefficient, (W/m^2.K)

F is the standard fin efficiency for straight fins with rectangular profile, given as (Duffie and Beckman, 1991).

$$F = \frac{tanh\left[\frac{m(W-D_i)}{2}\right]}{\frac{m(W-D_i)}{2}}$$

(3.3)

where :

$$m = \sqrt{\frac{U_L}{K\delta}}$$

(3.4)

$k\delta$ is the plate thermal conductivity and thickness product.

D_i is the internal diameter of tube.

3.6.2.2 Collector top loss

An approximate relation for collector top loss coefficient (U_{top}) is given by (Duffie and Beckman, 1991):

$$U_{top} = \frac{1}{\frac{N_G}{\frac{C}{T_{pm}}\left[\frac{T_{pm}-T_a}{N_G+f}\right]^e+\frac{1}{h_w}}} + \frac{[\sigma({T_{pm}}^2+{T_a}^2)][T_a+T_{pm}]}{\frac{1}{\varepsilon_p+0.00591N_G h_w}+\frac{2N_G+f-1+0.133\varepsilon_p}{\varepsilon_g}-N_G}$$

(3.5)

where:

$$f = \left(1 + 0.089h_w - 0.1166h_w\varepsilon_p\right)(1 + 0.07866N_G)$$

(3.6)

$$C = 520[1 - 0.000051\beta^2]$$

(3.7)

$$e = 0.430\left(1 - \frac{100}{T_{pm}}\right)$$

(3.8)

N_G is the number of glass covers

β is the collector tilt (degrees)

ε_g is the emittance of glass (0.88) (Duffie and Beckman, 1991).

ε_P is the emittance of plate.

Ta is the ambient temperature (K)

T_{pm} is the mean plate temperature (K)

h_w is the sorrounding heat transfer coefficient (W/m^2.K)

3.6.2.3 Collector back loss (U_b)

The energy loss through the bottom of the collector is made up of conductive loss due to heat flow through the insulation and convection and radiation resistance to the environment. The magnitude of the conduction loss compared to the radiation loss is such that the radiation is negligible (Duffie and Beckman, 1991).Thus the back loss coefficient is estimated as (Duffie and Beckman, 1991).

$$U_b = \frac{K_{bi}}{x_{bi}} \quad (3.9)$$

where:

$K_{bi}$is the thermal conductivity of material

x_{bi} is the thickness of material.

3.6.2.4 Collector edge loss (U_e)

The edge loss coefficient is the ratio of the thermal conductivity of the insulation at edge to its thickness; times the ratio of the area of edge to the collector effective aperture area. Rai (2008) recommended edge insulation of about the same thickness as the bottom insulation. The edge loss estimated by assuming one-dimensional sideway heat flow around the perimeter of the collector system is expressed as:

$$U_e = \frac{K_{ei}}{x_{ei}} \frac{A_e}{A_C} \quad (3.10)$$

where:

K_{ei} is the thermal conductivity of edge insulation materials.,

A_c is the collector area.

A_e is the edge insulation area.

x_{ei} is the insulation thickness at the edge

3.6.2.5 Collector overall heat loss coefficient

The overall heat loss coefficient for a flat plate collector is composed of the top loss coefficient, the edge loss coefficient and the back loss coefficient. A relation for collector overall heat loss coefficient, $U_{L,}$ is expressed as (Duffie and Beckman, 1991):

$$U_L = U_t + U_e + U_b \quad (3.11)$$

3.6.2.6 Collector useful energy

In steady state, the performance of a flat-plate solar collector can be described by the useful gain from the collector, Q_u, which is defined as the difference between the absorbed solar radiation and the thermal loss. Duffie and Beckman, (1991) expressed the useful energy gain of a solar collector for glazed or evacuated collectors as:

$$Q_u = A_C\left[S - U_L\left(T_{pm} - T_a\right)\right]^+ \quad (3.12)$$

$$Q_u = F_R[S - U_L(T_i - T_a)]^+$$

(3.13)

The + superscript indicates that only positive values of the terms in the square brackets are to be used. Thus, to produce useful gain greater than zero the absorbed radiation must be greater than the thermal losses.

where:

Q_u is the useful energy gain per unit time,

F_R is the collector heat removal factor,

U_L is the overall loss coefficient of the collector.

A_c (m^2) is the collector area,

S is the absorbed solar radiation.

T_i ,T_a are the collector fluid inlet and ambient temperatures, respectively.

The collector useful energy can also be defined as the quantity of energy absorbed by a fluid moving in the tubes of a solar collector to rise the fluid temperature from the fluid inlet temperature,T_i, to fluid outlet temperature, T_o. It is expressed as:

$$Q_u = \dot{m}C_p(T_o - T_i)$$

(3.14)

Equating equation (3.12a) and (3.13) and solving for the collector area gives:

$$A_C = \frac{\dot{m}C_p(T_o - T_i)}{[S - U_L(T_{pm} - T_a)]^+}$$

(3.15)

3.6.2.7 Convective heat transfer coefficient in collector tubes

Reynolds, Prandtl and Nusselt numbers are normally used to compute convective heat transfer coefficients. The values of the parameters defining these numbers are also known

to be dependent on temperature. For the evaluation of convective heat transfer coefficients by simulation a large database of physical properties of these parameters is needed. The exact temperature at which a certain evaluation is to be carried out will not be possible. One quick and simple solution is to build temperature dependent models. The nature of flow is determined by using a reliable indicator, known as the Reynolds number, where if the Reynolds number is less or equal to 2200 the flow is considered laminar and if Reynolds number is greater than 2200 flow is considered turbulent (Fallziah and Balbir, 2003). The indicator is also useful especially in evaluating the Nusselt number, which is used in the computation of the convective heat transfer coefficient. The general correlation for obtaining the convective heat transfer coefficient in tubes is expressed as (Jaime, 2009):

$$h_f = \frac{K_f Nu_D}{D_i} \tag{3.16}$$

where:

h_f is the convective heat transfer coefficient in tubes

K_f is the thermal conductivity of the fluid in the tube

Nu_D is the nusselt number

D_i is the internal diameter of the tube

However, the Nusset number is a function of the Reynolds number, which is an indicator of the nature of flow which can be calculated for laminar flow as the case in thermosyphon system.

For the evaluation of the Nusselt number, Nu_D, for a turbulent flow where Reynold number is greater than 2200 , Fallziah and Balbir, (2003),correlated the Nusset number as:

$$Nu_D = \frac{(fn/8)RePr}{K_1 + K_2(fn/8)^{1/2}\left(Pr^{2/3} - 1\right)} \tag{3.17}$$

where:

$$K_1 = 1 + 1.3fn \tag{3.18}$$

$$K_2 = 11.7 + \frac{1.8}{P_r{}^{1/3}} \tag{3.19}$$

$$fn = [1.82\log(Re) - 1.64]^{-2} \tag{3.20}$$

For Re <2200 flow is considered laminar and Fallziah and Balbir, (2003).correlated the Nusset number as:

$$Nu_D = 3.7 + \left[\frac{0.0534\left(\frac{RePrD_i}{L}\right)^{1.15}}{1+0.0335\left(\frac{RePrD_i}{L}\right)^{0.82}}\right] \tag{3.21}$$

where:

Re is the Reynolds number expressed by Incropera, *et al*.(2007) as:

$$Re = \frac{4\dot{m}}{\pi D_i \mu} \tag{3.22}$$

P_r is the Prandtl number expressed by Duffie and Beckman (1991) as:

$$Pr = \frac{C_p \mu}{K_f} \tag{3.23}$$

where:

Nu_D is the Nusselt number

D_i is the inner tube diameter

$\dot{m}$ is the fluid flow rate

μ is the dynamic viscosity,

Cp, is the specific heat capacity of the fluid

K_f is the thermal conductivity of the fluid

L is the tube length

3.6.2.8 Thermo-physical properties of water.

The following expressions estimate the thermo-physical parameters of water as a function of temperature (Koffi *et al*., 2008).

Density of water:

$$\rho = 1001 - 0.08832T - 0.003417T^2$$

(3.24)

Specific heat:

$$C_p = 4226 - 3.244T + 0.0575T^2 + 0.0002656T^3$$

(3.25)

Kinematic viscosity:

$$\upsilon = \left(\frac{1}{0.5155+0.0192T} - 0.12\right) X10^{-6}$$

(3.26)

Thermal conductivity:

$$K_f = 0.557 + 0.002198T - 0.00000708T^2$$

(3.27)

Thermal cubic expansion coefficient:

$$\beta' = (0.3 + 0.116T - 0.0004T^2)X10^{-4}$$

(3.28)

Dynamic viscosity

$$\mu = \upsilon\rho$$

(3.29)

Prandtl number

$$P_r = 39.5345T^{-0.144} - 18.8396$$

(3.30)

3.6.3 System load calculations.

3.6.3.1 Sensible heat requirement

The sensible heat requirement is the energy needed to raise the temperature of water to the desired temperature. If water flowing at the rate of $\dot{m}_L$ is to be heated from a mains supplied temperature T_i to a desired temperature T_L, the energy requirement over a specified time horizon may be expressed as follows (Koffi *et al*., 2008).

$$Q_s = \dot{m}_L C_p (T_L - T_i) \quad (3.31)$$

where:

Q_s is the rate of quantity of heat required to meet the load

T_L is the desired load (hot water) temperature, ^{o}C

$\dot{m}_L$ is the desired load mass flow rate, kg/s

3.6.3.2 Pipe/Ducts losses

These can be estimated by conventional methods. For any well-designed system the losses from ducts should be small and can be approximated to an adequate degree of accuracy in terms of the inlet and outlet temperatures as (Duffie and Beckman, 1991):

$$Q_p = U_i A_i (T_i - T_a) + U_o A_o (T_o - T_a) \quad (3.32)$$

where:

U_i is the loss coefficient of collector inlet pipe plus insulation

U_o is the loss coefficient of collector outlet pipe plus insulation

A_i is the surface area of the collector inlet pipe

A_o is the surface area of the collector outlet pipe

3.6.3.3 Storage tank losses

Losses from the storage tank may be significant. The rate of tank losses is estimated from the tank loss coefficient-area product $(UA)_{st}$ and the ambient temperature,T_a, surrounding the tank, calculated as (Govind, 2006):

$$\dot{Q}_{StL} = U_{st}A_{st}(T_{st} - T_a) \tag{3.33}$$

where

$U_{st}$is the tank loss coefficient

$A_{st}$is the tank surface area

$T_{st}$is the storage temperature

For a cylindrical tank, the surface area of the tank is related to the storage volume of the tank by the following equation (Kulkarni, *et al*., 2006).

$$A_{st} = 1.845\left(2 + \frac{h}{d}\right)V_{st}^{\frac{2}{3}} \tag{3.34}$$

where:

V_{st} is the volume of the cylindrical tank

h is the height of the cylindrical tank

d is the diameter of the cylindrical tank

3.6.4 System performance evaluation

3.6.4.1 Collector mean fluid and absorber plate temperature

To evaluate the collector performance, it is necessary to know the fluid properties and heat transfer coefficient which can be obtained at a mean fluid temperature expressed by (Klein *et al,*1974; Duffie and Beckman, 1991) as:

$$T_{fm} = T_{ci} + \frac{Q_{u/A_c}}{F_R U_L}(1 - F'') \tag{3.35}$$

where

T_{ci} is the collector inlet fluid temperature

T_{fm} is the collector mean fluid temperature

F'' is the collector flow factor

$F''$is the collector flow factor, which is defined as the ratio of the heat removal factor,F_R, to the collector efficiency factorF'expressed as (Duffie and Beckman, 1991).

$$F'' = \frac{F_R}{F'} = \frac{\dot{m}C_p}{A_c U_L F'}\left[1 - exp\left(-\frac{A_c U_L F'}{\dot{m}C_p}\right)\right] \quad (3.36)$$

The mean absorber plate temperature is always greater than the mean fluid temperature due to the heat transfer resistance between the absorbing surface and the fluid. This temperature difference is usually small for liquid systems, but may be significant for air systems (Duffie and Beckman, 1991). The mean plate temperature is evaluated in an iterative manner using the equation

$$T_{pm} = T_{ci} + \frac{Q_{u/A_c}}{F_R U_L}(1 - F_R) \text{ (Duffie and Beckman, 1991).} \quad (3.37)$$

A reasonable guess for T_{Pm} for liquid heating collector operated at typical flow rates of 0.01 to 0.02kg/m^{2}s is giving by (Duffie and Beckman, 2006):

$$T_{pm} = T_{ci} + 10\ (C^o) \quad (3.38)$$

3.6.4.2 Collector outlet temperature in the flow direction

On the basis of Pierson and Javelas (1983) and Duffie and Beckman (1991) analysis, the collector hourly outlet hot fluid temperature,T_{co}, is determined by the absorber thermal equilibrium equation given by:

$$T_{co} = T_{ci} + \left[T_a - T_{ci} + \frac{I_T(\tau\alpha)}{U_L}\right]\left[1 - exp\left(-\frac{U_L A_c}{\dot{m}C_p}\right)\right] \quad (3.39)$$

where:

T_{co} is the collector outlet temperature

T_{ci} is the collector inlet temperature

I_T is the hourly solar radiation on tilted surface.

Temperature at the inlet of the storage tank could be predicted from the expression (Koffi *et al,*. 2008):

$$T_{sti} = T_{co} + \left(T_{fco} - T_a\right)\left[1 - exp\left(-\frac{U_o \pi d_o L_o}{\dot{m} C_p}\right)\right] \quad (3.40)$$

By neglecting the thermal wall resistance, the heat exchange coefficient between the connecting pipes and the ambient conditions can be determined by the equation (Qin, 1997):

$$U_o = \frac{1}{\frac{1}{2\pi k_{ins}} Ln\left(1+\frac{2t_{ins}}{d_o}\right)+\frac{1}{\pi(d_o+2t_{ins})h_w}} \quad (3.41)$$

where:

U_o is the Loss coefficient of collector outlet pipe plus insulation

T_{sti} is the storage tank inlet temperature

L_o is the length of the pipe from the collector outlet to the tank inlet

d_o is the outer diameter of collector outlet pipe

t_{ins} is the thickness of insulation material

T_{ci} is the fluid inlet temperature

$C_p$is the fluid specific heat capacity

$\dot{m}$ is the mass flow rate of fluid in the collector

k_{ins} is the thermal conductivity of insulation material

h_w is the natural convection heat coefficient from the insulation surface to surrounding.

3.6.4.3 Storage tank temperature

Assuming solar radiation intensity on tilted surface, ambient temperature, and load demand to be constant over the specified time step. Solution of the energy balance equation of the

solar water heating system of Figure 3.1 can be obtained using simple Euler's integration, to solve for the tank storage temperature T_{St}^{+} as (Duffie and Beckman, 1991) :

$$T_{St}^{+} = T_{st} + \frac{\Delta t}{(\rho V_{st} C_p)_s}\left[\dot{Q}_u - \dot{Q}_{Ls} - U_{st}A_{st}(T_{st} - T_a)\right] \quad (3.42)$$

T_{St}^{+} is the storage tank temperature after an additional time interval of one hour from the previous time and Δt is the time horizon which may be a day, a month or a year depending on the period of interest. For satisfying the entire thermal demand, (solar fraction S.F=1) storage tank temperature during the time of the demand must be greater than the desired load temperature.

$$T_{st} \geq T_L \quad (3.43)$$

When the storage tank temperature is less than the load temperature ($T_{st} < T_L$), the desired load temperature requirement can be met by an auxiliary heater. The duty of auxiliary heater is given by the following formula (Govind *et al*,. 2006).

$$Q_{aux} = (m_L)C_p[T_L - T_{st}] \quad (3.44)$$

where

Q_{aux} is the auxiliary energy requirement to meet the desired load

C_p is the specific heat of fluid.

T_{st} is the storage tank temperature

m_L is the desired load mass flow rate, kg/s

When water is used as the working fluid, the system cannot be designed for two-phase condition. The storage tank temperature, therefore, has to be always less than the boiling temperature of the working fluid.

$$T_{st} \leq T_{sat} < 100 \quad (3.45)$$

3.6.4.4 System solar fraction

Solar fraction, is the fraction of the total hot water energy that is supplied by solar system, it is calculated using the equation from Buckles and Klein (1980),

$$SF = \frac{Q_s - Q_{Aux}}{Q_s} \quad (3.46)$$

where:

$Q_s$is the total energy required to meet the required load

Q_{Aux} is the total auxiliary energy required to be supplied to the system to support the portion of the total load that is not provided by the solar energy.

The solar fraction is a better indicator of the system performance compared to the other parameters such as collector efficiency or heat removal factor, since it manifests the overall performance of the entire system not a component.

3.6.4.4 Collector efficiency

The Hottel-Whillier equation defines the efficiency for a solar collector in terms of the collector heat removal factor F_R, given in equation form as (Govind *et al*., 2008):

$$\eta_C = \frac{Q_u}{H_T A_c} = \frac{F_R[S - U_L(T_i - T_a)]^+}{H_T} \quad (3.47)$$

The + superscript indicates that only positive values of the terms in the square brackets are to be used.

3.7 System Design Approach and Calculations

Satisfactory performance and reliability of a solar water heating system requires adequate sizing of its components as well as accurate prediction of the system performance (i.e delivered useful energy and outlet water temperature, solar fraction, and thermal efficiency, etc). Therefore, proper sizing of system components and the determination of system characteristics through calculation of system design parameters is very important to

achieving satisfactory performance. To calculate these design parameters and evaluate the sensitivity and effect of some design parameters on the performance of thermosyphon solar water heating (TSWH) system, the following design method was adopted:

3.7.1 Determination of the design month

The design month is defined as the month with the least value of the energy ratio, E_R. The energy ratio, E_R, is the ratio of monthly average daily solar radiations on the collector surface to the monthly average daily solar system load expressed as:

$$E_R = \frac{H_T}{Q_s} \tag{3.48}$$

where:

H_T is the monthly average daily solar radiation on the tilted collector surface(kJ/m^{2}day)

Q_s is the monthly average daily load. (kJ/day).

The demand on the system for the design month is usually the highest and therefore the calculation of system design parameters and subsequent components sizing was done based on the design month average daily solar radiation and weather data of Zaria. To determine the design month, the monthly average daily weather data and solar radiations on the surface of the collector for all months obtained from the weather data processor (type 109 component) of TRNSYS 16 software was used as input into programme codes (appendix A) written in MATLAB to calculate the energy ratio, E_R, (equation 3.48). The month with the least energy ratio, E_R, is considered the design month. The results obtained were tabulated and shown in Tables 4.1 and 4.2.

3.7.2 Determination of design parameters.

System design parameters and characteristics were calculated from the programme codes developed in MATLAB programming language (appendix A) from equations (3.1) to (3.47). The monthly average daily solar radiation and weather data of Zaria, obtained from

the weather data processor of TRNSYS 16 were used as inputs for the calculations. The system calculated parameters are presented in Tables 4.1, 4.2 and 4.3.

3.7.3 Design parameters optimisation.

The system design parameters optimisation procedure was done in two parts. The first was performed to study the effect and sensitivity of the flat plate collector design parameters on the heat removal factor, F_R, in order to determine the proper system characteristics that will give satisfactory performance. Solar radiation, meteorological data and monthly average daily system characteristics for the design month were used as input data into the programme codes written in MATLAB programming language (Appendix B to Appendix E). These programme codes (Appendix B to Appendix E) were used to study the effects of varying some selected system characteristics (ie cupper tube diameter, number of glass covers, absorber plate thickness, and centre to centre tube distance) on the chosen design objective function (ie collector heat removal factorF_R) . The results of these studies are presented in Figure 4.1 to 4.7

The second part of the optimisation was conducted using TRNSYS 16 software to simulate and predict the system performance (load temperature) using different system component sizes. The software used has the graphical ability to visualise the effect of varying the components sizes on the objective function (load temperature). The set of components sizes and system design parameters which meet system design load (load temperature) after simulation were chosen as the final adopted system component size as presented in Table 4.4.

3.7.4 System performance simulation

The performance of the system was numerically simulated using TRNSYS 16 software based on Typical Meteorological Year (TMY) weather data for the location (Zaria) with

the system characteristics as indicated in Table 4.4. The system schematic model used for simulation s as shown in figure3.3.Theresults of the simulation is shown in Figure 4.8 to Figure 4.19.

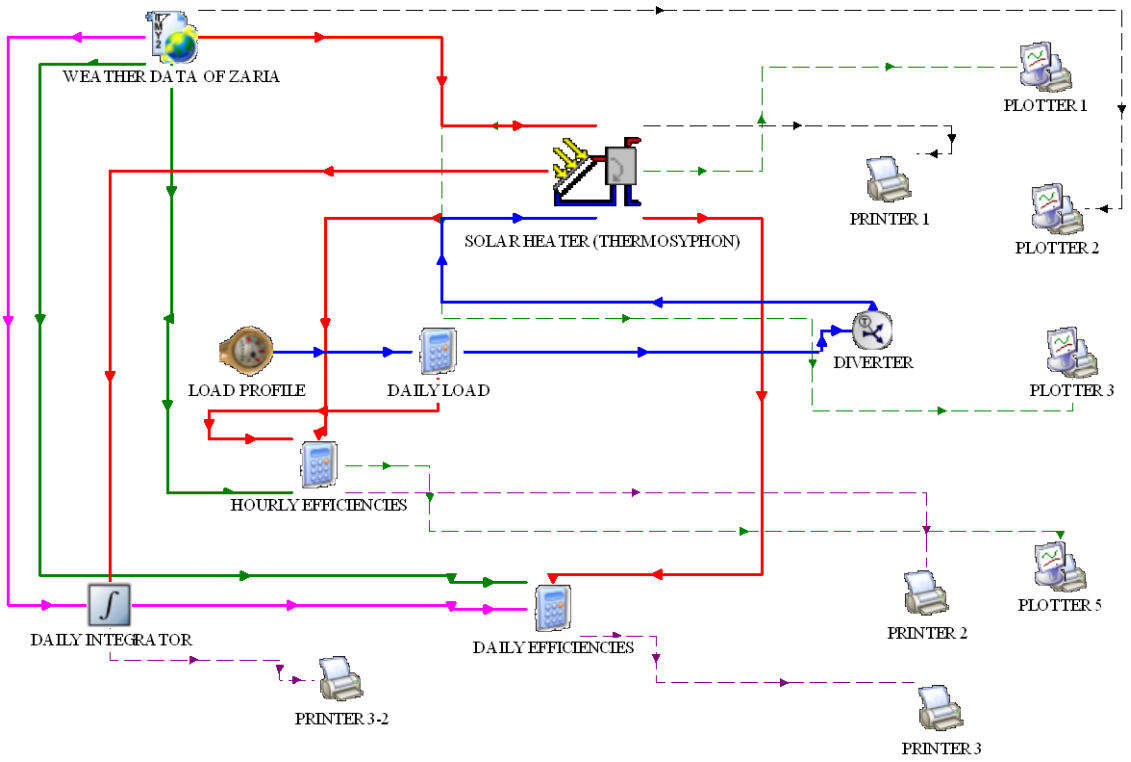

Figure3.3: Schematic representation of system model in TRNSYS 16 simulation studio. (Beckman *et al.*, 2004)

Figure 3.4 shows the flow chart for the simulation of the performance of the thermosyphon water heating system in a TRNSYS software simulation studio,

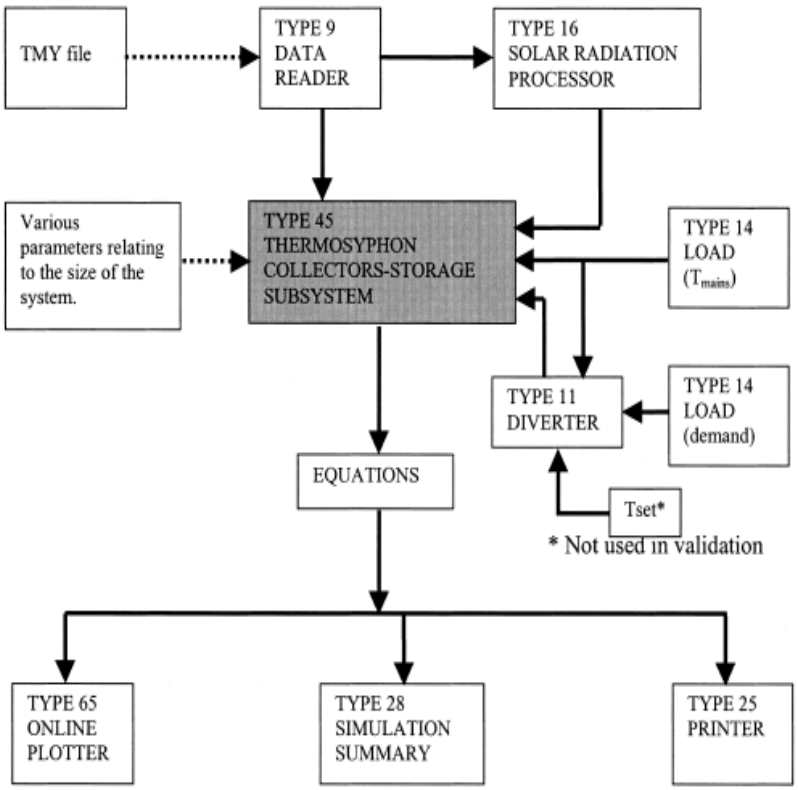

Figure.3.4: Information flow diagram for the simulation of the thermosyphon solar water heating
system. (Soteris and Christos 2000)

3.8 Construction of the System.

The system was constructed in Mechanical Engineering Department workshop of Ahmadu Bello University (A.B.U) Zaria based on the optimum system dimensions of Table 4.4. Details of the construction steps are shown in Table 3.1

3.8.1 Construction of the flat plate solar collector

The construction and assembling of the flat plate solar collector is carried in the following sequence:

- The copper pipe grid was built from 15mm diameter copper pipe with the traditional top and bottom headers with vertical riser tubes spaced 10mm across the width of the collector base.

- The absorber was made from aluminum strips with grooves that snuggly fit over the copper pipes.
- The absorber plate (fin) was fitted into copper pipe grid frame by screws and staplers.
- The copper grid casing where the grid was installed was then constructed from aluminum square pipes insulated with wood and fiber glass.
- The glass glazing was installed on the top of the grid casing.

The details of the construction process is shown in Tables 3.1 to 3.3

Table 3.1 show the construction process, the materials and the equipment used for the construction of the flat plate solar collector.

Table 3.1: Construction of the flat plate solar collector

Component	**Materials**	**Construction Process**	**Equipment used**
Copper Pipe Grid	Two rolls of 15mm diameter copper pipe (15m long each), 20 pieces of copper T-joint fittings and 4 pieces of copper elbow-joint fittings	A 1600mm x1200mm copper grid was made from the copper pipes which were fitted into each other to form the grid by means of copper T and elbow joints. The vertical riser tubes of the grid were spaced 10mm from each across the width of the collector base. The first riser gets a T-fitting (this will be where water flows into the collector), and the last riser gets an elbow fitting. On the other end of the collector, the elbow was fitted on the first riser, and the T-joint was fitted on the last riser (where water will exit the collector). See plate 1 in appendix F. **Copper Grid Leak- Test:** The grid was supported up in a vertical position with the outlet end at the lower end blocked. Water was poured into the high end until the grid was completely full. The water was allowed for	Hack saw, Pair of pliers, Soldering flux, Iron brush, Measuring tap

		a good while to settle and then checked all the joints for leaks.	
Absorber Board	1600mm x1400mm x 5.5mm,Aluminum sheet, 1600mm x 1400mm x 30mm plywood, 1600 x 1200mm formed copper pipes grid. Black paint, Silicon bead.	30mm thick plywood was cut to the size of 1600mm x 1400mm (equal to the collector area A_c**).** This plywood was used to lay out the copper grid. The plywood formed the base to tightly secure the aluminum sheet (absorber plate) over the copper pipes grid. But before the copper grid was placed over the plywood, a 5mm thick aluminum sheet was first placed under the copper tube. The idea of adding the flat strip under the copper pipe was to provide an additional heat transfer path from the aluminum fin into the bottom of the copper pipe grid. Grooves to snugly fit over copper pipe grid for proper transfer of heat were created on the aluminum sheet. For the sheet to be tightly secured to the plywood, silicon bead was added to grooves on the fin to fill any tiny gap remaining between the fin and the copper. The fin was Stapled firmly to the plywood on both sides of the copper pipes. The heat absorber board was painted black with high temperature barbeque paint**.** See plate 3.	Cutting saw, hammer, screw driver, paint sprayer, measuring tape, Iron set square.
Collector casing	30mm x 150mm polished wood, 4mm thick white glass, wood spray fiber wool.	Two pieces of 30mm x150mm wood of length 1600mm and two pieces 30mm x150mm wood of length 1400mm were cut and joined to produce the rectangular frame for the casing of the absorber board. The woods were polished and painted to avoid absorption of moisture to prevent change in dimension. After the frame was constructed, it is covered at the bottom by plywood of 10mm thick. A 30mm thick layer of	Cutting saw, paint sprayer, hammer, nails and screws,

		saw dust is immediately laid on the frame and the absorber board was installed on this insulating material. Finally, two rectangular glasses 1595mmx1395mm of 4mm thick were used to cover the collector casing at the top at a distance of 30mm from each other to form the glazing of the flat plate solar collector. See plates 2 , 3 and 4.	

3.8.2 Construction of the storage tank

Table 3.2 show the construction process, the materials and the equipment used for the construction of the storage tank

Table 3.2: Construction of the storage tank

Component	**Materials**	**Construction Process**	**Equipment used**
Storage Tank	Fiber glass, chemicals, casting mould	First, a casting mould needed to produce the water storage tank was produce by cutting a 6mm thick iron sheet to the required dimensions (1319mm x 900mm) and then rolled on a roller to produce a cylindrical mould of 100 liters. Chemical pastes formed from fiber glass mixed with the moulding chemicals were poured into the casting mould to produce a cylindrical tank of length 0.9m and radius 0.21m (100L capacity). The produced tank has thermocouples installed at the tank water inlet and outlet to record the tank water inlet and outlet temperatures. The tank was insulated with several layers of fiber wool. Plumbing operation was carried out on the storage tank to create the tank water inlets and outlets. The connection of the tank to the	Iron mould, sand paper, plumbing bar, and glues.

		flat plate collector and other parts of the system was made by plastic pipes connected by means of different types of plumbing joints. See plates 5,6, 7and 8 for details.	

Table 3.3 show the construction process, the materials and the equipment used for the construction of the Supporting Frame.

3.8.3 Construction of the Supporting Frame

Table 3.3: Construction of the Supporting frame

Component	Materials	Construction Process	Equipment used
Supporting frame	Mild steel, rectangular pipe (20mmx40 mm) of 4mm thickness	A rectangular mild steel pipe was cut into various pieces representing the dimensions of the frame as shown in the working drawing number 2using hack saw and measuring tape and welded by means of electric arc to produce the main frame used for supporting the storage tank and solar collector. See plate 9. The various components were then assembled to form the complete system. See plates 10, 11 and 12.	Hawksaw, Electric arc welder, measuring tape

3.9 System Cost Estimation

Table 3.4 shows the estimated cost for the production of different components of the thermosyphon water heating system broken down into parts A, B and C.

Table 3.4: System cost estimation for the production of the thermosyphon water heating system

as at 20 July, 2014

PartA: Storage Tank (Volume: 0.15m^3)

S/N	Item	Qty	Unit Price	Total Price
1	5mm thick sheet Metal	2	5000	10000
2	Fiber Wool Mat	1	15,000	15000

3	4 litres Binder	5	2000	10000
4	20 litres resin Chemicals	3	3000	9000
5	Labour		10,000	10,000
	Total			**54,000**

PartB:Solar Collector (Area: 2.24m^2)

S/N	Item	Qty	Unit price	Total price
1	Wood:30mmX100mmX1600mm	2	1000	2000
2	Wood:30mmX100mmX1200mm	2	1000	2000
3	Ply wood:2mmX1200mmX2000mm	2	4500	9000
4	Plastic pipe:2000mm long, 15mm diameter	3	300	900
5	White glass :4mmX 1595mmX1195mm	2	3000	6000
6	Aluminum sheet:5mmX1595mmX1195mm	2	1500	3000
7	Copper pipe:1550 mm long, 15 mm diameter	2	5000	10000
10	Thermocouples wires	4	3000	12000
11	Paints	3	2000	6000
12	Labour			12000
	Total			**62,900**

PartC: Supporting Frame.

S/N	Item	Qty	Unit price	Total price
1	Rectangular iron pipes:30mmX50mmX2000mm	5	1500	7500
2	Wood:30mmX100mmX1200mm	2	1000	2000
3	Pack of electrodes	3	1000	3000
4	Labour		5000	5000
5	Miscellaneous	1	10000	10000
	Total			**27,500**
	GRANT TOTAL			**144,400**

3.10 Validation of Simulation Model

A model is always a simplification of the complex reality of natural phenomena. This simplification has the merit of representing the reality in all its extents. However, the constructed system model may not be capable of producing a response that is entirely in line with the behavior of the observed phenomenon (Julien *et al.*, 2013).

In order to validate the predicted system performance obtained from the model, the water temperature in the storage tank and weather data measured during the experiment were used as the validation parameters. The temperature of the water in the storage tank was chosen as the validation parameter because this temperature is a very important parameter

both for the designer and for the end user. No water was removed during the experiment to simplify the validation process. Water temperature in the storage tank and weather data (solar radiation and ambient temperature) were experimentally measured at an interval of one hour starting from 8 am to 5pm daily and the results recorded. This procedure was repeated for 3 consecutive days. The daily records were compared with the system simulated results. The results are as shown in Figures 4.21 to 4.27.

To validate the predictive power of the model, the Root Means Square Error (RMSE) and the Nash-Sutcliffe Coefficient of Efficiency (NSE) were employed. These statistical criteria are considered objective and provide unbiased indicators of the model predictive power (Julien *etal.*, 2013). The RMSE measures the differences between values predicted by a hypothetical model and the observed values. In other words, it measures the quality of the fit between the actual data and the predicted data from the model (Julien *et al.*, 2013). RMSE is one of the most frequently used measures of the goodness of fit of generalised regression models. In the application of regression models, unless the relationship or correlation is perfect, the predicted values are more or less different from the actual observations. The RMSE of a model prediction with respect to the estimated variable X_{model} is defined as the square root of the mean squared error (Neil, 2010).

$$RMSE = \sqrt{\frac{\sum_{i=1}^{n}\left(X_{obs,i}-X_{model,i}\right)^2}{n}} \tag{3.49}$$

where X_{obs} is observed values and X_{model} is modeled values at time/place *i*.

The lower the Mean Absolute Error or the Bias Percentage value, the better the performance of the model (Neil, 2010).Furthermore, the Nash-Sutcliffe Coefficient of Efficiency (NSE) defined as follow was determined

$$NSE = 1 - \frac{\sum_{i=1}^{n}\left(X_{obs,i}-X_{model,i}\right)^2}{\sum_{i=1}^{n}\left(X_{obs,i}-\bar{X}_{obs}\right)^2} \tag{4.50}$$

where:

X_{obs} is the observed value

X_{model} is the modelled value at time/place *i*.

$\bar{X}_{obs}$ is the mean of the observed value.

Nash-Sutcliffe efficiencies can range from -∞ to 1. An efficiency of 1 (NSE = 1) corresponds to a perfect match between model and observations. An efficiency of 0 indicates that the model predictions are as accurate as the mean of the observed data, whereas an efficiency less than zero (-∞< E < 0) occurs when the observed mean is a better predictor than the model (Julien *et al.*, 2013).

3.10.1 Description of the experimental set-up

The constructed thermosyphon solar water heating system whose characteristics and configurations are as described in Figure 3.1, Tables 4.3 and Table 4.4was installed in the Department of Mechanical Engineering, Ahmadu Bello University Zaria and were used to carry out the experiments. The tilt of the collector with respect to the horizontal plane is 12^{o} towards south. A picture of the setup is shown in Plate 12 of appendix F.

3.10.2 Experimental procedure

On each day within this test period, experiment was started and completed by measuring the initial and end of day inlet and outlet water temperatures in the storage tank and solar collector at one hour intervals. To accomplish the above, thermocouples were fixed at the inlet and outlet parts of the storage tank and solar collector. Also, each day's experiment was started by emptying the water tank and charging it with fresh water. During the experimentation, no water was drawn off from the system during daytime. The thermosyphonic flow solar water heater was tested for 3 days between 8.00 hrs and 18.00 hrs. The amount of solar radiation on the collector surface and the ambient temperature

were measured with a Zonen pyranometer and digital thermometer, respectively. The solar irradiance was measured and recorded every fifteen minutes and integrated over an hour. During the experiments the K-type thermocouple wires were used to measure the inlet and outlet temperatures of the storage tank and the solar collector. In order to measure these temperatures accurately, all thermocouples were calibrated against a high accuracy temperature recorder to ±0.3 ^{o}C accuracy. A graphical comparison of the simulated system performance and the test performance is presented in Figures 4.21 to figure 4.29

CHAPTER FOUR

RESULTS AND DISCUSSION

4.1 System Design Calculations

Table 4.1 shows the monthly average daily environmental variables (solar radiation and weather data) determined from the TMY solar data of Zaria, Nigeria (lat. 11.2^{o} N and long. 7.8^{o} E), for recommended average day of the months using the weather data processor (TYPE 109) of TRNSYS 16 software and the programme codes (appendix A) developed in MATLAB (Brian *et a.*, 2001). It can be seen from this table that the clearness index, $\overline{K}_T$,for the months of January to April and month of December is above 0.7 indicating that over 70% of extraterrestrial solar energy, $\overline{H}_o$, is received on a horizontal surface in the said location (Zaria).The clearness index decreased to values slightly below 0.7 from the months of May to November and increase to 0.73 in December. The worst values of $\overline{K}_T$were found in July and August. This implies that August which has the least clearness index has the least amount of solar energy received on the surface of the earth for this location (Zaria).The annual average value of $\overline{K}_T$ for this location (Zaria) is 0.64, indicating a good solar potential for all solar system design. The variation in monthly average value of $\overline{K}_T$ can be explained from the fact that for this location (Zaria), the amount of cloud cover in the sky from the months of January to April is lesser. This period corresponds to the dry season of this location. The worst values of $\overline{K}_T$ found in July and August is an indication that the sky at this period (peak rainfall) is covered by heavy cloud due to high amount of rainfall.

Table 4.1: Simulated monthly average daily solar and weather data for Zaria.

	$\bar{V}$ (m/s^2)	$\bar{T}_a$ (°C)	$\bar{H}_o$ (J/m^2.day)	$\bar{H}$ (J/m^2.day)	$\bar{H}_b$ (J/m^2.day)	$\bar{R}_b$	$\bar{K}_T$
JAN	2.60	38	31414623.3	22658400	18425800	1.222	0.721
FEB	2.57	38	34167274.8	24854400	19870000	1.134	0.727
MARCH	2.70	40	36695102.7	27025200	21486500	1.034	0.736
APRIL	2.31	32	37982188.4	28209600	19906100	0.931	0.743
MAY	2.80	35	37814449.5	18014400	12500520	0.854	0.496
JUNE	3.50	32	37350825.9	23644800	12287500	0.819	0.633
JULY	2.91	26	37403591.6	18125000	10813100	0.834	0.485
AUGUST	**3.08**	**28**	**37674087.9**	**16095600**	**8491700**	**0.898**	**0.427**
SEPT	1.56	32	36966765.4	24310800	11327100	0.992	0.658
OCT	2.57	36	34746668.2	22251600	14802500	1.101	0.640
NOV.	3.39	35	31962730.9	21535200	17297700	1.198	0.674
DEC.	2.00	33	30477090.9	22237100	17181600	1.247	0.730
Annual AV.	**2.67**	**33.75**	**35387950.0**	**22413508.3**	**15365843.3**	**1.020**	**0.640**

Source: Researcher's calculated result

Table 4.2 shows the calculated monthly values of energy absorbed by the collector $\bar{S}_R$, the collector useful energy Q_u, system monthly average daily design load, Q_L,and the total collector area$A_c$required to meet the system monthly average daily design load. It can be seen from the table that the month of August has the least energy ratio (E_R) of 0.66 and the maximum required collector area A_c of 5.89m^2. This implies that if the solar system is to meet all domestic hot water load of 0.1m^3 set at 70°C (i.e solar fraction S.F =1) in August, a minimum collector area of 5.89m^2 is required. The table also shows that the collector area required to meet the same domestic hot water load varies from months to month, with the least area of 1.15m^2 in March. This indicates that if an annual average monthly collector area of 2.24m^2 is adopted for this design, the system would be capable of meeting all year round design load (ie S.F=1)for all months except for the months of July and August where only a portion of the load would be met because the adopted collector area of 2.24m^2 would be inadequate to meet the design load in these months. To meet design load for these months, additional means of heating to load temperature is required. Therefore, for all year round satisfactory system performance and economy, the annual

average collector area of 2.24m^2 is adopted for this design. This implies that the domestic hot water need for some months which require collector area higher than the annual average of 2.24 m^2 will have to be met by the auxiliary energy source.

Table 4.2: System design calculation for the determination of design month.

	$\overline{S}_R$ (MJ/m^{2}day)	$\overline{H}_T$ (MJ/m^{2}day)	$\overline{Q}_L$ (MJ/m^{2}day)	$\overline{Q}_s$ (MJ/day)	$\overline{Q}_u$ (MJ/m^{2}day	$\overline{E}_R$	A_c (m^2)
JAN	21.8	26.75	8.400	17.43	13.37	1.535	1.303
FEB	22.4	27.52	8.385	17.43	14.05	1.579	1.241
MARCH	22.7	27.74	8.467	16.34	14.20	1.698	1.150
APRIL	21.7	26.77	8.176	20.70	13.51	1.293	1.532
MAY	13.0	16.14	8.346	19.06	4.67	0.847	2.082
JUNE	16.9	21.25	8.404	20.69	8.50	1.027	2.434
JULY	13.0	16.25	8.127	23.96	4.86	0.678	4.925
AUGUST	**12.1**	**15.17**	**8.211**	**22.87**	**3.87**	**0.661**	**5.897**
SEPT	19.2	24.02	8.059	20.69	11.13	1.160	1.859
OCT	19.2	23.66	8.330	18.51	10.83	1.278	1.709
NOV.	20.4	24.96	8.465	19.06	11.89	1.310	1.602
DEC.	21.5	26.47	8.150	20.15	13.35	1.314	1.510
A. AV	**18.6**	**23.06**	**8.290**	**19.70**	**10.40**	**1.200**	**2.240**

Source: Researcher calculated result

Table 4.3 shows the calculated monthly average daily system overall heat loss coefficient, U_L, storage tank loss coefficient U_{st}, collector heat removal factor F_R, glass covers transmittance-absorptance product, $\tau\alpha$, and the wind loss coefficient, h_w. The table indicatesthat the monthly average daily values of these calculated design parameters vary significantly for some design parameters and insignificantly for others. This variation in the design parameters could be explained from the fact that the solar radiations and weather data which served as input for the calculation of some of these parameters are highly random and vary significantly throughout the year. The monthly average daily values of these design parameters (Table 4.3) are useful parameters for the determination of system performance during these months through simulation using TRNSYS software.

Table 4.3 : Calculated monthly average daily system design parameters

MONTH	$\overline{U}_L$ (W/m^{2}k)	$\overline{U}_{st}$ (W/m^{2}k)	$\overline{F}_R$	$\overline{\tau\alpha}$	$\overline{h}_w$ (W/m^{2}k)
JAN	8.26	0.123	0.822	0.81	10.60
FEB	8.27	0.123	0.837	0.81	10.51
MARCH	8.38	0.122	0.855	0.82	10.90
APRIL	8.00	0.125	0.782	0.81	9.73
MAY	7.97	0.121	0.422	0.81	11.20
JUNE	8.10	0.116	0.607	0.80	13.30
JULY	7.74	0.120	0.369	0.80	11.53
AUGUST	**7.80**	**0.119**	**0.311**	**0.80**	**12.04**
SEPT	7.84	0.131	0.722	0.80	7.48
OCT	8.11	0.123	0.737	0.81	10.51
NOV.	8.26	0.117	0.752	0.82	12.97
DEC.	7.98	0.127	0.788	0.81	8.80

Source: Researcher calculated result

4.2 Collector Design Parameters Optimisation

4.2.1 Collector tilt angle (β)

Figure 4.1 shows the effect of varying the collector tilt angle on the amount of monthly average daily solar radiation received on the collector surface on a typical recommended average day for the month of August (16August). From the figure, the incident solar radiation increases as the tilt angle increase from zero, reaching the maximum amount of 16.28 MJ/m^{2}day at a collector tilt angle of 12^o. Further increase in the tilt angle resulted in a decrease in amount of solar radiation received on the collector surface. The 12^o collector tilt was adopted as the optimum tilt angle for the design.

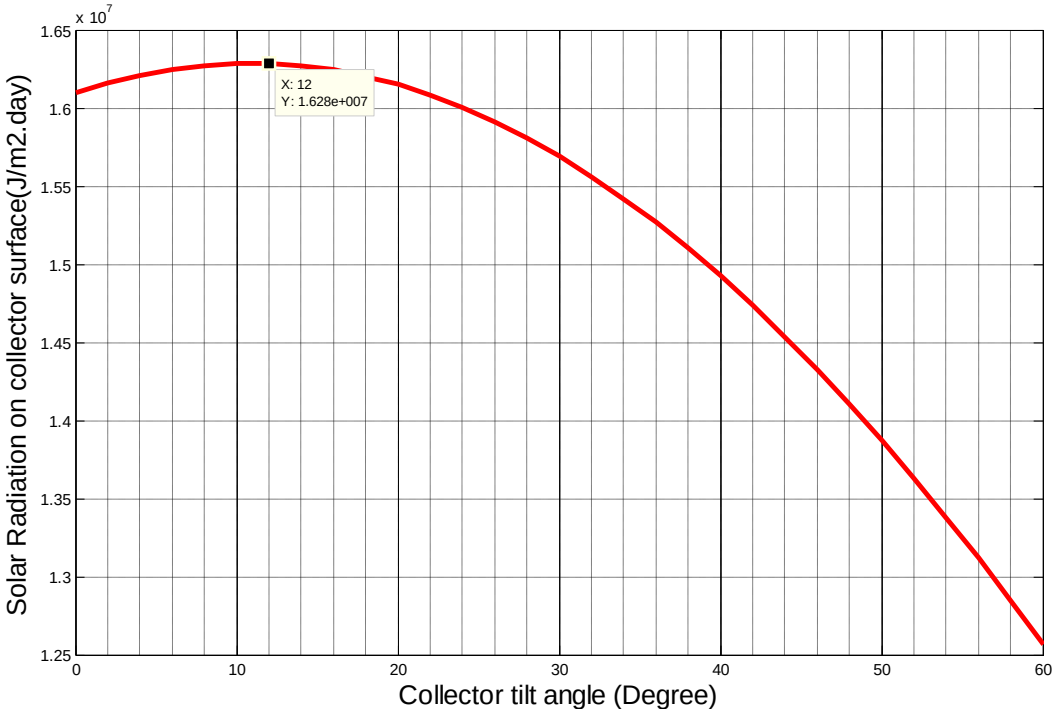

Figure 4.1: Optimum tilt angle for annual performance of solar water heating system.

4.2.2 Collector tube diameter and centre to centre distance.

The effect of varying tube centre to centre distance (W) on the collector heat removal factor,F_R, over a range of tube internal diameter D_i (0.002m to 0.0035m), for a single glazing flat plate collector, keeping the collector heat loss coefficient h_{fi} (7.80W/m^{2}K), collector area A_c (2.24m^2) and plate thickness (6mm) constant is shown in Figure 4.2.The graph shows that as W increases from 0 to 2m, $F_R$for a tube diameter of 0.03m increases from a minimum value of 0.446, reaching a maximum value of 0.575 representing an increase of 28.92 % at a centre to centre distance of 0.30m. The heat removal factor, F_R, again decreases from a value of 0.575 to 0.350 representing a drop of 39.13% as W was further increased from 0.3 to 2.0m. This trend is also observed for collector diameters lower than 0.03m as seen from the figure. The graph also reveals that the heat removal factor is improved as the collector tube internal diameter decreases. A collector tube

diameter of 0.02m is observed to have the maximum value of the heat removal factor of 0.6 at a centre to centre distance of 0.2m

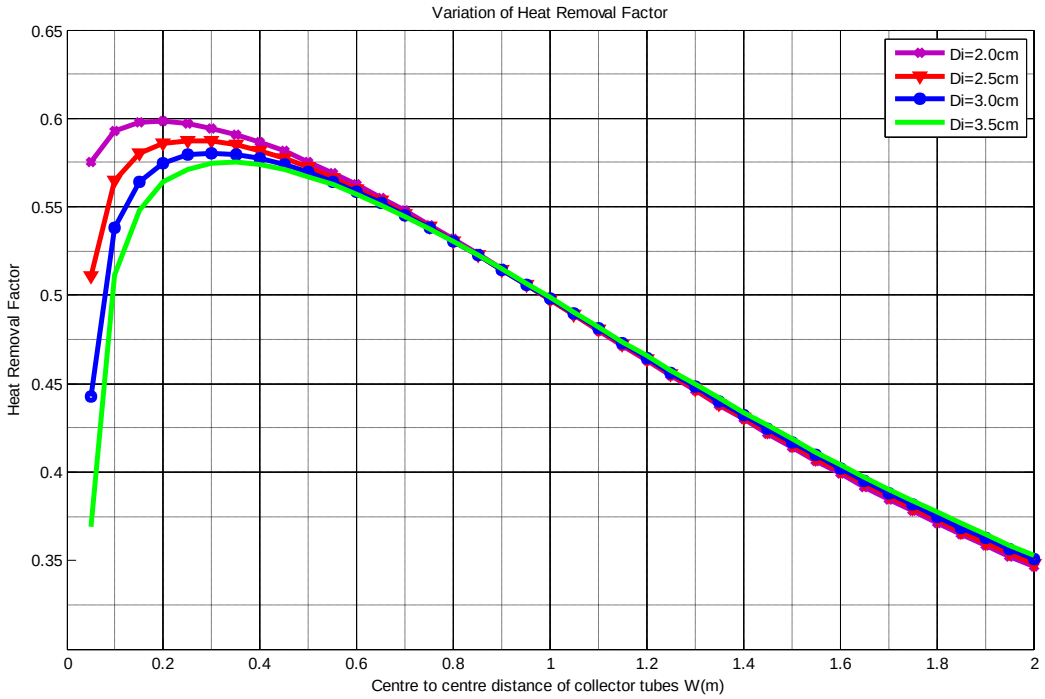

Figure 4.2: Effect of collector tube centre to centre distance (W) on heat removal factor
(F_R) for a range of tube internal diameter (Di).

Therefore, considering system fabrication difficulties, and commercially available sizes of system component (tube), a collector tube with internal diameter of 1.5cm (0.015m) and a tube centre to centre distance W of 15cm (0.15m) was selected as the optimum for this design.

4.2.3 Collector absorber plate thickness

Figure 4.3 shows the effect of varying the absorber plate thickness on the heat removal factor of a single glazing flat plate solar collector for the selected collector characteristics from Figure 4.1 and Figure 4.2. The figure shows that the heat removal factor increases from a value of 0.6178 to 0.6195 as the plate thickness increases from 0.003m to 0.075m. This increase in F_R represents an increase of 0.31% in heat removal factor as the thickness

of the plate is increased from 0.003m to 0.075m. This increase is considered very insignificant. Considering the system cost in relation to system performance and commercially available size, a 0.006m (6mm) thickness plate is selected as the absorber plate thickness for this design.

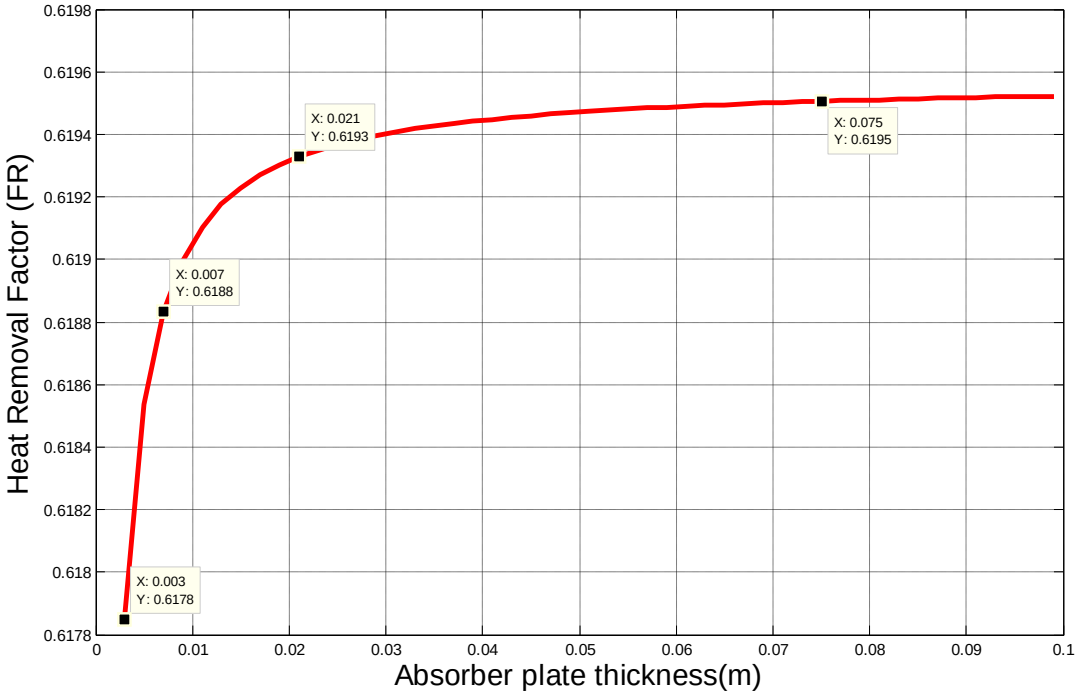

Figure 4.3: Effect of the variation of collector absorber plate thickness on heat removal
factor for given collector characteristics

4.2.4 Collector number of glazing

The effect of varying the number of glazing keeping other design parameters constant on the heat removal factor of the solar collector is shown in Figure 4.4 and Figure 4.5.The figures reveal that as the number of glazing increases, the heat removal factor increases. The figure shows an improvement in the heat removal factor of the collector from 0.6553 to 0.9165as the number of glazing increases from 1 to 10. When the collector glazing is increased from 1 to 2, the heat removal factor increased from 0.6553 to 0.7714, representing a significant increase of 15.44%. Additional increase in the number of glazing

from 2 to 3 increased the heat removal factor from 0.77 to 0.82. This again represents a slight improvement of 6.45%. The improvement in F_R as the number of glass cover, N_g, increases can be explained from the fact that the overall heat loss coefficient, U_L, decreases with increase in $N_g$as shown in Figure 4.5.

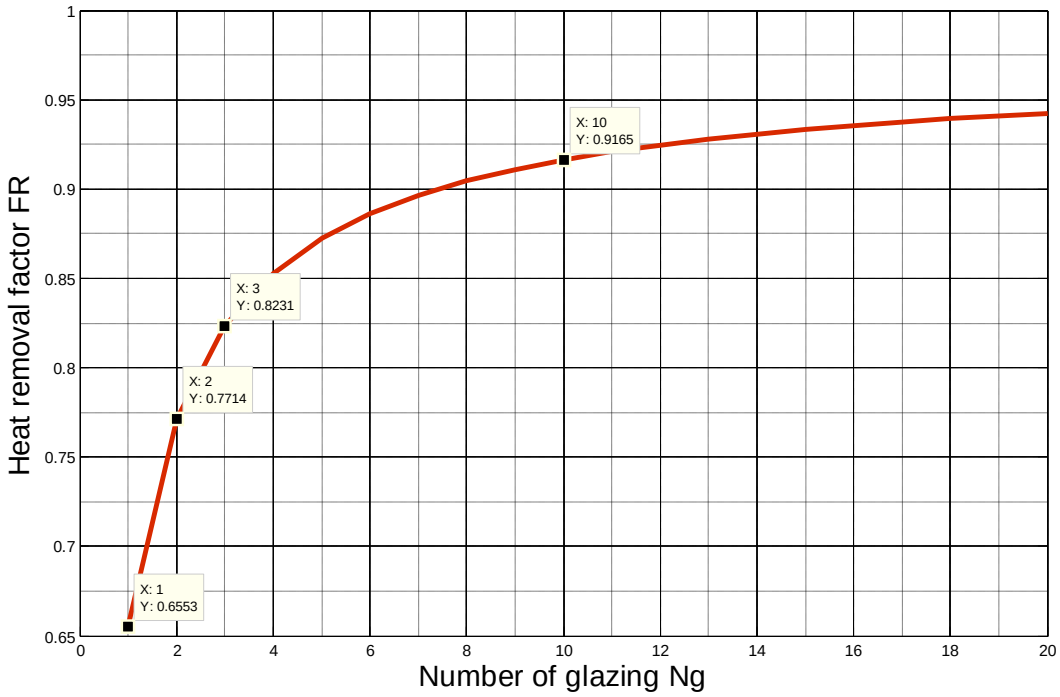

Figure 4.4: Effect of the variation of collector number of glass on heat removal factor (F_R) for given collector characteristics

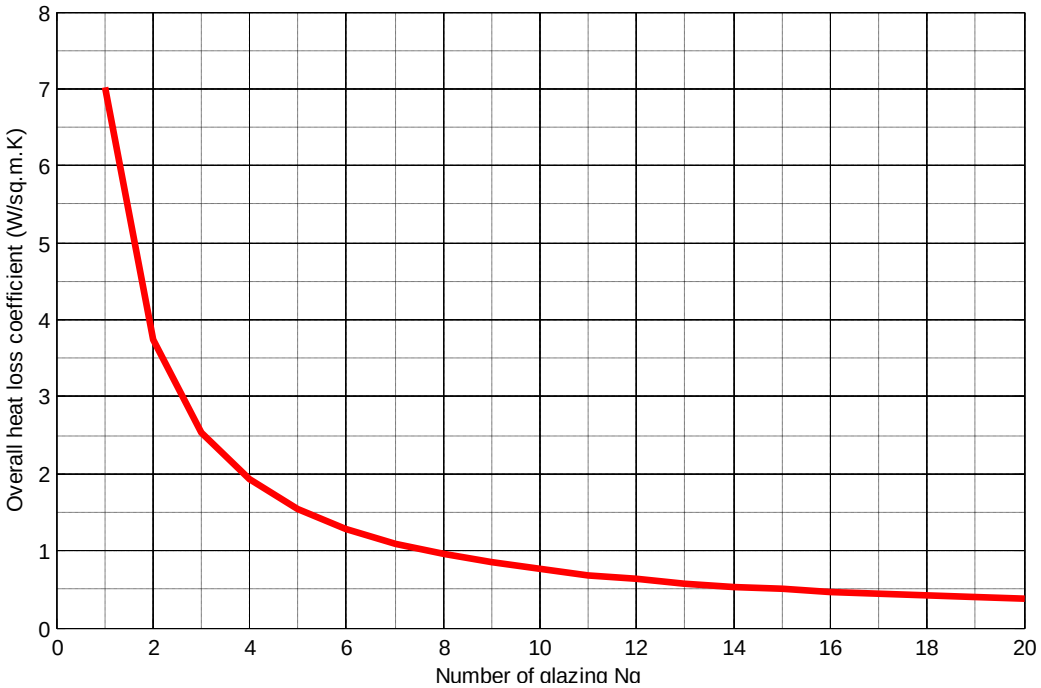

Figure 4.5: Effect of the variation of collector number of glass on overall heat lost coefficient

(U_L) for given collector characteristics

4.3 System Optimum Parameters and Simulation

Table 4.4 and Table 4.5 show the final system characteristics and design parameters adopted for the system performance simulation using TRNSYS 16 software. The results of the predicted performance of the system at the end of the day for a typical recommended average day of each month of the year are shown in Figures 4.6 to 4.17.

Table 4.4: System characteristics

Description	**Value/Type**
Total aperture area	2.24 m^2
Storage tank capacity	100L
Riser tubes material	Copper
Number of riser tubes	12
Absorber surface	Painted matt black
Glass type	4 mm low iron glass
Collector insulation	Saw dust 30 mm thick for both sides and back insulation.

Table 4.5: System final optimum design parameters and components size.

Parameter	Description	Values
A_C	Collector area (m^2)	2.24
$F_R(\tau\alpha)_n$	Intercept of the efficiency vs. (Ti-Ta)/I_T curve	0.63
$F_R U_L$	Negative of the slope of the efficiency vs. (Ti-Ta)/I_T (kJ/h m^2 C)	14.26
β	Collector slope (degrees)	12.0
N_R	Number of parallel collector risers	12
d_R	Riser diameter (m)	0.02
H_d	Header diameter (m)	0.02
H	Header length (m)	1.4
h_c	Vertical distance between collector outlet and inlet (m)	0.33
h_o	Vertical distance between outlet of tank and inlet of collector (m)	0.37
d_i	Diameter of collector inlet pipe (m)	0.02
L_i	Length of collector inlet pipe (m)	1.55
NB_1	Number of right angle bends (or equivalent) in inlet pipe	2
U_i	Loss coefficient of collector inlet pipe plus insulation (kJ/h m^{2o}C)	0.625
L_o	Length of collector outlet piping (m)	0.80
NB_2	Number of right angle bends (or equivalent) in collector outlet piping	2
U_o	Loss coefficient of collector outlet pipe plus insulation (kJ/h m^{2o}C)	0.625
V_t	Tank volume (m^3)	0.100
H_t	Tank height (if vertical) or diameter (if horizontal) (m)	0.40
H_R	Height of collector return to tank above bottom of tank (m)	0.39

Figure 4.6 shows the simulated hourly tank inlet, collector inlet, and tank average temperature of the system as predicted using TRNSYS 16 softwarefor recommended average day of January (16 January, 2013). The figure shows a continous rise in tank inlet

temperature from an initial temperature of 30^{o}C at 8.00hours reaching its peak of 80^{o}C at 15 hours.This is again followed by a drop in temperature from 16 hours to a temperature of 58^{o}C at hours. This observed drop in temperature is due to the lower amount of solar radiation received on the collector surface at this time of the day. On the other hand, the collector inlet temperature remains constant from the start of simulation (8.00 hours) to 13 hours. At about 13 hours , the collector inlet temperature started to rise.It could also be seen from the figure that at the end of the simulation time (18 hours), the tank average temperature remains greater than the collector inlet temperature. This reveals stratification of the storage tank temperature; the implication is a non uniform storage tank water temperature at the end of the day. That is,the temperature of water at the top layer of the storage tank is higher than the temperature of water at in the bottom layer of the storage tank at the end of the day.

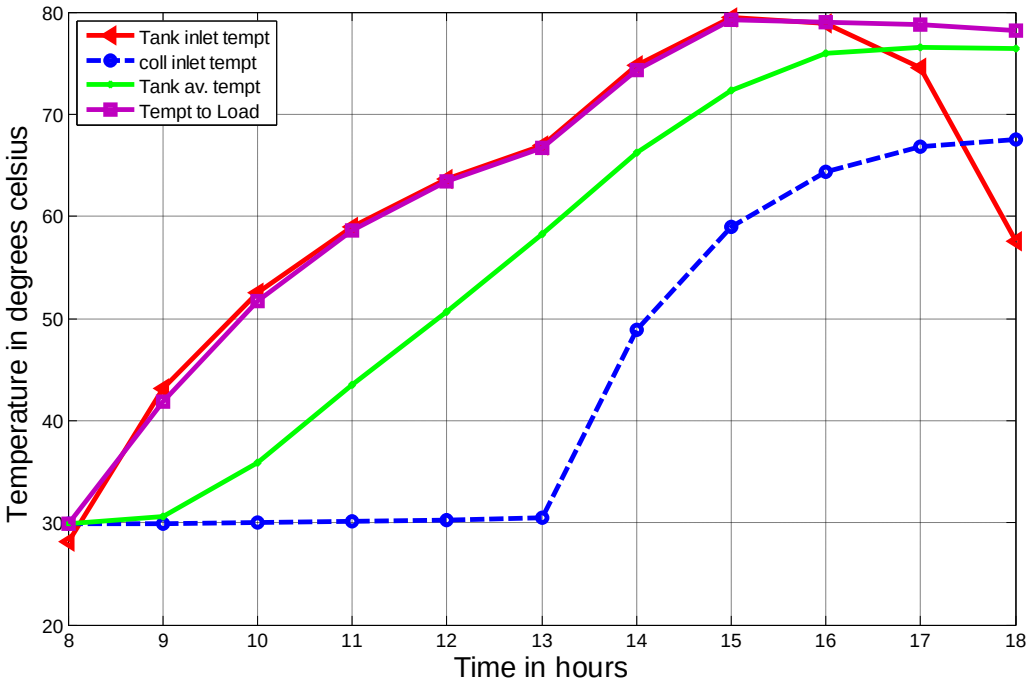

Figure 4.6: Temperatures variation for a recommended average day in January. (17 January)

Figures 4.7 to 4.17 show the hourly performance of the system for recommended average day of the months of February to December. This figures show a similar trend in hourly performance of the system as in the month of January. However, the peak temperatures and the time at which the peak temperatures are achieved differ for different months. Figure 4.13 shows that a maximum tank inlet temperature of 59^{o}C for the month of August. This performance is the worst of all the months. The figures also reveal that the month of March has the best performance with the highest tank inlet temperature 82^{o}C (see Figure 4.8).The implication of the low performance of the system in May, August and October where tank average temperature less than 70^{o}C is that additional heat will be required to meet the desired load temperature. However, for the months of January, February, March, April, June, July, September, November and December with average tank temperature of 70^{o}C and above, additional heat source will not be required to meet the desired load temperature.

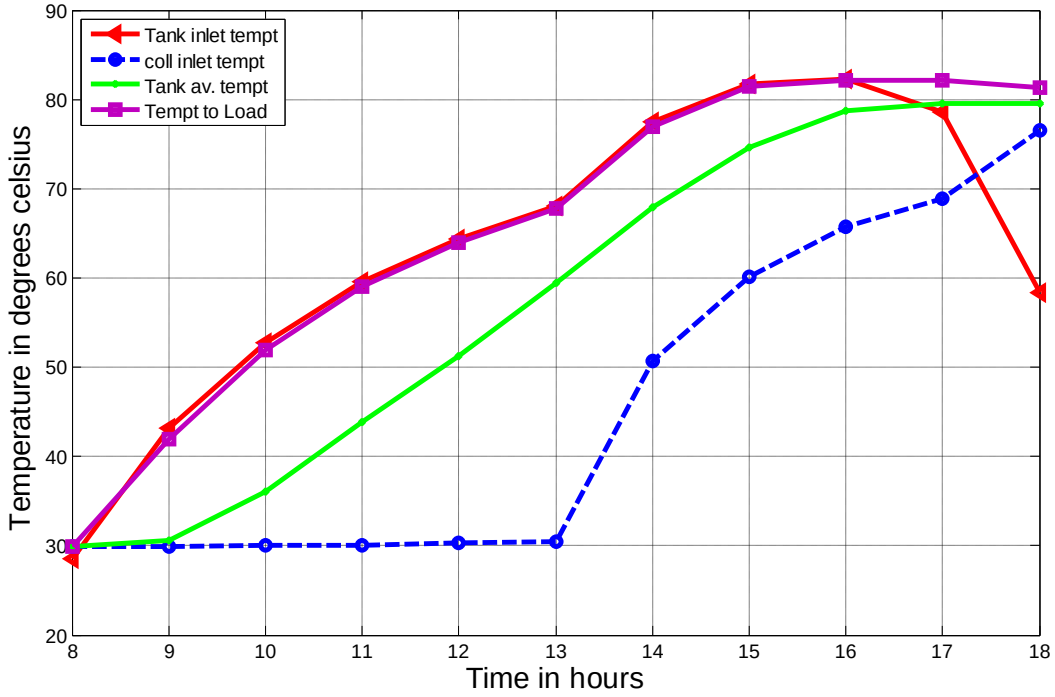

Figure 4.7: Temperature variation for a recommended average day in February. (16 February)

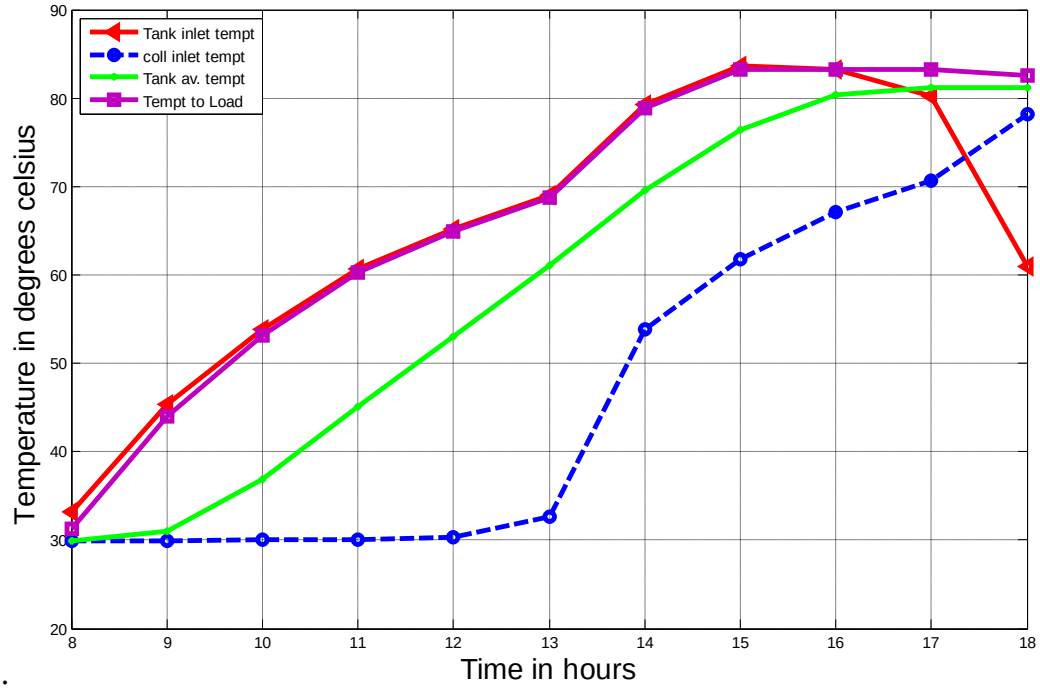

.

Figure 4.8: Temperature variation for a recommended average day in March. (16 March)

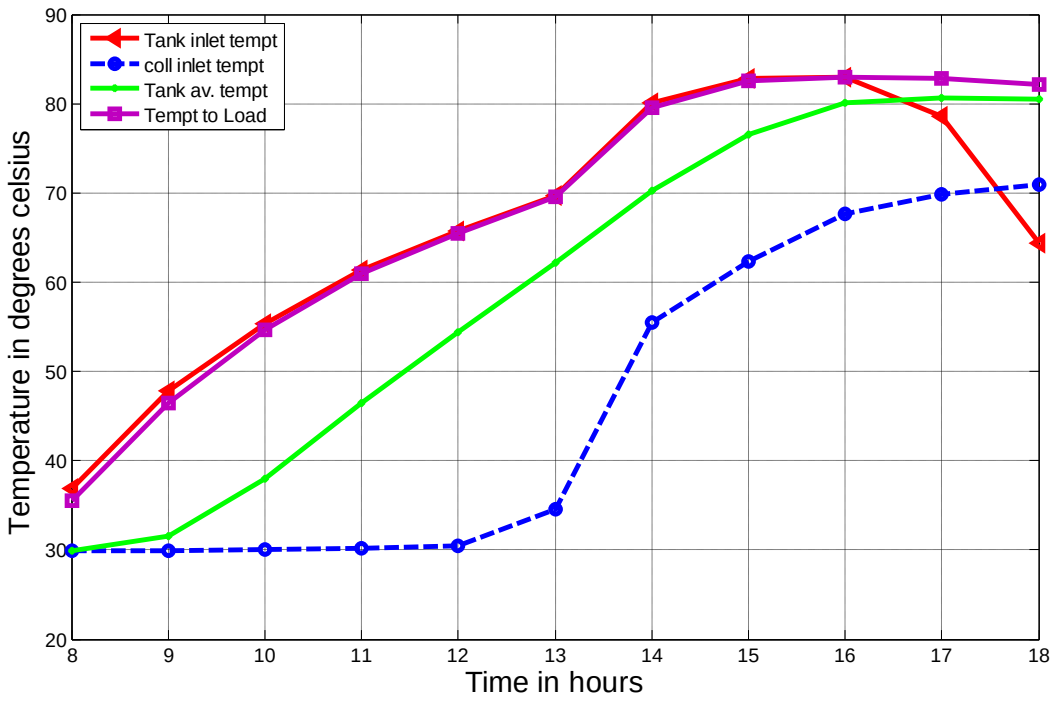

Figure 4.9: Temperature variation for a recommended average day in April. (15 April)

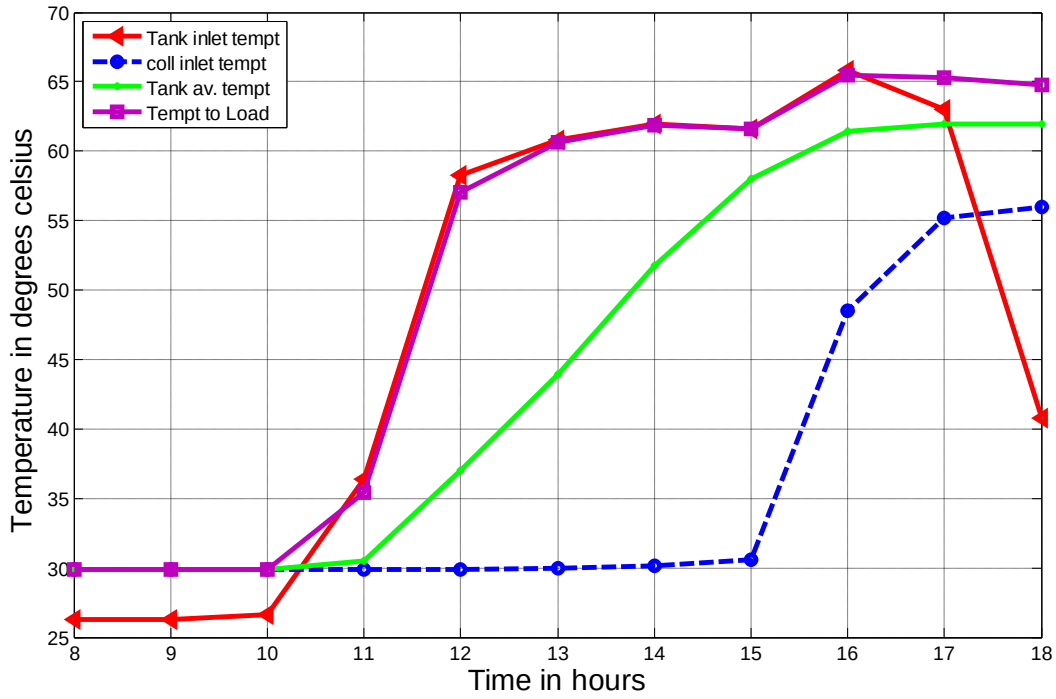

Figure 4.10: Temperature variation for a recommended average day in May. (15 May)

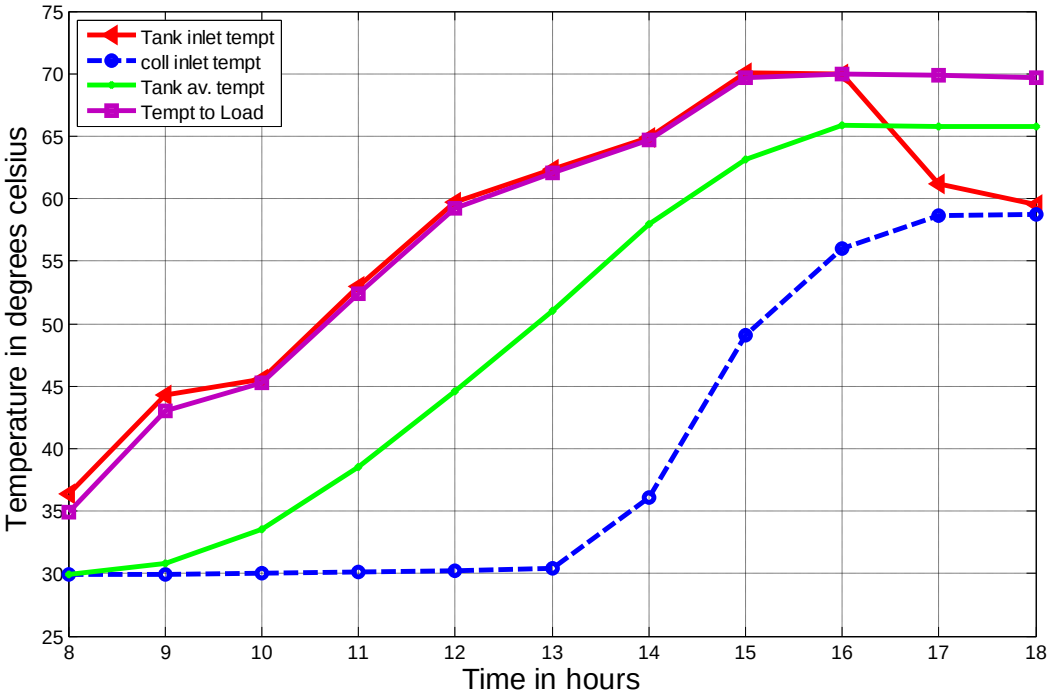

Figure 4.11: Temperature variation for a recommended average day in June. (11 June)

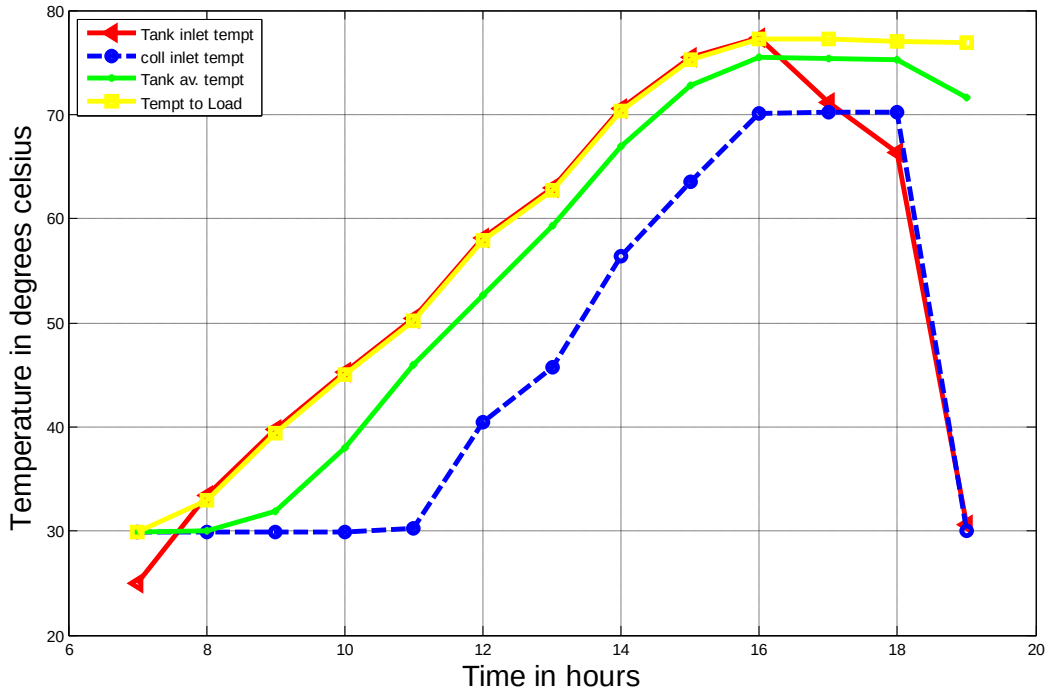

Figure 4.12: Temperature variation for a recommended average day in July. (17 July)

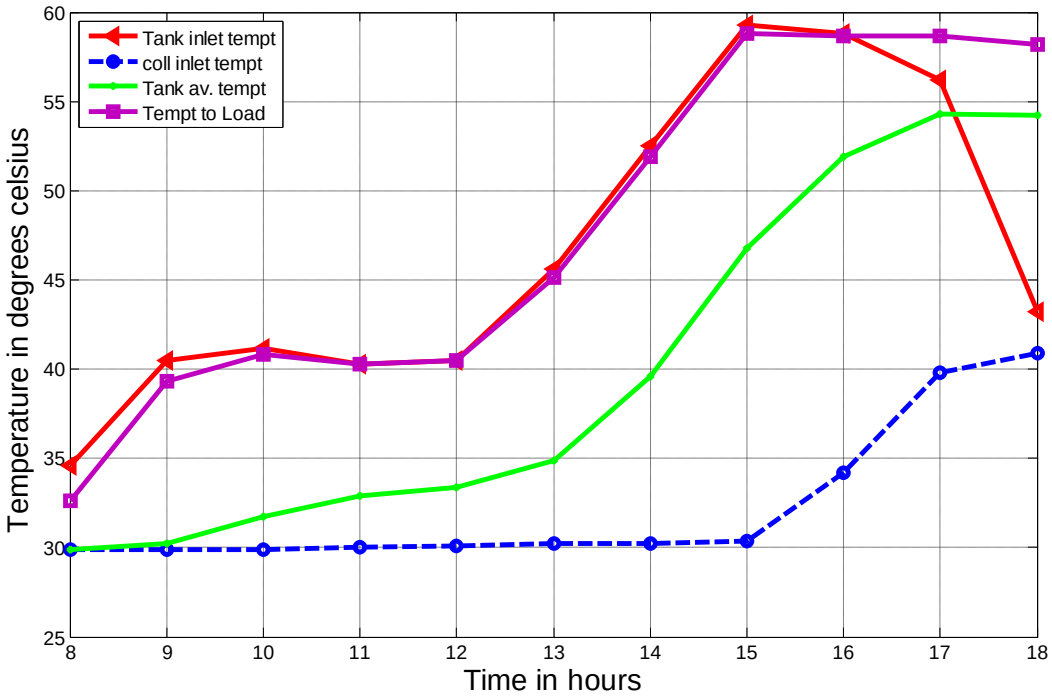

Figure 4.13: Temperature variation for a recommended average day in August. (16th Aug)

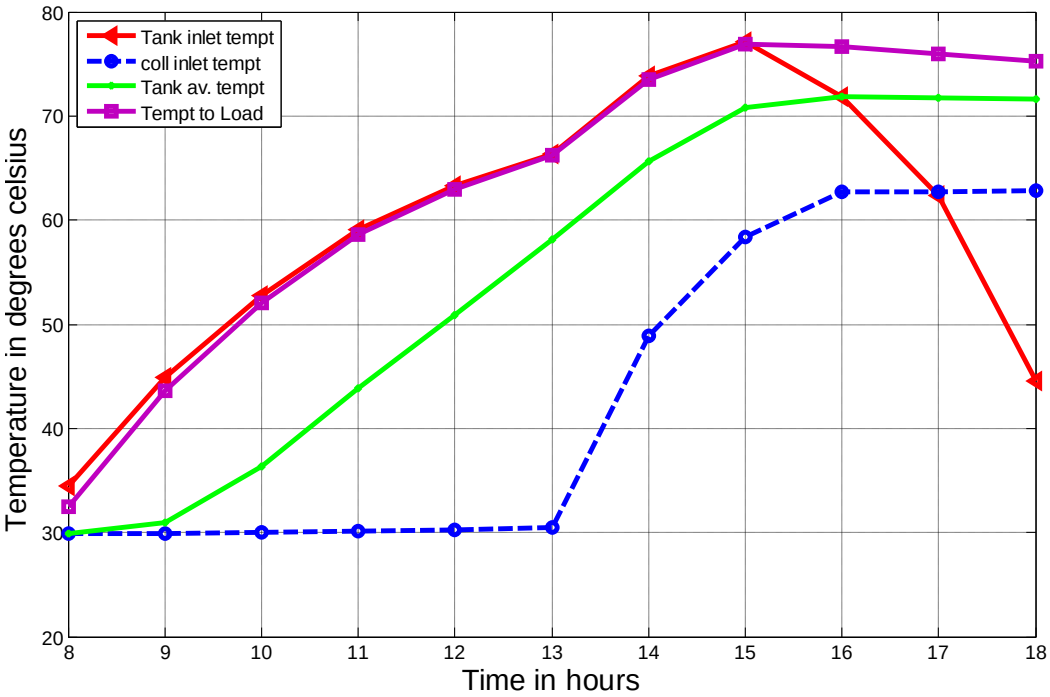

Figure 4.14: Temperature variation for a recommended average day in September. (15 Sept.)

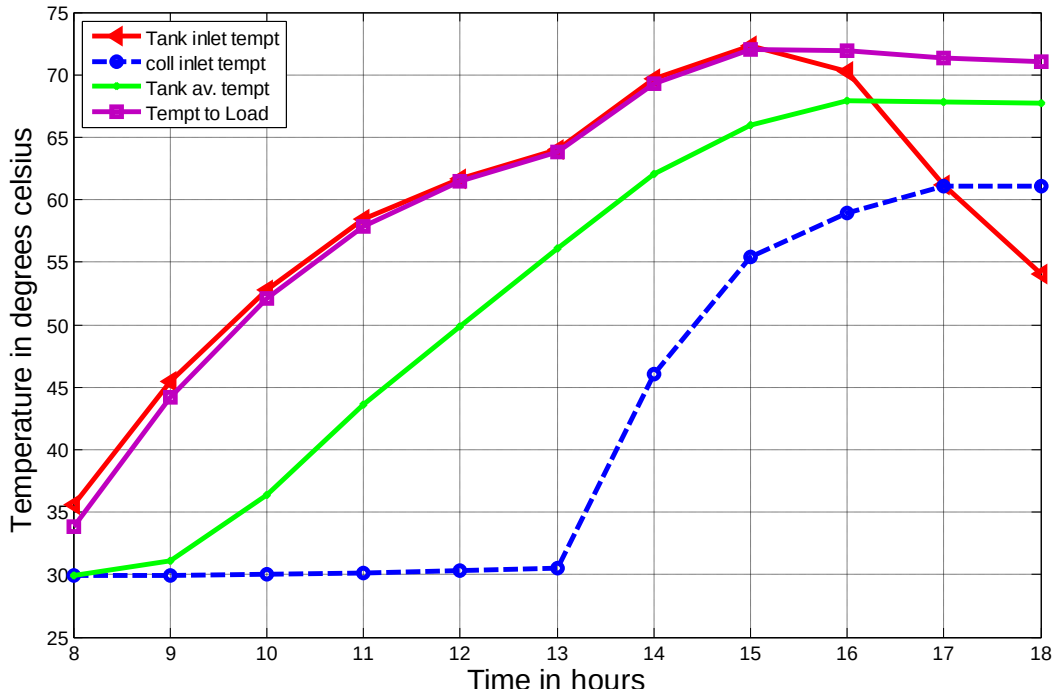

Figure 4.15: Temperature variation for a recommended average day in October. (15 Oct)

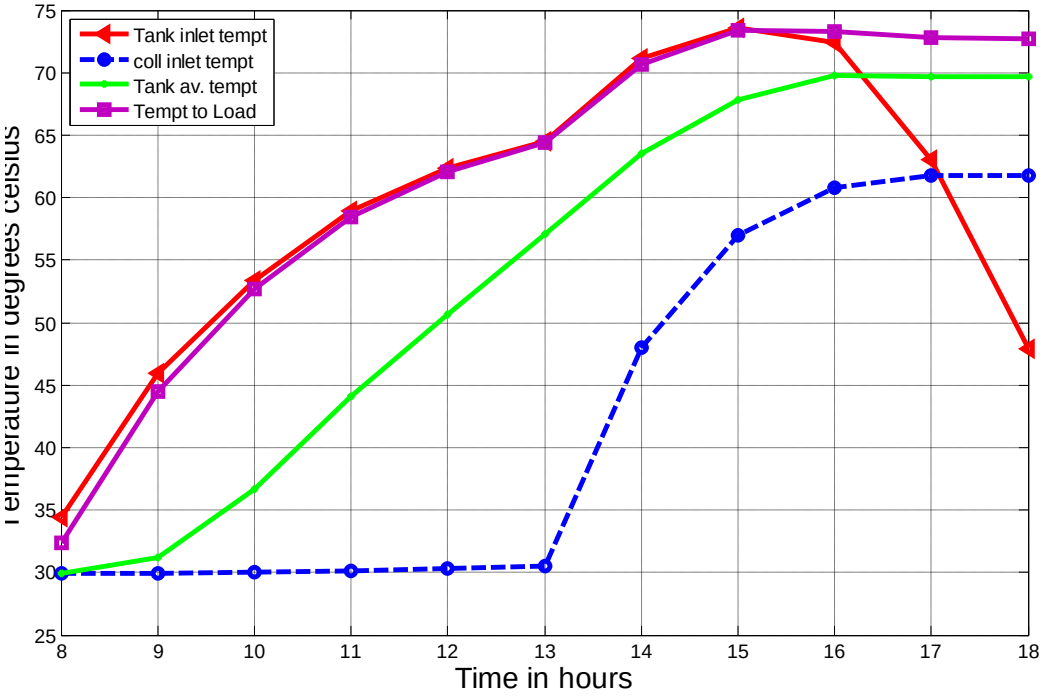

Figure 4.16: Temperature variation for a recommended average day in November. (14 Nov.)

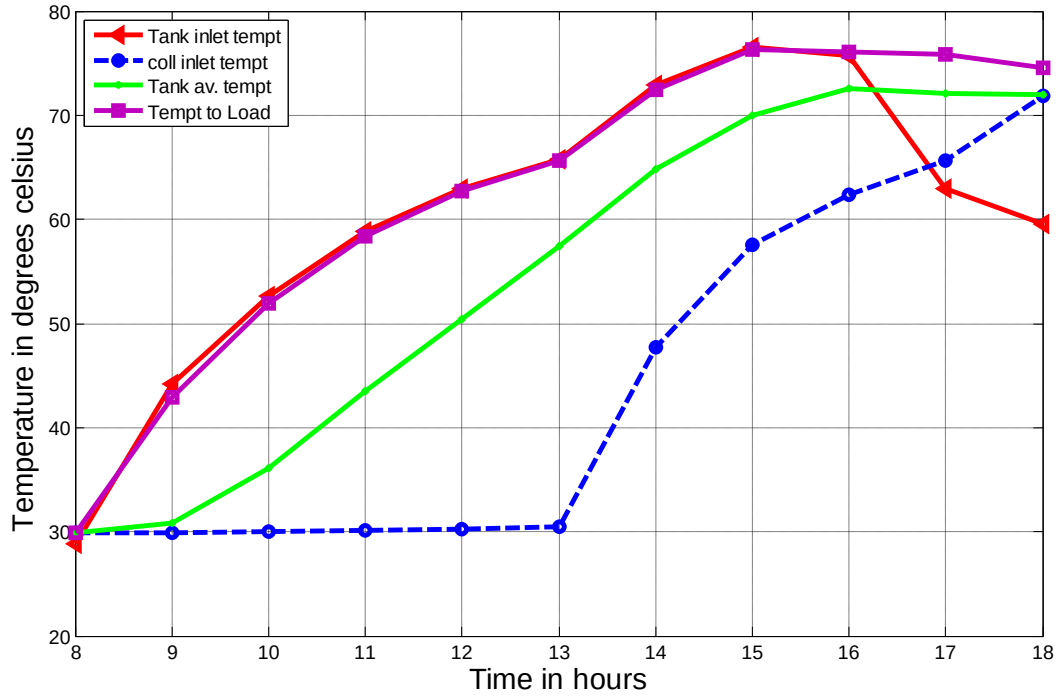

Figure 4.17: Temperature variation for a recommended average day in December. (10 Dec.)

4.4 System Performance Evaluation

To evaluate the performance of the system, the experimental results of 29 March, 2014 was used to calculate the hourly collector efficiency from equation (3.47).The experimental result was compared with the simulated one and the result is shown in Figure 4.18. The result shows slight deviation between the experimental and simulated collector efficiency. It can also be seen from the figure that the experimental efficiency of the collector increases from 24% at 8.0 hours reaching its peak value of 66% at 10.0 hours and then decreases again to 19% at 17.0 hours. The graph also shows that the highest experimental efficiency of 66%of the solar collector was at 10 hours. Figure 4.18 shows that the hourly experimental efficiencies are higher than the estimated (simulated) efficiencies from 8 hours to 11 hours. However, the simulated efficiencies are higher than the experimental efficiency from 12 hours to 17 hours. This was as a result of the inability of software to exactly predict the weather conditions due to its highly random nature with time.

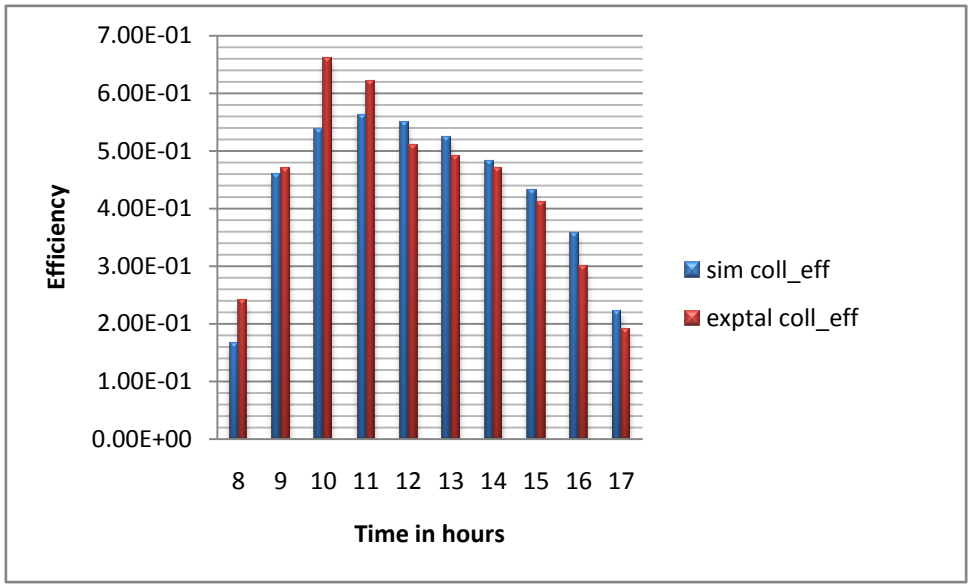

Figure 4.18: Comparison of solar collector simulated efficiency with experimental efficiency.

4.5 Validation of Simulated Results

The validation of the performance of the system as predicted by the system simulation model using TRNSYS 16 software was performed in two parts. Firstly, the system experimental results (i.e the measured solar radiation , weather data, system collector temperature and storage tank temperature obtained during the 3 day experiment were compared to the simulated results. The aim was to obtain the trend and the level of agreement of the experimental results with the simulated ones. Secondly, two statistical tools namely; the Roots Mean Square Error (RMSE) and the Nash-Sutcliffe coefficient of efficiency (NSE) were employed to analyse the predictive power of the simulation software.

4.4.1 Comparison of simulated results with experimental results.

Figures 4.19 and figure 4.20 show the comparison of the experimental hourly solar radiation and hourly ambient temperature with the predicted result from the model (solar data processor, Type 109 of TRNSYS). Figure 4.19 shows that the model slightly over estimates the hourly solar radiation for most part of the day for the said location (Zaria) on 29 March, 2014. However the computed Root Mean Square Error (RMSE)value of 283022 KJ/hr.$m^2$and NSE value of 0.926as shown in Table 4.9 between the measured (experimental) solar radiation and the simulated ones indicate that the error is low and that the model is 92.6 % accurate in predicting the actual solar radiation on 29 March, 2014.

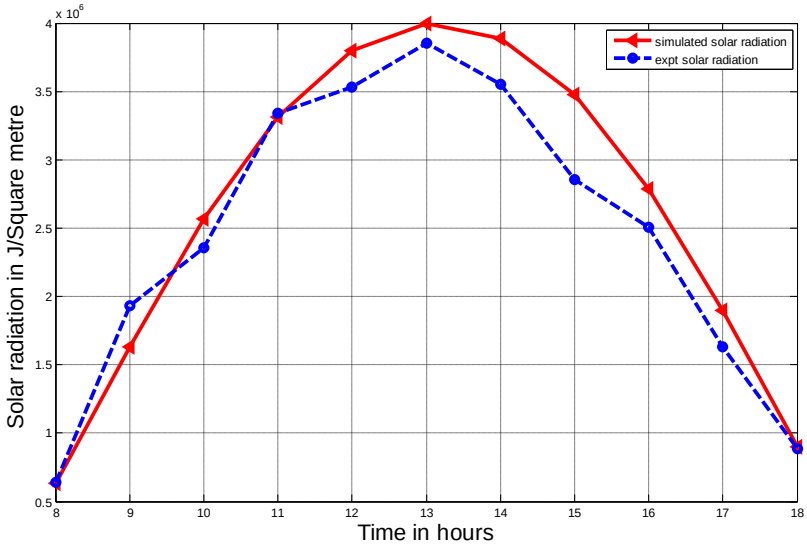

Figure 4.19: Comparison of hourly solar radiation of Zaria recorded during the experiment with the values obtained using TRNSYS 16 software. (29 March, 2014.)

The hourly solar radiation values as predicted by the model are slightly larger than the experimental ones as shown in Figure 4.19.

The experimental and simulated ambient temperature shown in Figure 4.20 also shows the same trend as shown in Figure 4.19.

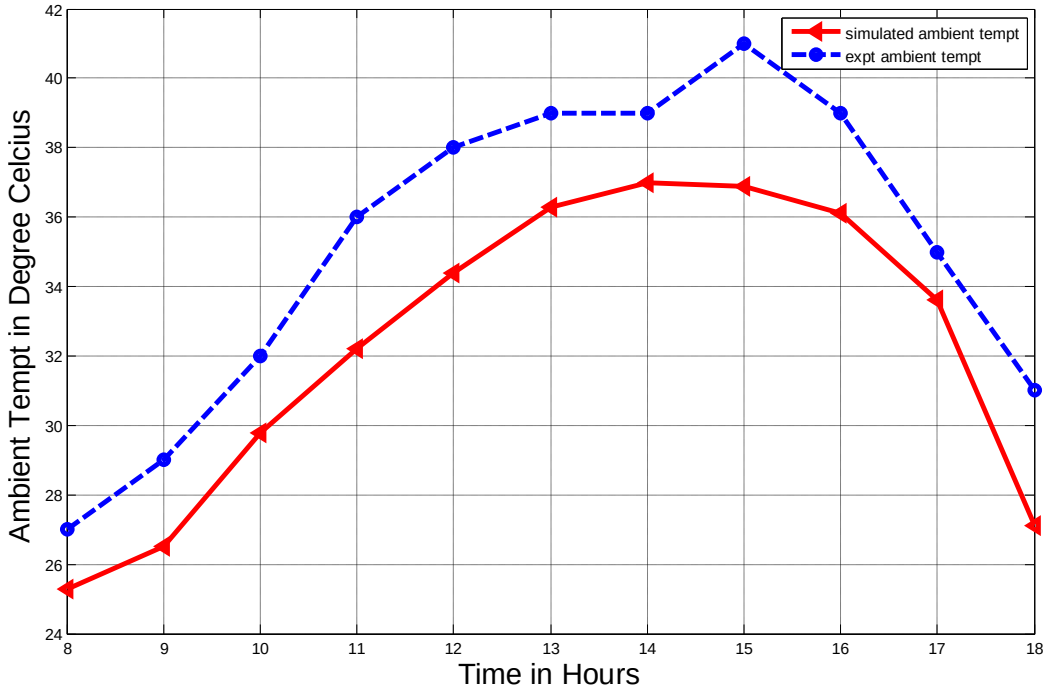

Figure4.20: Comparison of hourly ambient temperature of Zaria recorded during the experiment
with the values obtained using TRNSYS 16 software. (29 March, 2014.)

Figure 4.21 shows the variation of the storage tank and solar collector hourly inlet temperatures recorded during the experiment in comparison with the simulated results. The figure shows an increase in experimental tank inlet temperature from an initial temperature of 38^{o}C at the start of the experiment at 8.00 hours reaching its peak value of 81.5 ^{o}C at 15.00 hours. The figure also reveals that the storage tank inlet temperature started decreasing after 15.00 hours to a value of 55^{o}C at the end of the experiment at 18hours. The variation in hourly collector inlet temperature also follows the same trend, with the maximum temperature of 72 ^{o}C recorded at 16.00 hours. However the computed Root Mean Square Error (RMSE) value of 8.09^{o}C and NSE value of 0.66 as shown in Table 4.6 between the measured (experimental) storage tank inlet temperature and the simulated ones indicate that the error is low (8.09^{o}C) and that the model is 66% accurate in predicting the actual storage tank inlet temperature on 29 March, 2014.

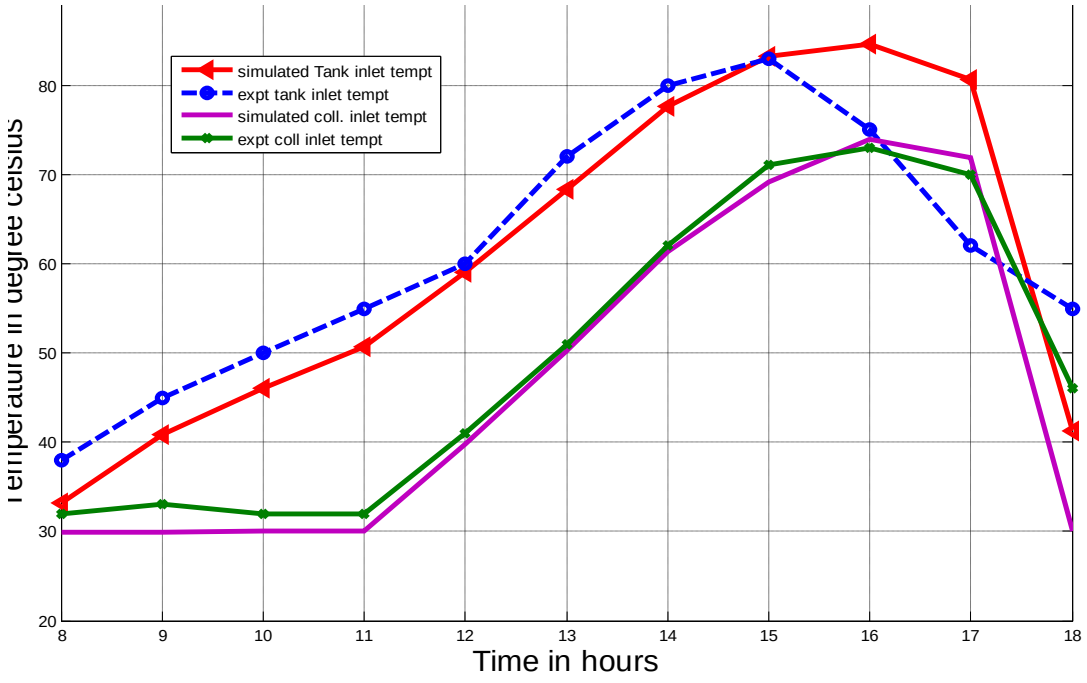

Figure 4.21: Comparison of hourly simulated inlet temperatures of storage tank and solar collector with experimental results (29 March, 2014)

Figures 4.22to 4.24 and Figures 4.25 to 4.27 show the results of the experiment conducted on the 30March and 31 March 2014 respectively in comparison with the simulated results. The results from these figures show very similar trend as those reported on the 29 March 2014.

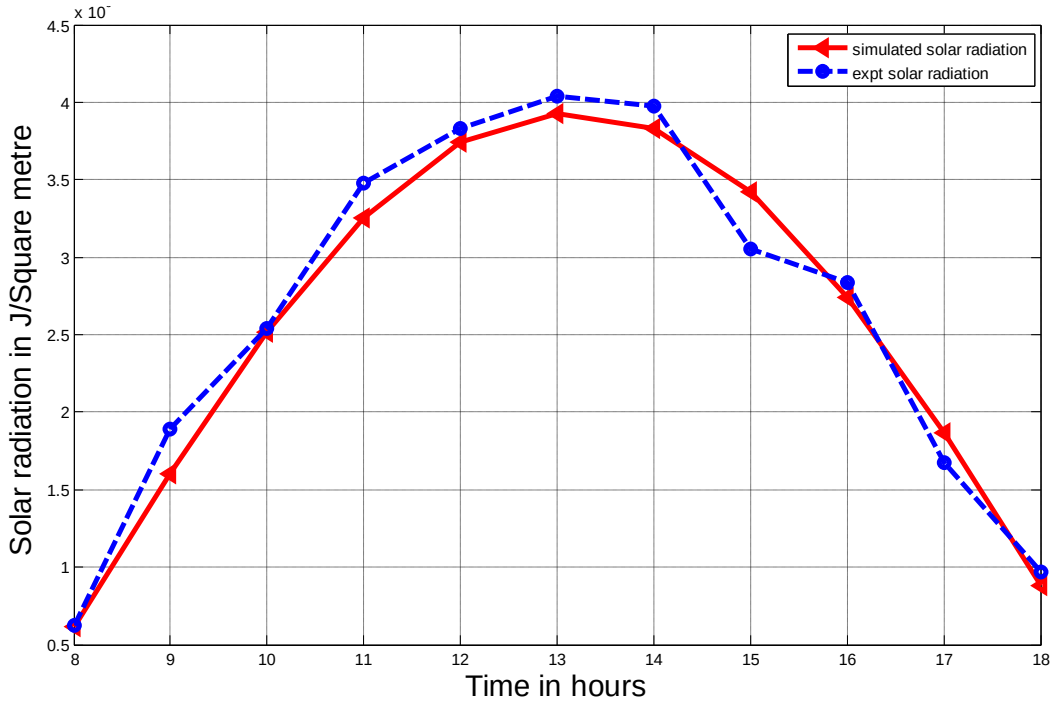

Figure.4.22: Comparison of hourly solar radiation of Zaria recorded during the experiment with the values obtained using TRNSYS 16 software. (30 March, 2014.)

The computed NSE value of 0.956 and of 0.885 as shown in Tables 4.7 and4.8 between the measured (experimental) storage tank inlet temperature and the simulated ones indicate that the model is 95.6% and 88.5% accurate in predicting the actual storage tank inlet temperature on 30th and 31 March, 2014 respectively. The experiments of 30 March and 31March were conducted to ensure that the simulation model could be used to predict the system performance with good repeatability.

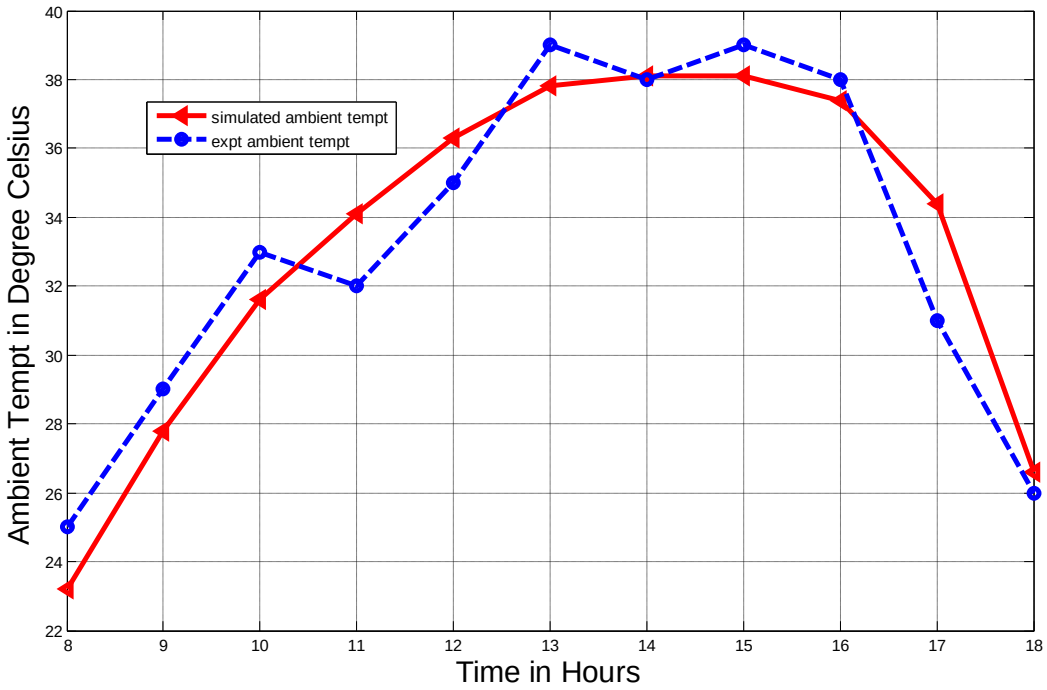

Figure 4.23: Comparison of hourly ambient temperature of Zaria recorded during the experiment

with the values obtained using TRNSYS 16 software. (30 March, 2014.)

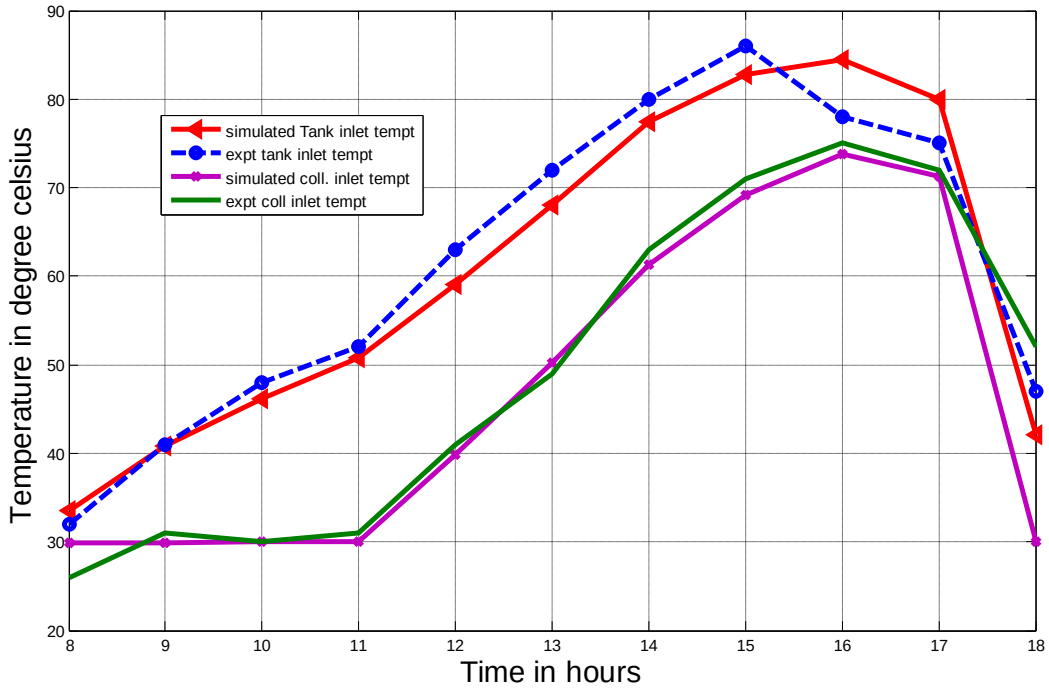

Figure 4.24 Comparison of hourly simulated inlet and outlet temperatures of storage tank and

solar collector with experimental results (30 March, 2014)

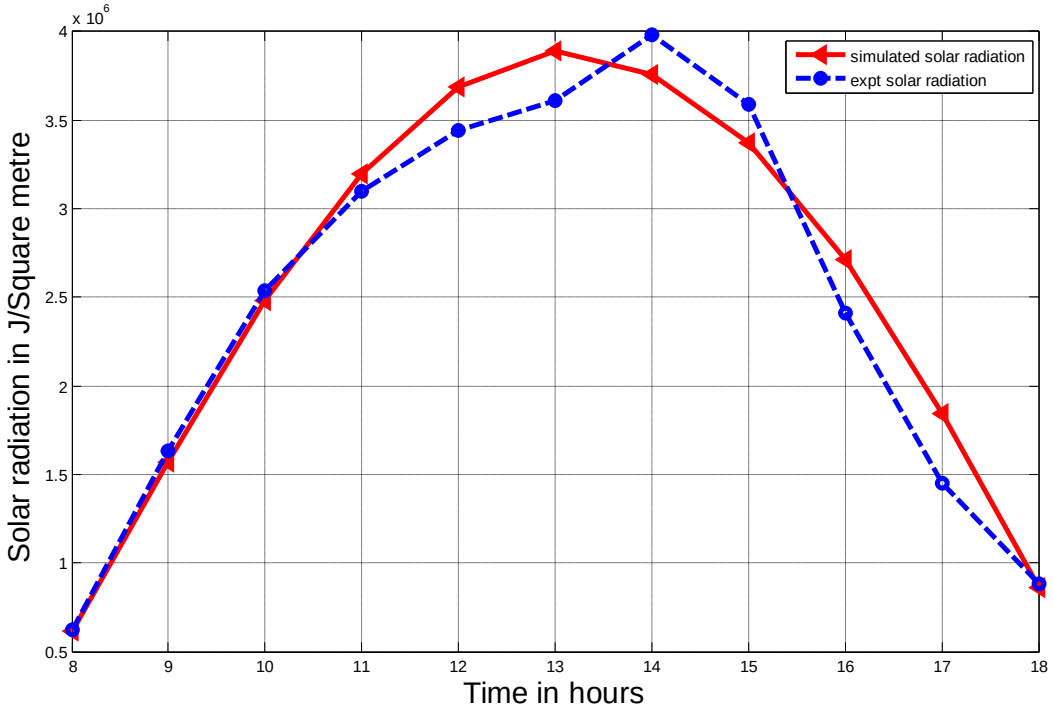

Figure.4.25: Comparison of hourly solar radiation of Zaria recorded during the experiment with

the values obtained using TRNSYS 16 software. (31 March, 2014.)

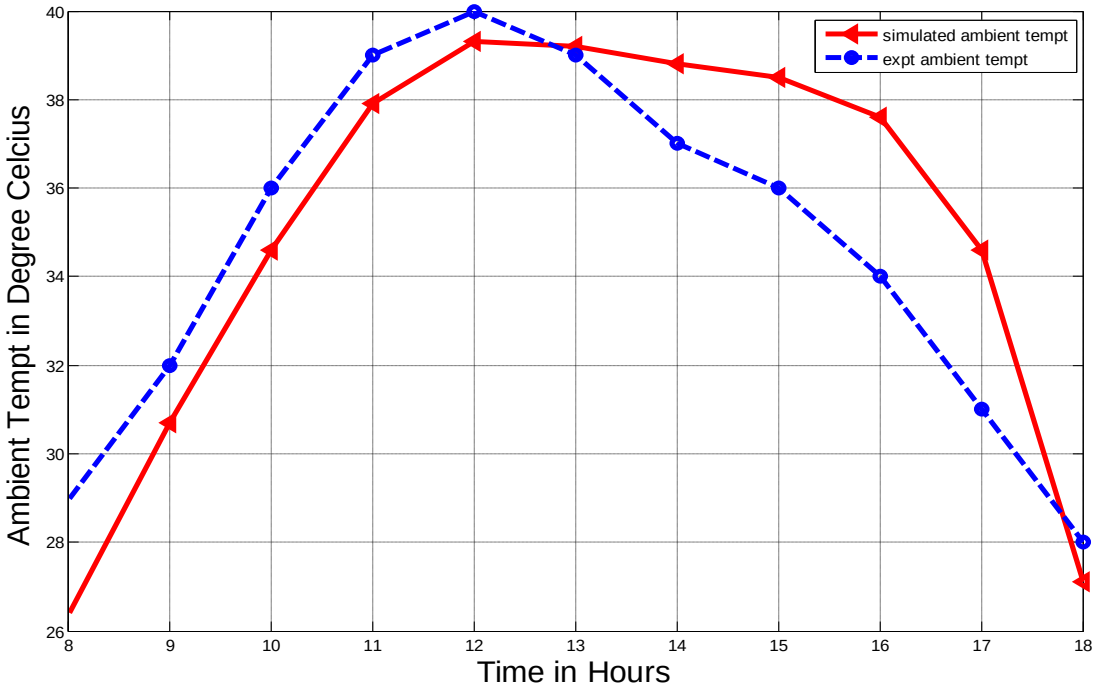

Figure 4.26: Comparison of hourly ambient temperature of Zaria recorded during the experiment

with the values obtained using TRNSYS 16 software. (31 March, 2014.)

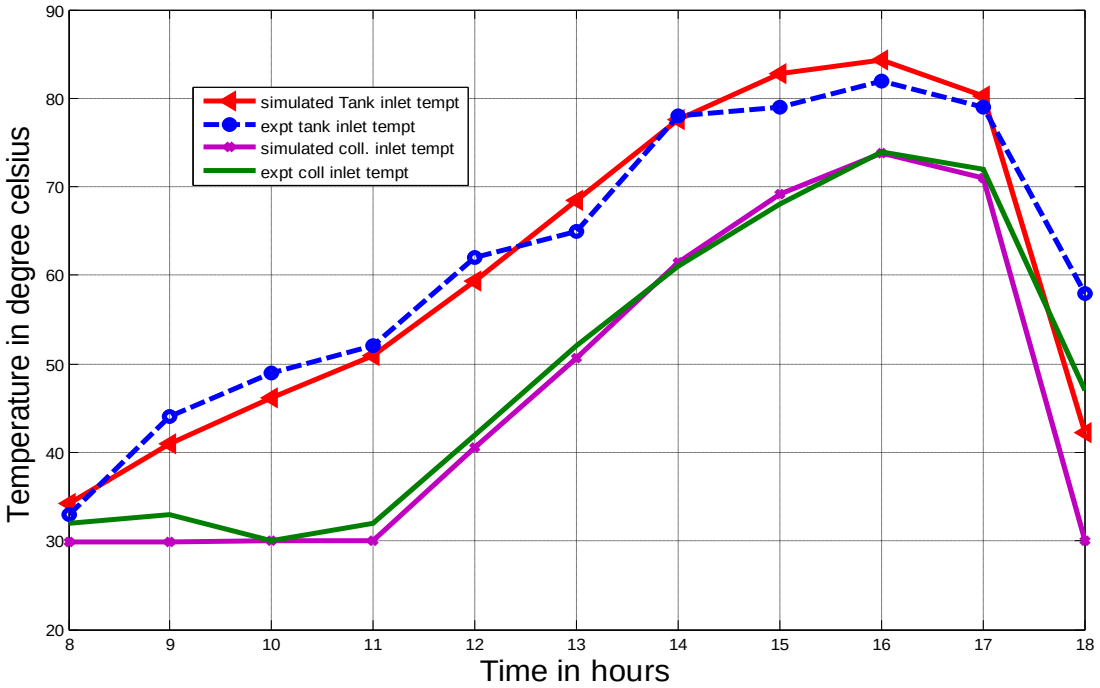

Figure 4.27: Comparison of hourly simulated inlet and outlet temperatures of storage tank and solar collector with experimental results (31 March, 2014)

Figures 4.28 to 4.30 show the temperature variation of the upper and lower glazing of the solar collector recorded during the three days experiment. From the results, it can be seen that the hourly temperature of the upper glazing (T_2 top) is lower than the hourly temperature of the lower glazing (T_1 top) for all the days on which the experiment was conducted. This could be explained from the fact that the double glazing reduces the effect of the wind velocity on the lower glazing thereby greatly reducing the heat lost from the top of the lower glazing due to the wind speed. The implication of this reduction in heat lost from the lower glazing is that the absorber plate temperature is improved thereby improving the thermal efficiency of the system as indicated in by the increase of heat removal factor F_R (Figure 4. 4) of the simulated result.

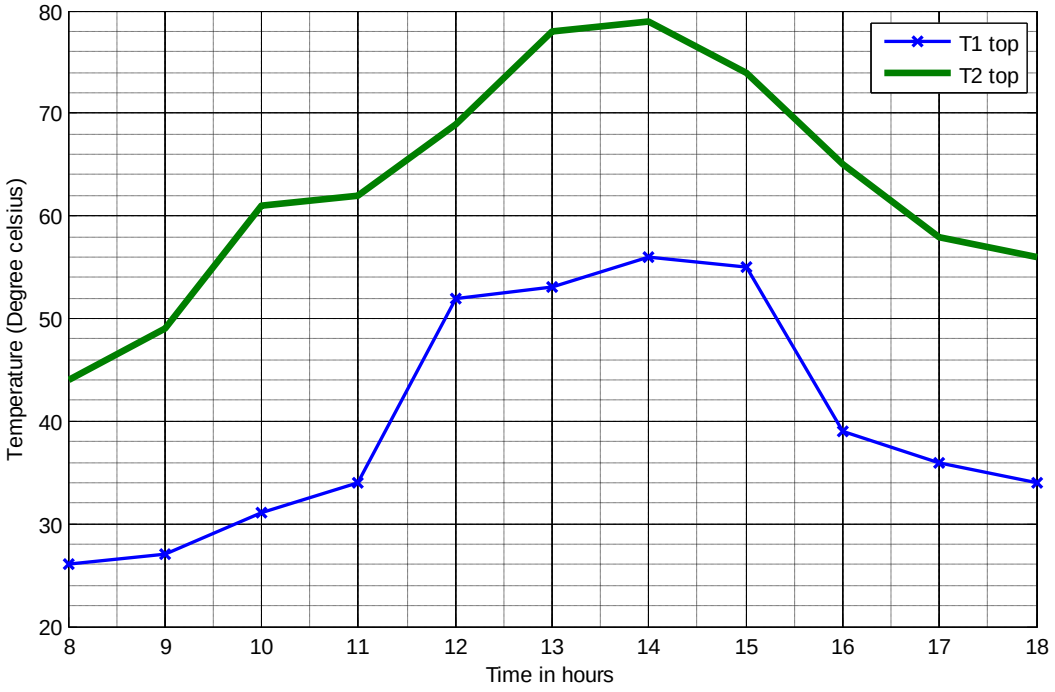

Figure4.28: Hourly temperature variation of the top surface of the first glazing (T_1 top) and second glazing (T_2 top) recorded during the experiment on 29 March, 2014

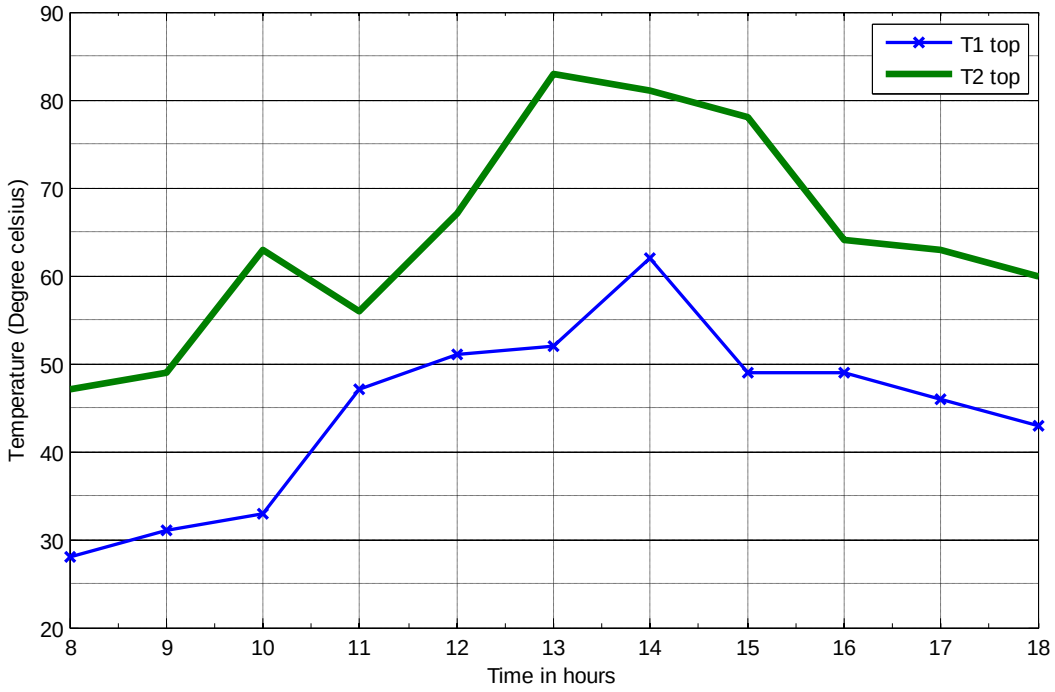

Figure 4.29: Hourly temperature variation of the top surface of the first glazing (T_1 top) and

second glazing (T_2 top) recorded during the experiment on 30 March, 2014

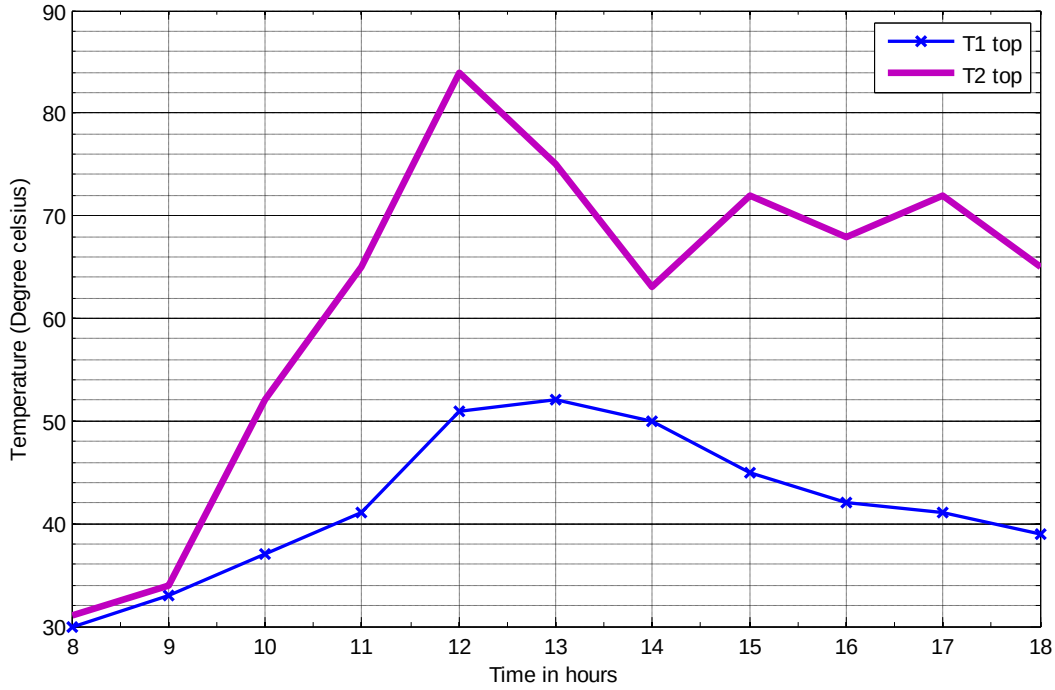

Figure4.30: Hourly temperature variation of the top surface of the first glazing (T_1 top) and second glazing (T_2 top) recorded during the experiment 31 March, 2014

4.4.2. Analysis of the predictive power of the simulation software (TRNSYS 16)

Tables 4.6 to 4.8 show the results of statistical analysis (RMSE and NSE) employed to analyse the predictive power of the system model (TRNSYS 16) based on the simulated and experimental storage tank inlet temperature obtained on the 29 to 31 March, 2014 respectively.

The result of Table 4.6 shows a RMSE value of 8.06^{o}C and a NSE value of 0.667 between the model and the experimental results. This RMSE value means that the error between the experimental storage tank inlet temperature and the simulated storage tank inlet temperature is 8.06 ^{o}C. The NSE value of 0.667 indicates that the model can predict the hourly storage tank inlet temperature with 66.7 % degree of accuracy. This also implies good quality of fit between the experimental data and the simulated data since the closer the NSE value to 1, the better the predictive power of the model (Julien *et al*, 2013). The analysis in Table 4.7 gives the RMSE and NSE values of 3.64^{o}C and 0.956 respectively. This value again implies that the error between the experimental hourly storage tank inlet

temperature and the simulated ones is 3.64^{o}C. The NSE value of 0.956 indicates that the model can predict the hourly storage tank inlet temperature of 30 March, 2014 with 95.6 % degree of accuracy. Table 4.8 gives the RMSE and NSE values of 5.31^{o}C and 0.885 between the measured hourly storage tank inlet temperature and the simulated ones of 31 March, 2014 respectively. The result also indicates high predictive power of the model since the RMSE is low and the NSE value is positive and approaches 1 (Julien *et al.*, 2013).

Table 4.6: Validation of simulated result with experimental result of 29 march 2014 using the RMSE and NSE statistical tools.

			RMSE Calculation		**NSE Calculation**
Time	**TK_{sim}**	**TK_{expt}**	$[TK_{sim} - TK_{expt}]$	$[TK_{sim} - TK_{expt}]^2$	$[TK_{expt} - \overline{TK}_{expt}]^2$
8.00	**33.20**	**38.00**	-4.80	23.04	545.69
9.00	40.80	45.00	-4.20	17.64	267.65
10.0	46.10	50.00	-3.90	15.21	129.05
11.0	50.70	55.00	-4.30	18.49	40.45
12.0	59.10	60.00	-0.90	0.81	1.85
13.0	68.30	72.00	-3.70	13.69	113.21
14.0	77.60	80.00	-2.40	5.76	347.45
15.0	83.20	83.00	0.20	0.04	468.29
16.0	84.60	75.00	9.60	92.16	186.05
17.0	80.60	62.00	18.60	345.96	0.41
18.0	41.30	55.00	-13.70	187.69	40.45
$\sum_{i=1}^{n}$,	**665.5**	**675.0**		**720.49**	2140.55
Ave.	**60.50**	**61.36**			

$$RMSE = \sqrt{\frac{\sum_{i=1}^{n}[TK_{sim} - TK_{expt}]^2}{n}}$$

$$= \sqrt{\frac{720.49}{11}} = 8.09^{o}\text{C}$$

$$NSE = 1 - \frac{\sum_{i=1}^{n}[TK_{sim} - TK_{expt}]^2}{\sum_{i=1}^{n}[TK_{expt} - \overline{TK}_{expt}]^2}$$

$$= 1 - \frac{720}{2140.55} = 0.66340825$$

Table 4.7: Validation of simulated result with experimental result of 30 march 2014 using the RMSE and NSE statistical tools.

			RMSE Calculation		**NSE Calculation**
Time	**TK_{sim}**	**TK_{expt}**	$TK_{sim} - TK_{expt}$	$[TK_{sim} - TK_{expt}]^2$	$[TK_{expt} - \overline{TK}_{expt}]^2$
8.00	**33.5**	**32.0**	1.50	2.25	856.73
9.00	40.8	41.0	-0.20	0.04	410.87
10.0	46.1	48.0	-1.90	3.61	176.09
11.0	50.8	52.0	-1.20	1.44	85.93
12.0	59.0	63.0	-4.00	16.00	2.99
13.0	68.1	72.0	-3.90	15.21	115.13
14.0	77.4	80.0	-2.60	6.76	350.81
15.0	82.8	86.0	-3.20	10.24	611.57
16.0	84.4	78.0	6.40	40.96	279.89
17.0	80.0	75.0	5.00	25.00	188.51
18.0	42.1	47.0	-4.90	24.01	203.63
$\sum_{i=1}^{n} X$	**665.0**	**674.00**		**145.52**	**3282.18**
Ave.	**60.45**	**61.27**			

$$RMSE = \sqrt{\frac{\sum_{i=1}^{n}[TK_{sim} - TK_{expt}]^2}{n}}$$

$$= \sqrt{\frac{145.52}{11}} = 3.64^{o}\text{C}$$

$$NSE = 1 - \frac{\sum_{i=1}^{n}[TK_{sim} - TK_{expt}]^2}{\sum_{i=1}^{n}[TK_{expt} - \overline{TK_{expt}}]^2} = 1 - \frac{145.52}{3282.18} = 0.9556$$

Table 4.8: Validation of simulated result with experimental result of 31 March 2014 using the RMSE and NSE statistical tools.

			RMSE Calculation		**NSE Calculation**
Time	**TK_{sim}**	**TK_{expt}**	$[TK_{sim} - TK_{expt}]$	$[TK_{sim} - TK_{expt}]^2$	$[TK_{expt} - \overline{TK}_{expt}]^2$
8.00	**34.2**	**33.0**	1.20	1.44	799.19
9.00	41.0	44.0	-3.00	9.00	298.25
10.0	46.2	49.0	-2.80	7.84	150.55
11.0	50.9	52.0	-1.10	1.21	85.93
12.0	59.3	62.0	-2.70	7.29	0.53
13.0	68.5	65.0	3.50	12.25	13.91
14.0	77.6	78.0	-0.40	0.16	279.89
15.0	82.8	79.0	3.80	14.44	314.35
16.0	84.3	82.0	2.30	5.29	429.73
17.0	80.2	79.0	1.20	1.44	314.35
18.0	42.2	58.0	-15.80	249.64	10.69
$\sum_{i=1}^{n} X$	**667.2**	**681.0**		**310.00**	**2697.40**
Ave.	**60.65**	**61.91**			

$$RMSE = \sqrt{\frac{\sum_{i=1}^{n}[TK_{sim} - TK_{expt}]^2}{n}}$$

$$= \sqrt{\frac{310.00}{11}} = 5.31^{o}\text{C}$$

$$NSE = 1 - \frac{\sum_{i=1}^{n}[TK_{sim} - TK_{expt}]^2}{\sum_{i=1}^{n}[TK_{expt} - \overline{TK}_{expt}]^2}$$

$$= 1 - \frac{310.00}{2697} = 0.8850$$

Table 4.9: Computation of RMSE and NSE values between the simulated solar radiation and experimental solar radiation of 29 March 2014.

			RMSE Calculation		NSE Calculation
Time	R_s **(kJ/hr.m^2)**	R_{exp} **(kJ/hr.m^2)**	$[R_s - R_{exp}]$ **(kJ/hr.m^2)**	$[R_s - R_{exp}]^2$ **(kJ/hr.m^2)**	$[R_s - \overline{R}_{exp}]^2$ **(kJ/hr.m^2)**
8.00	6.35E+05	6.43E+05	-8.43E+03	7.11E+07	3.31E+12
9.00	1.63E+06	1929600	-2.96E+05	8.75E+10	2.83E+11
10.0	2.57E+06	2356050	2.16E+05	4.66E+10	1.12E+10
11.0	3.31E+06	3337750	-2.43E+04	5.90E+08	7.67E+11
12.0	3.80E+06	3531250	2.72E+05	7.38E+10	1.14E+12
13.0	4.00E+06	3854000	1.42E+05	2.01E+10	1.94E+12
14.0	3.89E+06	3553750	3.34E+05	1.11E+11	1.19E+12
15.0	3.48E+06	2852100	6.23E+05	3.89E+11	1.52E+11
16.0	2.79E+06	2508800	2.82E+05	7.98E+10	2.20E+09
17.0	1.90E+06	1630400	2.69E+05	7.25E+10	6.91E+11
18.0	9.00E+05	884700	1.56E+04	2.44E+08	2.49E+12
$\sum_{i=1}^{n}$	2.89E+07	2.71E+07	1.83E+06	8.81E+11	1.20E+13
Ave.	2.63E+06	2.46E+06	1.66E+05	8.01E+10	1.09E+12

$$RMSE = \sqrt{\frac{\sum_{i=1}^{n}[TK_{sim} - TK_{expt}]^2}{n}}$$

$$= \sqrt{\frac{8.81E+11}{11}} = 283022 \text{ kJ/hr.m}^2$$

$$NSE = 1 - \frac{\sum_{i=1}^{n}[TK_{sim} - TK_{expt}]^2}{\sum_{i=1}^{n}[TK_{expt} - \overline{TK}_{expt}]^2}$$

$$= 1 - \frac{8.81E+11}{1.09E+12} = 0.926$$

CHAPTER FIVE

SUMMARY, CONCLUSIONS AND RECOMMENDATIONS

5.1 Summary

A thermosyphon solar water heating system to supply 100 litres at a minimum temperature of 59^{o}C has been successfully designed, simulated, constructed and tested in the Department of Mechanical Engineering, Ahmadu Bello University (A.B.U) Zaria, Nigeria (latitude 11.2^{o}N and longitude 7.8^{o} E).The design approach was in three parts; firstly the typical meteorological year (TMY) solar data of Zaria was processed to obtain the monthly average daily solar radiation of Zaria for recommended average day of the months. The month of August with the worst amount of the average daily solar radiation was considered as the design month and solar radiation and weather data of this month was used as input data for system design and parametric studies.

Secondly, a parametric studies which studies the effect and sensitivity some selected system components (i.e copper tube diameter, number of glass covers, absorber plate thickness, and centre to centre tube distance) on the design objective function (the heat removal factor. F_R) were studied through programs written in MATLAB programming language in order to determine the appropriate components size for each component based on solar radiation for the design month.

Thirdly the annual performance (collector and storage tank temperature) of the system was simulated under weather data of Zaria using TRNSYS 16 software. The system was then constructed based on the component sizes and system dimensions used for the simulation of the system. A 3 day test was conducted to experimentally evaluate the performance of the system and the results were compared with the simulated results. The RMSE and NSE

statistical tools were employed to compare the experimental results with the simulated results in order to determine the predictive power of the simulation software.

5.2 Conclusions

The results of this research led to the following conclusions**:**

1 A thermosyphon solar system with collector area of 2.24 m^2 and tilted at angle of 12^o to the horizontal operated under the weather condition of Zaria, would be capable of producing daily domestic hot water of 0.1m^3 at a minimum temperature of 59^{o}C at the end of the day for the worst month and 81^{o}C for the best month.

2 The parametric study reveals that for a solar collector with collector area of 2.24m^2 and collector tubes diameter of 0.2m,the heat removal factor is affected in the following ways:

   i. The heat removal factor, F_R,for a tube diameter of 0.03m increases from a minimum value of 0.446, reaching a maximum value of 0.575 representing an increase of 28.92 % as the tube centre to centre distance, W, was increase from 0 to 0.3m. Further increase in W from 0.3m to 2.0m, decreased the heat removal factor from a value of 0.575 to 0.350 representing a drop of 39.13%.

   ii. The heat removal factor increases from a value of 0.6178 to 0.6195 as the plate thickness increases from 0.003m to 0.075m. The increase in F_R represents an insignificant increase of 0.31% in heat removal factor..

3 The computed values of Nash-Sutcliff coefficient of 0.663, 0.956 and 0.885 and the low RMSE values of 8.09^{o}C, 3.64^{o}C and 5.31 ^{o}C between the modeled tank inlet temperature and the observed tank inlet temperature for the three day test confirm that the model formulation using TRNSYS software proposed here for the

performance simulation of the system is valid, realistic and is a representative of the real system and can be used confidently to estimate the dynamic behavior of the real system owning to the good quality of fit between experimental results and the simulated results.

4 The collector hourly average efficiency varied with time. The efficiency increased from 16.5% in the morning (8.00 hours) to 66.1% at 10.00 hours and decreased to a value of 19.0 % at the end of the day (17 hours).

5.3 Recommendations

The absorber plate of the solar collector in this study was placed above the copper tubes carrying the circulating water. It would be important here again to recommend that an investigation should be conducted to know if the absorber plate placed below the collector copper tube will give better performance of the system.

It is also recommended that the annual life cycle savings (ALCS) analysis should be conducted so as to compare the difference between the overall cost of a conventional plant that supplies all the desired hot water, and the overall cost of the solar water heating system so as to justify the huge capital investment in the solar system.

.

REFERENCES

Alireza, H. and Kamran, S. (2009). Optimal design of a forced circulation solar heating system

for a residential unit in cold climate using TRNSYS. *Solar Energy*, 83 (5) ,700–714.

Alternative Energy Tutorials. (2012). *Alternative and Renewable energy.* Retrieved July 20,

2012 from http://www.alternative-energy-tutorials.com/.

Anna, H. (2006). *Conceptual design of a solar-thermal heating system with seasonal storage for*

avashon greenhouse. (Unpublished master's thesis) University of Washington. Retrieved January 20. 2012, from **http://f**aculty.washington.edu/malte/pubs/Anna_Thesis.pdf.

Buckles, W.E., and Klein, S.A. (1980). Analysis of solar domestic hot water heaters. *Solar Energy, 25* (5), 417–424.

Belessiotis, V., and Mathioulakis, E. (2002). Analytical approach of thermosyphon solar domestic hot water system performance. *Solar Energy*. *3* (72), 7–15.

Brian, R. H., Ronald L. L., and Jonathan, M. R. (2001). *A guide to MATLAB*: for *beginners and*

experienced users. Cambridge University Press *New York, NY, USA.*

Chaurasia P.B.L. and Twidell J.W. (2001). Collector cum storage solar water heaters with and

without transparent insulation material, *Solar Energy*, 70 (5), 403-416,

Christopher, A. , and Homola, P.E . (2006).*Solar domestic hot water heating systems design,*

installation and maintenance. Retrieved January 20, 2012, from http://www.solar-rating.org.

Duffie, J.A. and Beckman, W.A (1991).*Solar engineering of thermal processes*, 2nd Edition,

Toronto: John Wiley and Sons.

Delfín, S. S., Carlos R. E., and Valentín,C .H. (2000).*Simulation of a solar domestic water heating system, with different collector efficiencies and different volume storage tanks*. Retrieved March 13, 2011 from http://sel.me.wisc.edu.

Fallziah, S., and Balbir, S. M. (2003).Simulation of convective heat transfer coefficient in the

receiver tube of a parabolic trough concentrator.

Fanney, A,H, and Klein S.A (1985). Thermal Performance Comparisons for Solar Hot Water

System Subjected to Various collector array flow rate. *Proceeding of Inyersci*. 85, Montreal, Canada

Govind, N.K., Shireesh, B.K., and Santanu, B. (2008). Design of solar thermal systems utilizing

pressurized hot water. *Solar Energy*, *82* (23), 686–699.

Govind N. K, Shireesh B. K, and Santanu B. (2006) Determination of design space and optimization of solar water heating systems. *Solar Energy, 32* (6), 263-276.

Hay, J.E., Davies, J.A., 1980. Calculations of the solar radiation incident on an inclined surface.

In: Hay, J.E., Won, T.K. (Eds.), Proc. of First Canadian Solar Radiation Data Workshop, 59. Ministry of Supply and Services, Canada.

Incropera, F.P., DeWitt, D.P, Bergman, T.L., and Lavine, A.S.(2007). *Fundamentals of heat and*

mass transfer, 6th Ed., Hoboken : NJ, John Wiley & Sons,

ISO 9459-3:1997(E). (1997). *Performance tests for solar plus supplementary systems. international standards organization*, Geneva, Switzerland.

Intergovernmental Panel on Climate Change (IPCC). (2001). *IPCC third assessment report on*

climate change: Summary for policy makers. Geneva, Switzerland.

Jae-Mo, K. (1999). *Development of a flat plate solar collector design programme*. (Doctoral dissertation, University of Wisconsin). Retrieved March 13, 2011 from http://sel.me.wisc.edu/theses.

Julien, G. A, Emmanuel, L., Clément, A., Rufin, O. A., and Brice, A. S. (2013). Modeling solar

energy transfer through roof material in Africa Sub-Saharan Regions. *ISRN Renewable Energy 34(7), 632-645*.

Jaime, (2009).An improved and extended general correlation for heat transfer during Condensation in plain tubes. *American Society of Heating, Refrigerating and Air-Conditioning Engineers, 15 (5), 225-237,*

Kudish, A.I., Santamaura, P., and Beaufort, P.(1985). Direct measurement and analysis of thermosyphon flow. *Solar Energy*,35 (23), 167-173.

Klucher (*1979).* A refinement of the diffuse sky radiation. *Solar Energy*, 2, (23), 93-184

Beckman W.A.,Mitchell J.W.,Duffie.J.A.,Duffie. N.A., and Freeman T.L. (2004).*TRNSYS Simulation software and its utility programs*. Retrieved March 13, 2011 from http://sel.me.wisc.edu/trnsys.

Kulkarni, G.N., Kedare, S.B., and Bandyopadhyay, S. (2006). The concept of design space for

sizing solar hot water systems. *Solar Energy, 12*(3), 283-298.

Koffi, P.M.E., Andoh, H.Y., Gbaha P., Toure S., and Ado G. (2008).Theoretical and experimental study of solar water heater with internal exchanger using thermosiphon system .*Energy Conversion and Management,49* (23), 2279–2290.

Mryna , B. (1997). *High performance in low flow solar domestic hot water system.* (Unpublished master's thesis, University of Wisconsin) Retrieved March 13, 2011 from http://sel.me.wisc.edu/theses.

Mirunalini, T., Iniyan ,S., and Ranko, G. (2010). A review of solar thermal technologies. *Renewable and Sustainable Energy Reviews*, 14, (3) 312–322

Morrison, G.L., and Braun, J.E. (1985).System modeling and operation characteristics of thermosyphon solar water heaters. *Solar Energy*; 34 (24), 389-405.

Neil, J. S.(2010). *Encyclopedia of research design*. Online ISBN: 9781412961288 | Publisher: SAGE Publications, Inc.

Pierson, P., Javelas, R. (1983). Theoretical and experimental study of a natural circulation type

solar water heater with exchanger. *Re´v Ge´nThermique*; 259 (21), 67–82.

Qin L. (1998). *Analysis modeling and optimum design of solar domestic hot water system*. (Doctoral dissertation, University of Wisconsin).Retrieved March 13, 2011 from http://sel.me.wisc.edu/theses.

Rai, G.D. (2008). *Solar energy utilization: A text book for engineering students.* 5th Edition,

Delhi, Khanna.

Rhushi, P.R., Byregowda, H.V., and Gangavati, P.B. (2010). Experimental analysis of flat plate.

European Journal of Scientific Research, 53 (23), 57-64. Retrieved January 20, 2012 from http://www.eurojournals.com/ejsr.htm.

Rhushi, P.R., Byregowda, H.V., Gangavati, P.B., andShankaran K. P. (2011). Performance analysis of a solar water heater with flat plate collector using computer program. *European Journal of Scientific Research, 53* (23), 67-79. Retrieved Jan 20th 2012 from http://www.eurojournals.com/ejsr.htm

Retscreen Internatinal. (2004). *Solar water heating project analysis*. Retrieved January 20,

2012 from http//:www.redscreen.net

Reindl, D.T., Beckman,W.A., and Duffie, J.A. (1990). Evaluation of hourly tilted surface radiation models. *Solar Energy, 45*(9), 9–17.

Soteris, A.K (2004) Environmental benefits of domestic solar energy systems.

Energy Conversion and Management 45 (3), 3075–3092

Suleiman B.T. (2011). Modeling and simulation of a solar poweredadsorption refrigeration system.(Unpublished doctoral dissertation, of Ahmadu Bello University, Zaria.)

Soteris, A.K., and Christos P. (2000).Modeling of a thermosyphon solar water heating system

and simple model validation *Renewable Energy 21* (2000) 471-493. Retrieved October 20, 2012 from http//: www.elsevier.com/locate/renene

Shariah, A.M, andShialabi B.(1997). Optimal design for a thermosyphon solar water heater.

Renewable Energy, 11 (12), 351-361.

Unified Facilities Criteria (UFC), (2004). *Solar heating of buildings and domestic hot water*

Retrieved January 20, 2012 from http://dod.wbdg.org/.

www.eere.energy.gov. Retrieved October 20, 2012.

Young, D.K., Kyaw, T., Hitasha, K.B., Charanjit S.B., and Kim, C.N. (2012). Thermal analysis

and performance optimization of a solar hot water plant with economic evaluation. *Solar Energy*, 86 (7), 1378–1395 Retrieved October 20, 2012 from http//: www.elsevier.com/locate/solener.

APPENDIX A

SYSTEM DESIGN PROGRAMME CODES DEVELOPED USING MATLAB

```
clearall
T_L=70    %system design load temperature in degrees
Gsc=1367    % solar constant
beta=11.2    %collector tilt angle
LAT=11.2    % latitude of location(Zaria)
n1=1.51     %refractive index of glass
N=1     %number of glass
KL=0.0736 %glass extinction coefficient and length product
abst=0.98%plate absorbtance
rho_g=0.2 %ground reflectance
K_ins=0.04 %thermal conductivity of insulation material
Ep=0.96 %plate emmittance
Eg=0.88  %glass emmittance
zegma=5.67e-8 %Boltzman constant
density=1000 % density of water
volume=0.13 %volme of water
Cp=4190  %specific heat of water
Kb=0.04 %thermal conductivity of back insulation mat.
tb=50/1000 %back insulation thickness
Ke=0.04  %thermal conductivity of edge insulation mat
t_e=40/1000%edge thickness
y=120/1000 %hight of collector case
L=2000/1000 %length of collector
t_ins=30/1000 %back thickness
D_o=25/1000 %ext. dia. of collector tube
Di=20/1000  %internal. dia. of collector tube
K_p=211   %thermal conductivity of plate
Delta_p=5/1000 %plate thickness
W=50/1000 %center to center distance of tubes
h=1.2     %hight of tank
d=420/1000  %diameter of tank
Kt_ins=0.04
T_ins_t=50/1000 % tank insulation thickness
 DT=42/100 %tank diameter.
n=[17 47 75 105 135 162 198 228 258 288 318 344]'   %recomended days of the months
M=[1 2 3 4 5 6 7 8 9 10 11 12] %number of months in a year
P=pi/180
DLTA=23.45*sin(2*pi*((n+284)/365)%formula for monthly declination
w_s=(acos(-tan(LAT*P)*tan(DLTA*P)))*1/P %monthly sunset angle
w_sb=(acos(-tan((LAT-beta)*P)*tan(DLTA*P)))*1/P
w_s1=min(w_s,w_sb) %minimum of line 8 and 9.
A1=86400*Gsc/pi;
A2=(1+0.033*cos(360*n*P/365));
A3=cos(LAT*P).*cos(DLTA*P).*sin(P*w_s)+(pi.*w_s*sin(P*LAT).*sin(P*DLTA)/180);
Ho=A1.*A2.*A3 % calculation of extraterestetial radiation
% H next line is the measured values of monthly average daily solar radiation on
H=[22.6584  24.8544  27.0252  28.2096  18.0144  23.6448  18.125  16.0956  24.3108  22.2516  21.5352
22.2371]'*1e6
KT= H./Ho % clearness index
% calculation of radiation on tilted surface.
Hb=[18.4258  19.8700  21.4865  19.9061  12.50052  12.2875  10.8131  8.4917  11.3271  14.8025  17.2977
17.1816]'*1e6
Hd=H-Hb
```

```
Rb1=cos((LAT-beta)*P).*cos(DLTA*P).*sin(w_s1*P)
Rb2=(pi/180).*w_s1*sin((LAT-beta)*P).*sin(DLTA*P)
Rb3=cos(LAT*P).*cos(DLTA*P).*sin(w_s*P)
Rb4=(pi/180)*w_s.*sin(LAT*P).*sin(DLTA*P)
Rb=(Rb1+Rb2)./(Rb3+Rb4)
HT1=H.*(1-(Hd./H)).*Rb+Hd*(1+cos(P*beta))/2
HT2=H.*0.2*(1-cos(P*beta))/2
HT=HT1+HT2
Teta=[43;
41 ;
    37.5;
    38.9;
41.2 ;
43.0 ;
42.5 ;
39.5 ;
37.5 ;
39.5 ;
    41;
    43]
 a1=sin(P*Teta)
Teta_r=asin(a1/n1)*(1/P)
rho_p=(sin(P*(Teta_r-Teta))).^2./(sin(P*(Teta_r+Teta))).^2
rho_pp=(tan(P*(Teta_r-Teta))).^2./(tan(P*(Teta_r+Teta))).^2
rho=(rho_p+rho_pp)/2
 tao_rho1=(1-rho_pp)./(1+(2*N-1)*rho_pp)
 tao_rho2=(1-rho_p)./(1+(2*N-1)*rho_p)
tao_rho=(tao_rho1+tao_rho2)/2
tao_a=exp(-N*KL./cos(P*Teta_r))
tao=tao_rho.*tao_a
tao_ab=tao*abst./(1-(1-abst)*rho_g)
Teta_d=59.7-0.1388*beta+0.001479*beta^2 % incident angle of diffuse radiation
Teta_g=90-0.5788*beta+0.002693*beta^2 % incident angle of reflected radiation
%%%%%%%%%%%%%%%%%%%%%%%%%%%%%%%%%%%%%%%%%%%
 a1d=sin(P*Teta_d)
Teta_rd=asin(a1d/n1)*1/P
 rho_pd=(sin(P*(Teta_rd-Teta_d))).^2./(sin(P*(Teta_rd+Teta_d))).^2
 rho_ppd=(tan(P*(Teta_rd-Teta_d))).^2./(tan(P*(Teta_rd+Teta_d))).^2
rhod=(rho_pd+rho_ppd)/2
 tao_rho1d=(1-rho_ppd)./(1+(2*N-1)*rho_ppd)
 tao_rho2d=(1-rho_pd)./(1+(2*N-1)*rho_pd)
tao_rhod=(tao_rho1d+tao_rho2d)/2
tao_ad=exp(-N*KL./cos(P*Teta_rd))
taod=tao_rhod.*tao_ad
tao_abd=taod*abst./(1-(1-abst)*rho_g)
%%%%%%%%%%%%%%%%%%%%%%%%%%%%%%%%%%%%%%%%%%%%%%%%%%%%%%%%%%%%%%%%%%%%%
%%%%%%%%%
a1g=sin(P*Teta_g)
Teta_rg=asin(a1g/n1)*1/P
 rho_pg=(sin(P*(Teta_rg-Teta_g))).^2./(sin(P*(Teta_rg+Teta_g))).^2
 rho_ppg=(tan(P*(Teta_rg-Teta_g))).^2./(tan(P*(Teta_rg+Teta_g))).^2
rhog=(rho_pg+rho_ppg)/2
 tao_rho1g=(1-rho_ppg)./(1+(2*N-1)*rho_ppg)
 tao_rho2g=(1-rho_pg)./(1+(2*N-1)*rho_pg)
tao_rhog=(tao_rho1g+tao_rho2g)/2
tao_ag=exp(-N*KL./cos(P*Teta_rg))
taog=tao_rhog.*tao_ag
```

```
tao_abg=taog*abst./(1-(1-abst)*rho_g)
 SR1=Hb.*Rb.*tao_ab
 SR2=Hd*tao_abd*(1+cos(P*beta))/2
 SR3=H.*rho_g*tao_abg*(1-cos(P*beta))/2
 SR=SR1+SR2+SR3
t_a_pd=SR./HT
Tmax=[38 38 40 32 35 32 26 28 32 36 35 33]'
Tmin=[16 16 20 15 22 29 18 18 20 20 18 17]'
 Ti=Tmax
 V=[2.6 2.57 2.70 2.31 2.8 3.5 2.91 3.08 1.56 2.57 3.39 2.0]'
hw=2.8+3*V
 Uo1=(1/(2*pi*K_ins))*log(1+2*t_ins/D_o)
 Uo2=1./pi*(D_o+2*t_ins).*hw
Uo=(1./(Uo1+Uo2))
Tpm=Ti+25
 Tpm1=Tpm+273
 Ta=Tmax
Tat=[30.67 29.12 30.66 31.22 27.37 28.44 22.68 25.54 27.65 26.28 27.50 26]'
 Ta1=Ta+273
 f=(1+0.089*hw-0.1166.*hw*Ep)*(1+0.07866*N)
 C=520*(1-0.000051*beta^2)
 e=0.430*(1-(100./Tpm1))
 U_top1=((C./Tpm1).*((Tpm1-Ta1)./(N+f)).^e)+1./hw
 U_top2=(N./U_top1).^-1
 U_top3=zegma*(Ta1.^2+Tpm1.^2).*(Ta1+Tpm1)
 U_top4=(1./(Ep+0.00591*N*hw))+((2*N+f-1+0.133*Ep)/Eg)-N
U_top=U_top2+U_top3./U_top4
U_back=Kb/tb
U_tb=U_top+U_back
%calcualtion of sensible heat requirement
mass=density*volume
 Qs=mass*Cp*(T_L-Ti)
Qc_loss=U_tb*12*3600.*(Tpm-Ta)% collector heat loss
Qu=SR-U_tb.*12*3600.*(Tpm-Ta)  % collector usefull energy
 Ac=(Qs./Qu)% calculation of collector area.
 R_DM=SR./Qs
 R_DM2=HT./Qs
W_c=Ac./L
Ae=2*y*(L+W_c)
U_e=Ke*Ae./(t_e*Ac)
 U_L=U_top+U_e+U_back
 Qu2=SR-U_L.*12*3600.*(Tpm-Ta)
 Ac2=Qs./Qu2
Tfm=Ti
density=1001-0.08832*Tfm-0.003417*Tfm.^2
 KV=((1./(0.5155+0.0192*Tfm))-0.12)*1e-6 %kinematic viscocity
K_f=0.557+0.002198*Tfm-0.00000708*Tfm.^2% fluid thermal conductivity
 D_V=density.*KV %dynamic viscocity
Pr=Cp*D_V./K_f
mdot=150/(12*3600)
 Re=4*mdot./(pi*Di*D_V)
if Re>2100
fn=(1.82.*log10(Re)-1.64).^(-2)
   K_1=1+1.3*fn
   Pr_1=Pr.^0.333
   K_2=11.7+(1.8./Pr_1)
   NuD1=(fn./8).*Re.*Pr
```

```
  NuD2=K_1+K_2.*(fn/8).^(1/2).*(Pr.^(2/3)-1)
NuD=NuD1./NuD2 %nusset number
elseif Re<2100
    NuD1=0.0534*((Re.*Pr.* Di)./L).^1.15
    NuD2=1+0.0335*((Re.*Pr.*Di)./L).^0.82
NuD=3.7+(NuD1./NuD2)
else
NuD=0
end
h_fi=(K_f.*NuD)./Di
 m=((U_L./(K_p*Delta_p))).^0.5
 F=tanh(m*(W-Di)/2)./(m*(W-Di)/2) %fin efficiency
 F_prime1=1./U_L
 F_prime2=W.*(1./((U_L.*(Di+(W-Di).*F))+1./(pi.*Di* h_fi )))
F_prime=F_prime1./F_prime2
F_R1=(mdot.*Cp)./(Ac.*U_L )
F_R2=exp(-(Ac.* U_L.*F_prime)./(mdot.*Cp))
F_R=F_R1.*(1-F_R2) % heat removal factor
A_st=1.845*(2+h/DT)* volume^(2/3)%surface area of tank
% calculation of heat lost coeeficient of TANK
 UT1=(1/(2*pi*Kt_ins))*log(1+2*T_ins_t/D_o)
 UT2=1./pi*(DT+2*T_ins_t).*hw
U_st=(1./(UT1+UT2)) % daily tank lost coefficient
 g=0
```

APPENDIX B

A PARAMETRIC STUDY PROGRAMME CODES WRITTEN IN MATLAB TO STUDY THE EFFECT AND SENSITIVITY OF COLLECTOR TILT ANGLE ON THE TOTAL RADIATION RECEIVED ON COLLECTOR SURFACE.

```
Clear all
Gsc=1367
LAT=11.2
%recomended days of the months
n1=[228]' %recommended Average day of the year
for i=1:length(n1)
beta=0:2:60
P=pi/180                          %factor for the conversion from radian to degree.
DLTA=23.45*sin(2*pi*((n1(i)+284)/365))          %formula for monthly declination
w_s=(acos(-tan(LAT*P).*tan(DLTA*P)))*1/P %monthly sunset angle
w_sb=(acos(-tan((LAT+beta)*P).*tan(DLTA*P)))*1/P
w_s1=min(w_s,w_sb) %minimum of line 8 and 9.
A1=86400*Gsc/pi;
A2=(1+0.033*cos(360*n1(i)*P/365));
A3=cos(LAT*P).*cos(DLTA*P).*sin(P*w_s)+(pi.*w_s*sin(P*LAT).*sin(P*DLTA)/180);
Ho=A1.*A2.*A3 %annual average extrateresterial solar radiation of location
H=[12.6584]*1e6 % monthly average solar radiation for the month of August
KT= H./Ho
g=0
Hd1=0.775+0.00606*(w_s-90)
Hd2=(0.505+0.0045*(w_s-90)).*cos((115*KT-103)*P)
Hd=(Hd1-Hd2).*H
Hb=H-Hd
Rb1=cos((LAT+beta)*P).*cos(DLTA*P).*sin(w_s1*P)
Rb2=(pi/180)*w_s1.*sin((LAT+beta)*P)*sin(DLTA*P)
Rb3=cos(LAT*P)*cos(DLTA*P)*sin(w_s*P)
Rb4=(pi/180)*w_s*sin(LAT*P)*sin(DLTA*P)
Rb=(Rb1+Rb2)/(Rb3+Rb4)
HT1=(H.*(1-(Hd./H)).*Rb+Hd.*(1+cos(P.*beta))/2)'
HT2=(H.*0.2.*(1-cos(P*beta))/2)'
HT=(HT1+HT2)'
plot(beta,HT,'linewidth',2)
xlabel('Collector tilt angle (Degree)','fontsize',12)
ylabel('Solar Radiation on collector surface(J/m2.day)','fontsize',12)
title('Variation of Solar radiation on collector surface','fontsize',12)
holdon
end
holdoff
```

APPENDIX C

A PARAMETRIC STUDY PROGRAMME CODES WRITTEN IN MATLAB TO STUDY THE EFFECT AND SENSITIVITY OF COLLECTOR TUBE DIAMETER AND TUBE CENTRE TO CENTRE DISTANCE ON THE HEAT REMOVAL FACTOR

```
Clear all
k_p=211
u_L=7.4
delta_p=6/1000
 Di=[0.5/100:0.5/100:4/100]'
H_fi=113.13
mdot=0.0035
 AC=(2.2)
for i=1:length(Di)
 W=(5/100:5/100:200/100)'
 m1=((u_L./(k_p*delta_p))).^0.5
 f1=(tanh(m1*(W-Di(i))/2)./(m1.*(W-Di(i))/2))
 f_prime1=1./u_L
 f_prime2=(W.*(1./((u_L.*(Di(i)+f1).*(W-Di(i)))+1./(pi.*Di(i).* H_fi ))))
f_prime=f_prime1./f_prime2
f_R1=(mdot.*Cp)./(AC.*u_L )
f_R2=(exp(-(AC.* u_L.*f_prime)./(mdot.*Cp)))
f_R=(f_R1.*(1-f_R2))
plot(W,f_R,'r','linewidth',2)
xlabel('Center to centre distance of collector tubes (M)')
ylabel('Heat Removal Factor')
title('Variation of Heat Removal Factor')
holdon
end
g=0
```

APPENDIX D

A PARAMETRIC STUDY PROGRAMME CODES WRITTEN IN MATLAB TO STUDY THE EFFECT AND SENSITIVITY OF ABSORBER PLATE THICKNESS E ON THE HEAT REMOVAL FACTOR

```
k_p=211
u_L=7.4
 Di=0.5/100
H_fi=113.13
mdot=0.0035
 AC=(2.2)
delta_p=(5/1000:5/1000:35/1000)'
for i=1:length(delta_p)
 W=(5/100:5/100:200/100)'
 m1=((u_L./(k_p*delta_p(i)))).^0.5
 f1=(tanh(m1*(W-Di)/2)./(m1.*(W-Di)/2))
 f_prime1=1./u_L
 f_prime2=(W.*(1./((u_L.*(Di+f1).*(W-Di))+1./(pi.*Di.* H_fi ))))
f_prime=f_prime1./f_prime2
f_R1=(mdot.*Cp)./(AC.*u_L )
f_R2=(exp(-(AC.* u_L.*f_prime)./(mdot.*Cp)))
f_R=(f_R1.*(1-f_R2))
plot(W,f_R,'r','linewidth',2)
xlabel('Center to centre distance of collector tubes.W(m)')
ylabel('Heat Removal Factor')
title('Variation of Heat Removal Factor')
holdon
end
```

APPENDIX E

A PARAMETRIC STUDY PROGRAMME CODES WRITTEN IN MATLAB TO STUDY THE EFFECT AND SENSITIVITY OF NUMBER OF GLASS COVERS ON THE HEAT REMOVAL FACTOR

```
k_p=211
Di=1.5/100
hfi5=113.13
mdot=0.0035
AC=(2.2)
Ae5=0.511
abst=0.90
rho_g=0.2
beta5=11.2
hw5=10.4
V5=2.4
Tpm5=70+273
Ta5=311
Ep=0.95
zegma=5.67e-8
W=10/100
Ng=(1:1:10)'
f5=(1+0.089*hw5-0.1166*hw5*Ep )*(1+0.07866*Ng)
C =520*(1-0.000051*beta5^2)
e=0.430*(1-100/Tpm5)
U_top51=((C./Tpm5).*((Tpm5-Ta5)./(Ng+f5)).^e)+1./hw5
U_top52=(Ng./U_top51).^-1
U_top53=zegma*(Ta5.^2+Tpm5.^2).*(Ta5+Tpm5)
U_top5=(1./(Ep+0.00591*Ng*hw5))+((2*Ng+f5-1+0.133*Ep)/Eg)-Ng
U_topp=U_top52+U_top53./U_top5
U_back=Kb/tb
U_e5=Ke*Ae5./(t_e*AC)
 U_L5=U_topp+U_e5+U_back
 m5=((U_L5./(K_p*Delta_p))).^0.5
 F5=tanh(m5.*(W-Di)./2)./(m5.*(W-Di)./2) %fin efficiency
 F_prime51=1./U_L5
 F_prime52=W.*(1./((U_L5.*(Di+(W-Di).*F5))+1./(pi.*Di* hfi5 )))
 F_prime5=F_prime51./F_prime52
 F_R51=(mdot.*Cp)./(AC.*U_L5 )
F_R52=exp(-(AC.* U_L5.*F_prime5)./(mdot.*Cp))
F_R5=F_R51.*(1-F_R52) % heat removal factor
plot(Ng,F_R5,'linewidth',3)
xlabel('Number of glazing Ng','fontsize',18)
ylabel('Heat removal factor FR','fontsize',18)
g=0
```

APPENDIX F
FLOW CHAR FOR THE SYSTEM DESIGN PROGRAMME CODES DEVELOPED USING MATLAB

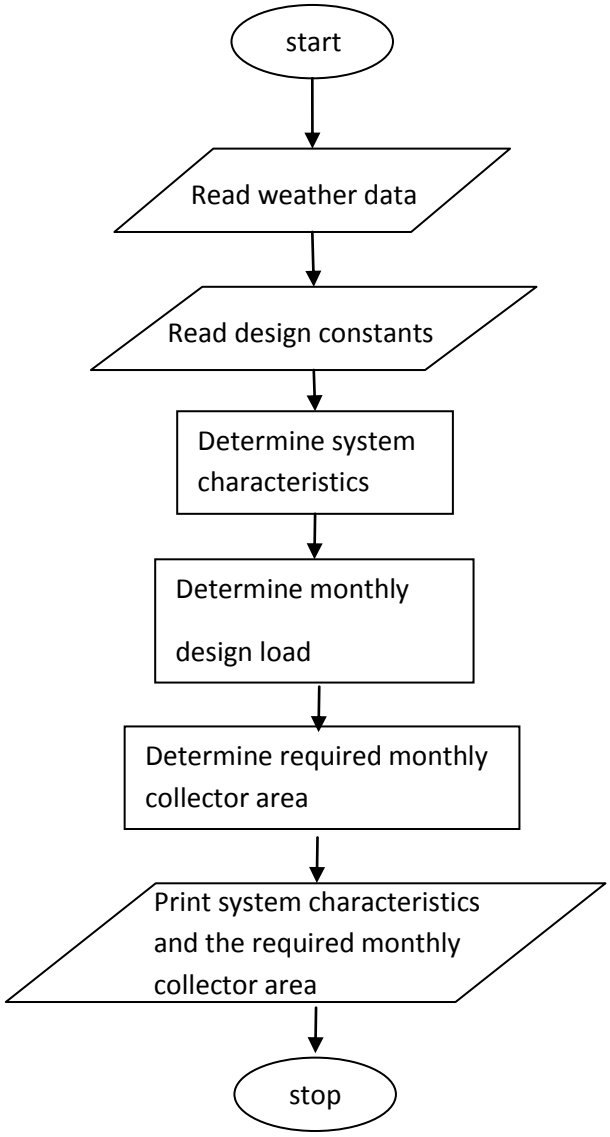

APPENDIX G

A FLOW CHART FOR A PARAMETRIC STUDY ON THE EFFECT OF THE TILT ANGLE ON THE AMOUNT OF SOLAR RADIATION ON COLLECTOR SURFACE

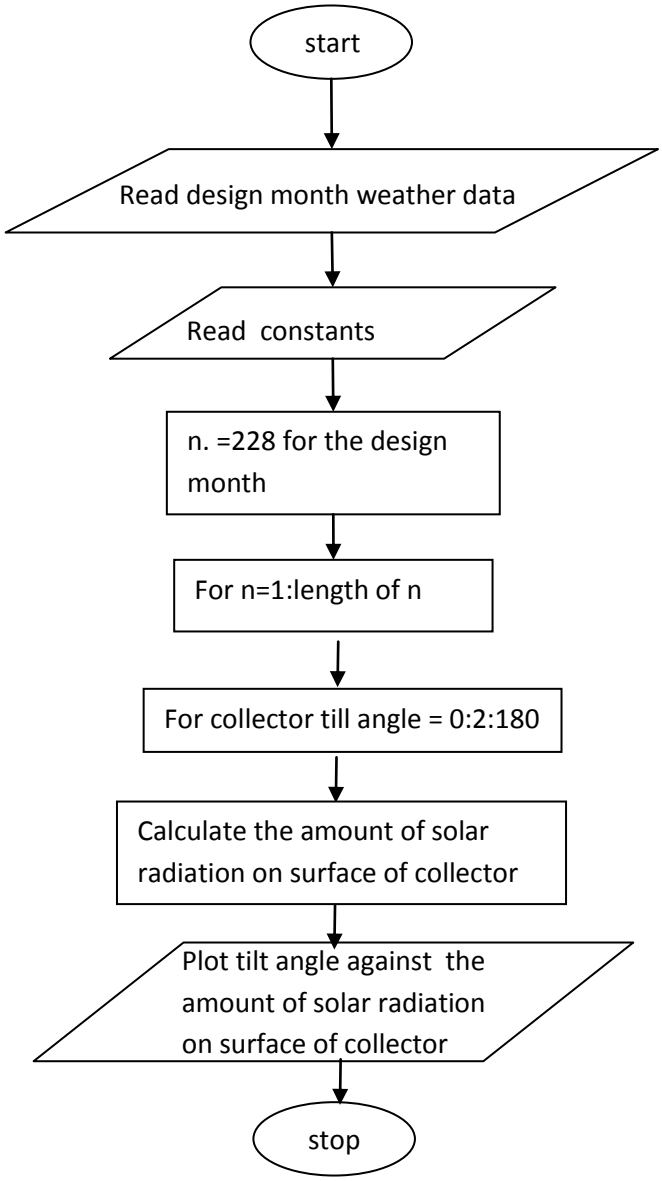

APPENDIX H

A FLOW CHART FOR A PARAMETRIC STUDY ON THE EFFECT OF THE TUBE DIAMETER ON THE HEAT REMOVAL FACTOR

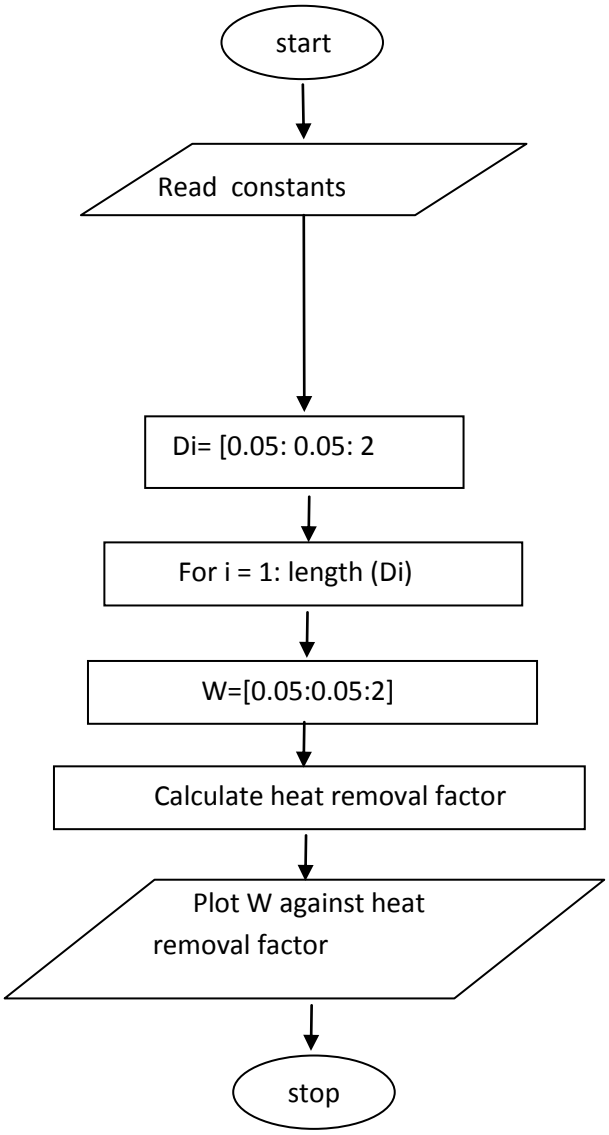

APPENDIX I

FLOW CHART FOR A PARAMETRIC STUDY ON THE EFFECT OF THE PLATE THICKNESS ON THE HEAT REMOVAL FACTOR

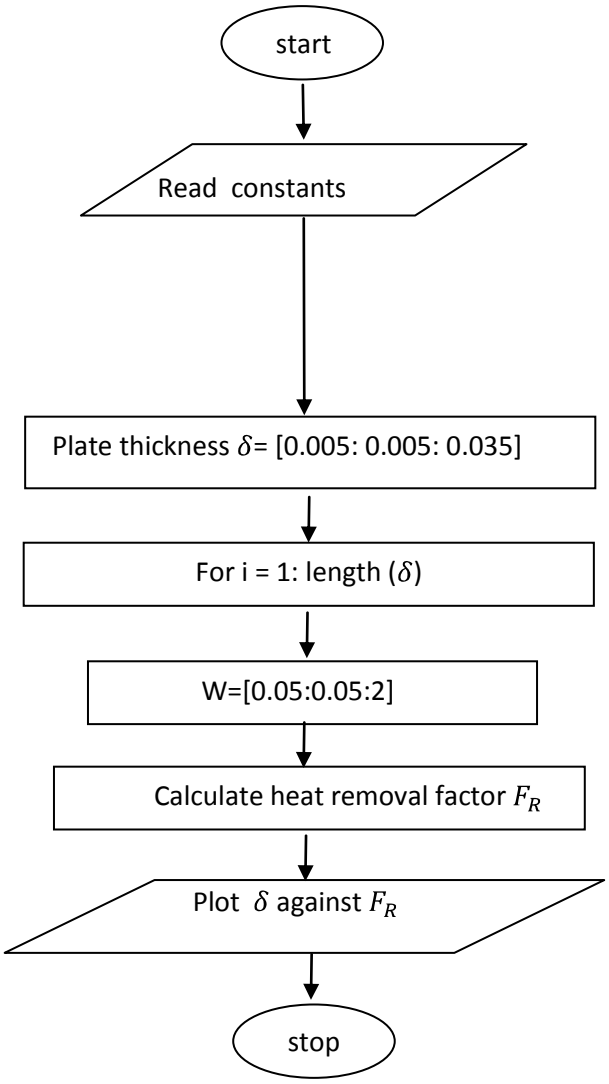

APPENDIX J

A FLOW CHART FOR A PARAMETRIC STUDY ON THE EFFECT OF NUMBER OF GLASS COVERS ON THE HEAT REMOVAL FACTOR

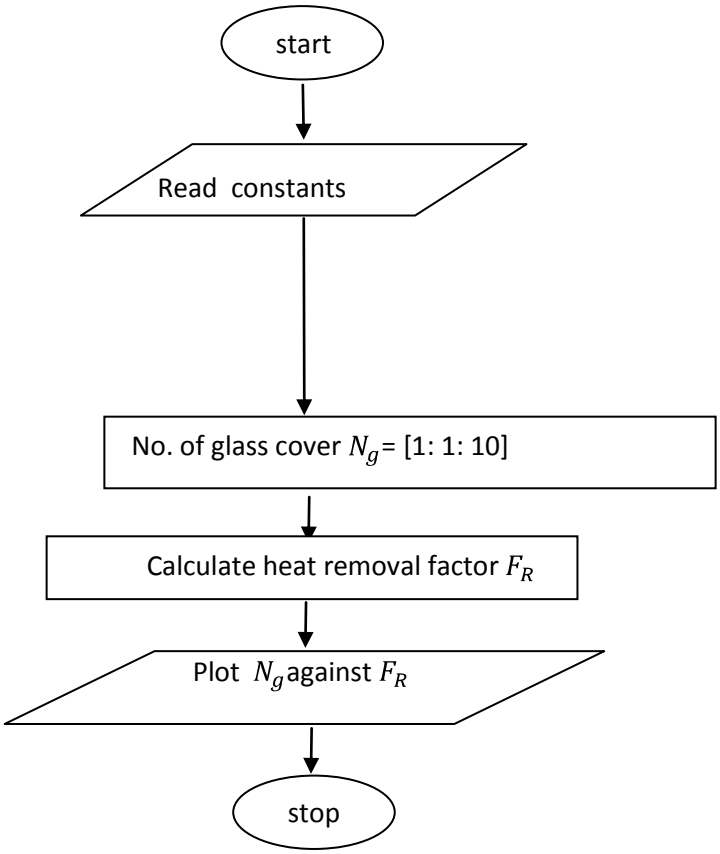

APPENDIX K

PHOTOGRAPHS OF CONSTRUCTED SYSTEM COMPONENTS

Plate 1: Construction of copper grid

Plate 2: Construction of collector casing from dry wood

Plate3: Copper grid and absorber plate fitted into the collector casing

Plate 4: Finished solar collector with double galzing.

Plate5: Two halves of the hot water storage tank moulded using fibre glass and chemical binders

Plate6: The two halves of the storage tank joint together to form the complete hot water storage tank.

Plate7: The hot water storage tank inside a metallic cylinder rimed with saw dust to prevent heat lost.

Plate 8: The side view of the hot water storage tank

Plate9: System supporting frame

Plate10: Side view of the assembled system

Plate11: front view of the assembled system

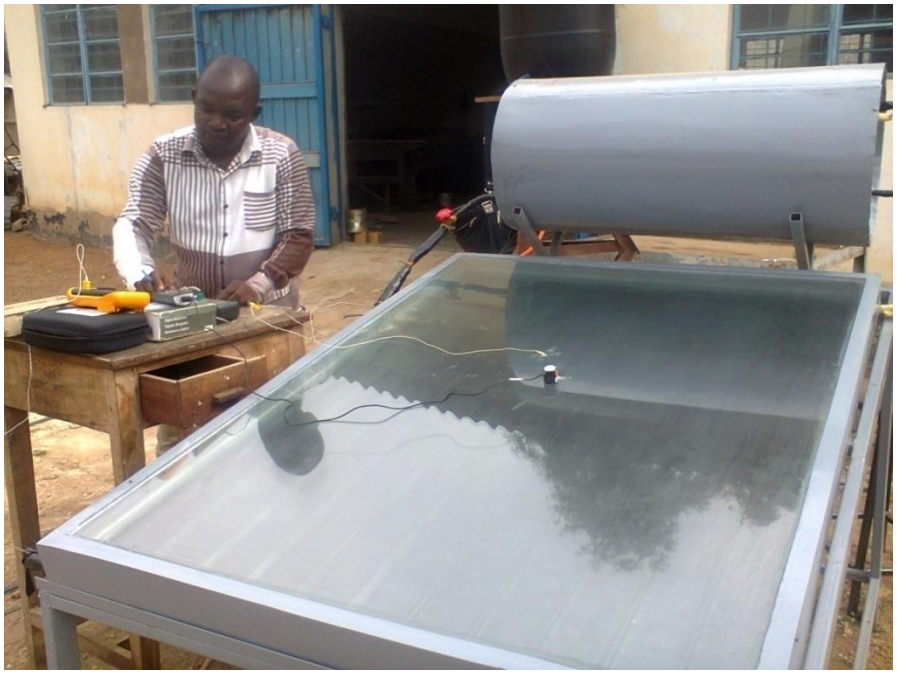

Plate12: System with experimental set up to measure system performance.